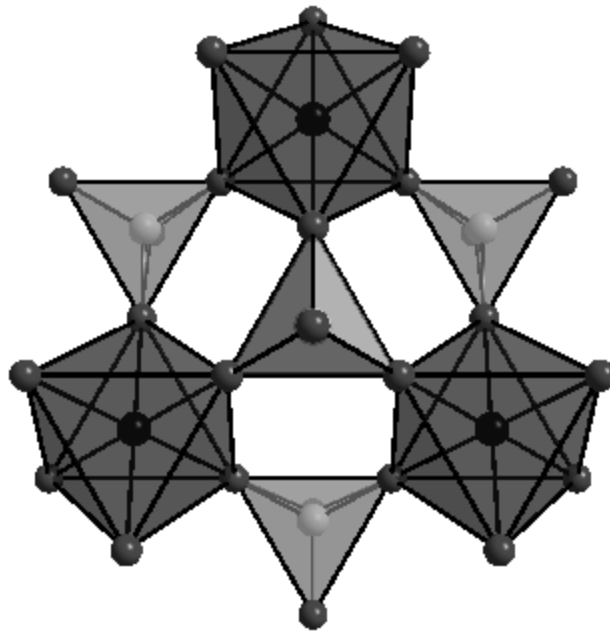


New Ternary Alkali Oxides and Quaternary Alkali Oxy-Nitrides of Molybdenum and Tungsten

Nachiappan Arumugam



Max-Planck-Institut für Festkörperforschung, Stuttgart
Universität Stuttgart
2005



New Ternary Alkali Oxides and Quaternary Alkali Oxy-Nitrides of Molybdenum and Tungsten

Von der Fakultät Chemie der Universität Stuttgart
zur Erlangung der Würde eines Doktors der Naturwissenschaften
(Dr. rer. nat.) genehmigte Abhandlung

Vorgelegt von

Nachiappan Arumugam

aus Sivagangai (Tamilnadu), Indien

Hauptberichter:	Prof. Dr. Dr. h. c. Martin Jansen
Mitberichter:	Prof. Dr. Ir. Eric Jan Mittemeijer
Mitprüfer und Prüfungsvorsitzender:	Prof. Dr. Thomas Schleid

Tag der mündlichen Prüfung: 25. Juli 2005

Max-Planck-Institut für Festkörperforschung, Stuttgart
Universität Stuttgart
2005

Dedicated to my

beloved parents and brothers

for their love, care, encouragement, and moral support throughout my graduate study.

*“I am always doing that which I cannot do,
In order that I may learn how to do it.”*

--Pablo Picasso

Acknowledgements

The work described in this doctoral thesis has been carried out under the guidance and supervision of Prof. Dr. Martin Jansen at the Max-Planck-Institut für Festkörperforschung in Stuttgart between July 2001 and June 2005. I consider myself to be endowed with immense luck in working under his supervision. His advice and guidance have been illuminating during my graduate study in Max-Planck-Institut für Festkörperforschung. My sincere thanks and gratitude are due to Prof. Dr. Martin Jansen for his inspiring motivation, suggestions, discussions and constant encouragement throughout the course of investigation. He created a pleasant environment for me and other group members. He encouraged independence, creativity and leadership. Words are insufficient to express the depth of my gratitude and appreciation for him. Yet, I would like to say 'Thank You', Prof. Dr. Martin Jansen.

I would also like to thank my dissertation committee members Prof. Dr. Thomas Schleid and Prof. Dr. Eric Jan Mittemeijer. Their tips and suggestions have been invaluable and helpful in completing this dissertation.

During the course of this research, many staff members of the Prof. Dr. Martin Jansen group helped me. Dr. Wilhelm Klein's and Dr. Mikhail Sofin's help in solving the crystal structure of many compounds, and also for the valuable discussions involved during the course of my stay deserves special mention. Whenever I approached them, they helped me without any hesitation and never said "NO", even if they are very busy. I express my sincere gratitude and appreciation to them. I also express my gratitude to Dr. Christian Oberndorfer for helping me with DTA/ TGA/ MS analysis, Mrs. Eva-Maria Peters and Dr. Jürgen Nuss for providing the solution to the single crystals and also with the EDX analysis, Dr. Dieter Fischer for his

assistance with MAPLE calculations, Mr. Denis Orosel and Mr. Klaus Hertel for Heating-Guinier measurements, and Mrs. Ortrud Buresch and Ms. Marie-Luise Schreiber for helping me with the elemental analyses.

I would like to thank Dr. Helmut Hass, Dr. Andreas Hönnerschied, Dr. Marcus Pompetzki and Mr. Claus Mühle for their timely help during the initial stages of my work. I would like to thank Prof. Dr. Hans Vogt and Mr. Wolfgang König for their assistance with the IR and Raman spectroscopy analyses and Ms. Eva for helping me with the magnetic measurements. I would like to thank Mr. Werner Giering for making precession photographs of crystals and Mr. Schmidt for assisting me with DSC measurements.

Over the last four years, the Jansen's group has been an extended family. Thanks to the leadership of Prof. Dr. Martin Jansen, this group functioned like a well-knit team. I express my deepest appreciation to all my group members, especially to my lab mates Kailu, Sascha (The King), Timo, Sannela, Pascal, Hanne, Andrei, Stephen and the rest of the group members, Angelika, Denitza, Sascha (1/2), Sanjeev, Bernt, Jan and Oli for their friendship, laughter, coffee breaks, and discussions. I would also like to thank all the Indians at MPI and at Būsnaer platz for making my stay wonderful and made me to feel at home. I would like to thank Max-Planck-Gesellschaft for providing me the funds through out my stay.

Finally, I take this as a golden opportunity to thank my parents, brothers (Karups and Pops) and friends (especially Sampi) for their moral support during this work. Without their encouragement, love, phone calls and care, I couldn't have accomplished what I have today.

Table of Contents

1. Chapter-1	12
1.1 Introduction.....	12
2. Chapter-2	27
2.1 Equipments and Work Techniques	27
2.1.1 Working under Inert Atmosphere	27
2.1.1.1 Vacuum and Inert Gas Glass Apparatus	27
2.1.1.2 Glove Box.....	30
2.1.2 Azide-Nitrate/Nitrite Route	30
2.1.3 Crystal Growing.....	32
2.2 Analyzing Techniques.....	32
2.2.1 Powder X-ray Diffraction	32
2.2.2 Heating-Guinier Method	33
2.2.3 Structure Solution and Refinement from Powder Diffraction	33
2.2.4 X-ray Diffraction on Single Crystals.....	34
2.2.4.1 Precession Technique	34
2.2.4.2 Four and Three Axes Diffractometers.....	35
2.2.5 Thermal Analysis.....	35
2.2.6 Measurement of the Specific Heat	36
2.2.7 IR-Spectroscopy.....	36
2.2.8 Measurements of Electrical Properties.....	36
2.2.9 Measurements of Magnetic Properties.....	37
3. Chapter-3	38
3.1 Alkali Oxynitrides of Molybdenum.....	38
3.2 Synthesis and Structure of $\text{Na}_3\text{MoO}_3\text{N}$	39

3.2.1	Synthesis	39
3.2.2	Thermal Analysis.....	40
3.2.3	Powder Diffraction Analysis	40
3.2.4	Structural Discussion	43
3.2.5	Second Harmonic Generation	46
3.2.6	MAPLE Calculation	48
3.3	Synthesis and Structure of $\text{Na}_5\text{MoO}_4\text{N}$	49
3.3.1	Synthesis	49
3.3.2	Thermal Analyses	50
3.3.3	Powder Diffraction Analysis	50
3.3.4	Single Crystal Data	52
3.3.5	High Temperature X-ray Analysis	53
3.3.6	MAPLE Calculation	56
3.3.7	Structural Discussion	58
4.	Chapter-4	62
4.1	Tripotassium Sodium Tungstate, $\text{K}_3\text{Na}(\text{WO}_4)_2$	62
4.1.1	Synthesis	63
4.1.2	Thermal Analysis.....	63
4.1.3	X-ray Analyses	64
4.1.3.1	Powder Diffraction Analyses.....	64
4.1.3.2	Single Crystal Diffraction Analyses.....	66
4.1.4	Phase Transition Analyses.....	66
4.1.4.1	Low Temperature DSC Measurement	66
4.1.4.2	High Temperature DSC Measurement	69
4.1.4.3	High Temperature X-ray Powder Diffraction	70
4.1.5	Crystal Structure Description	72
4.1.5.1	High-Temperature Phase	72
4.1.5.2	Low-Temperature Phase (Room Temperature Phase).....	77
4.1.5.3	MAPLE Calculation.....	79
4.1.5.4	Comparison of $\text{K}_3\text{Na}(\text{WO}_4)_2$ with Related Glaserites	82

5. Chapter-5	86
5.1 Synthesis and Structure of $K_6Mo_{10}O_{33}$	86
5.1.1 Synthesis	86
5.1.2 Thermal Analysis.....	87
5.1.3 Powder Diffraction Analysis	87
5.1.4 Single Crystal Data	88
5.1.5 Structure Description and Discussion	94
5.2 Oxynitrides of the Nominal Composition $A_3MO_{4-n}N_n$	102
5.2.1 K_3MoO_3N	103
5.2.1.1 Synthesis of “ $K_6Mo_2O_9$ ”	103
5.2.1.2 Powder Diffraction Analysis	103
5.2.1.3 Single Crystal Measurement	104
5.2.1.4 Thermal Analyses.....	105
5.2.1.5 Magnetic Measurement	105
5.2.1.6 DSC measurements	105
5.2.1.7 Chemical Analyses	105
5.2.1.8 Raman Measurement	106
5.2.1.9 Structure Description	107
5.2.2 Other Cubic Oxynitrides	111
5.2.2.1 Sodium Molybdenum Oxynitride, Na_3MoO_3N	111
5.2.2.2 Rubidium Molybdenum Oxynitride, Rb_3MoO_3N	113
5.2.2.3 Potassium Tungsten Oxynitride, K_3WO_3N	114
5.2.2.4 Potassium Niobate Oxynitride, K_3NbO_4	115
6. Chapter-6	117
6.1 Concluding Remarks.....	117
7. Summary	120

Zusammenfassung.....	125
References	130
Appendix.....	139

List of Figures

Figure 2-1: Vacuum and argon line system for handling air/moisture sensitive compounds.	28
Figure 2-2: Schlenk apparatus (upper cross sections: LV of 29, remaining cross sections LV 14.5) (a) Ampoules sealing part, (b) Capillary filling part.....	29
Figure 2-3: Drying tube (upper cross sections: LV of 29, remaining cross sections LV 14.5).	29
Figure 2-4: Reaction crucible. (a) Crucible (hexagonal, steel 9S29-K), (b) Inlays (Mo, Ag), (c) Inlay lid (Mo, Ag).	31
Figure 3-1: <i>Rietveld</i> -plot of $\text{Na}_3\text{MoO}_3\text{N}$. Shown is the observed pattern (circles), the best Rietveld plot (line), the Bragg Positions of $\text{Na}_3\text{MoO}_3\text{N}$ and Ag and the difference plot (Ag was used as a container material and is observed in a very small amount in the powder pattern and hence considered in the refinement).....	41
Figure 3-2: A view of a portion of $\text{Na}_3\text{MoO}_3\text{N}$ structure emphasizing the distorted hexagonal lattice network in $[0\ 0\ 1]$ direction.....	44
Figure 3-3: Crystal structure of $\text{Na}_3\text{MoO}_3\text{N}$ showing the isolated $[\text{MoO}_3\text{N}]$ tetrahedra.....	46
Figure 3-4: Arrangement of all $\text{NaO}_3\text{N-MoO}_3\text{N}$ tetrahedral in the crystal.	47
Figure 3-5: Obtained powder diffraction pattern of $\text{Na}_5\text{MoO}_4\text{N}$ with Cu- $K_{\alpha 1}$ radiation ($\lambda = 1.5406$) at room temperature.	52
Figure 3-6: HT X-ray pattern of $\text{Na}_5\text{MoO}_4\text{N}$. Region 1 indicates the silicon standard pattern obtained at RT. Region 2 indicates the pattern obtained at around $50\text{ }^\circ\text{C}$. Region 3 indicates the pattern obtained at $480\text{ }^\circ\text{C}$	53

Figure 3-7: X-ray profiles obtained at region 2 (50 °C) which is shown above and at region 3 (480 °C) shown below.	57
Figure 3-8: Perspective view of the crystal structure of Na ₅ MoO ₄ N.	59
Figure 3-9: The complex anion [MoO ₄ N] ⁵⁻	60
Figure 3-10: Elongated Na(3) atom along with selected Na, N and O atoms in the unit cell. The oxide and nitride anions are represented by black and white spheres respectively.....	60
Figure 4-1: Thermal analysis of K ₃ Na(WO ₄) ₂ . (TGA in blue and DTA in green)	64
Figure 4-2: Measured X-ray pattern of HT-K ₃ Na(WO ₄) ₂ , Mo-K _α , at 275 °C.....	65
Figure 4-3: Measured X-ray pattern of RT-K ₃ Na(WO ₄) ₂ , Mo-K _α , at 275 °C.....	65
Figure 4-4: X-ray single crystal diffraction patterns of the [0 k l], [h 0 l] and [h k 0] plane of the K ₃ Na(WO ₄) ₂ at room temperature (showing a monoclinic cell).	67
Figure 4-5: Heat capacity measurement of K ₃ Na(WO ₄) ₂ obtained. (powdered sample sealed in aluminum crucible)	70
Figure 4-6: X-ray patterns obtained at different temperatures K ₃ Na(WO ₄) ₂ (from RT to 300 °C).	71
Figure 4-7: X-ray patterns obtained at different temperatures of K ₃ Na(WO ₄) ₂ (from RT to 300 °C and 2θ between 10 and 15).....	72
Figure 4-8: <i>Reitveld</i> plot of HT-K ₃ Na(WO ₄) ₂ . Shown is the observed pattern (red circles), the best Rietveld plot (line), the Bragg Positions of the HT-K ₃ Na(WO ₄) ₂	73
Figure 4-9: Two hexagonal unit cells of HT-K ₃ Na(WO ₄) ₂ showing the opposite facing apices of WO ₄ tetrahedra.....	75

Figure 4-10: Perspective view along $[0\ 0\ 1]$ of the crystal structure of HT- $\text{K}_3\text{Na}(\text{WO}_4)_2$. Drawn are potassium atoms and the coordination polyhedra of tungsten (yellow tetrahedra) and sodium (green octahedra).	76
Figure 4-11: Unit cell of the crystal structure of HT- $\text{K}_3\text{Na}(\text{WO}_4)_2$ viewed along c-axis showing the two WO_4 tetrahedra inside.	80
Figure 4-12: Unit cell of RT- $\text{K}_3\text{Na}(\text{WO}_4)_2$ viewed along c-axis showing the two tilted WO_4 tetrahedra.	81
Figure 4-13: Coordination of K(1) and K(2) in HT-phase of $\text{K}_3\text{Na}(\text{WO}_4)_2$	83
Figure 4-14: Coordination of K(1) and K(2) in LT-phase of $\text{K}_3\text{Na}(\text{WO}_4)_2$	83
Figure 4-15: LT- $\text{K}_3\text{Na}(\text{WO}_4)_2$ with WO_4 tetrahedra and NaO_6 octahedra.	84
Figure 4-16: HT- $\text{K}_3\text{Na}(\text{WO}_4)_2$, drawn are WO_4 tetrahedra and NaO_6 octahedra. The hexagonal unit cell is drawn in blue, cell analogous to the monoclinic one in the LT-phase is drawn in red.	84
Figure 5-1: Measured X-ray powder diffractogram of $\text{K}_6\text{Mo}_{10}\text{O}_{33}$ with Mo- $\text{K}_{\alpha 1}$ radiation ($\lambda = 0.7103$) at room temperature.	88
Figure 5-2: Perspective view of the crystal structure of $\text{K}_6\text{Mo}_{10}\text{O}_{33}$ along $[0\ 0\ 1]$	95
Figure 5-3: The two symmetrically independent Mo_4O_{17} groups of the structure solution in $P1$, dotted lines represent bonds longer than 2.64 Å.	96
Figure 5-4: Mo_4O_{17} group of the centrosymmetric structure solution ($P\bar{1}$), positions of red oxygen atoms are half occupied, dotted lines represent bonds longer than 2.69 Å.	96
Figure 5-5: Mo_4O_{17} groups in polyhedral representation in $P1$	98
Figure 5-6: Crystal structure of $\text{K}_6\text{Mo}_{10}\text{O}_{33}$, viewing direction $[1\ 0\ 0]$	99
Figure 5-7: Crystal structure of $\text{Ag}_6\text{Mo}_{10}\text{O}_{33}$, viewing direction $[1\ 0\ 0]$	100

Figure 5-8: Crystal structure of $\text{Na}_6\text{Mo}_{10}\text{O}_{33}$. (The infinite chains identical in all structures shown are running parallel to viewing direction)	101
Figure 5-9: $[\text{Mo}_4\text{O}_{17}]$ chains in $\text{Na}_6\text{Mo}_{10}\text{O}_{33}$	101
Figure 5-10: X-ray powder diffraction analysis of $\text{K}_6\text{Mo}_2\text{O}_9$ with $\text{Cu-K}\alpha_1$ radiation ($\lambda = 1.5406$) at room temperature.	104
Figure 5-11: Raman spectrum of $\text{K}_3\text{MoO}_3\text{N}$ (shifts of MoO_4 tetrahedra units given in the brackets)	106
Figure 5-12: Crystal structure of $\text{K}_3\text{MoO}_3\text{N}$ with distorted MoO_3N polyhedra.	108
Figure 5-13: Molybdenum pseudo octahedron which is actually a disordered MoO_3N tetrahedra.	109
Figure 5-14: Probable electron density mapping of molybdenum polyhedra (Red sphere = Molybdenum, blue caps = Oxygen/Nitrogen).....	109
Figure 5-15: X-ray powder diffraction analysis of cubic $\text{Na}_3\text{MoO}_3\text{N}$ with $\text{Cu-K}\alpha_1$ radiation ($\lambda = 1.5406$) at room temperature.	113
Figure 5-16: X-ray powder diffraction analysis of cubic $\text{Rb}_3\text{MoO}_3\text{N}$ with $\text{Mo-K}\alpha_1$ radiation ($\lambda = 0.7103$) at room temperature.	114
Figure 5-17: X-ray powder diffraction pattern of cubic $\text{K}_3\text{WO}_3\text{N}$ with $\text{Mo-K}\alpha_1$ radiation ($\lambda = 0.7103$) at room temperature.	115
Figure 5-18: X-ray powder diffraction pattern of cubic K_3NbO_4 with $\text{Mo-K}\alpha_1$ radiation ($\lambda = 0.7103$) at room temperature.	116

List of Tables

Table 1-1: Crystallographic data for the few reported sodium molybdenum oxides*	15
Table 1-2: Crystallographic data of some reported potassium molybdenum oxides*	16
Table 1-3: List of few sodium and potassium tungstate compounds*	18
Table 1-4: Crystallographic data for univalent metal polymolybdates.....	19
Table 3-1: Crystallographic data and Structure Refinement of Na ₃ MoO ₃ N.	42
Table 3-2: Positional and isotropic displacement parameters for Na ₃ MoO ₃ N.	43
Table 3-3: Selected interatomic distances (Å) in Na ₃ MoO ₃ N.....	45
Table 3-4: Second-Harmonic Generation of Na ₃ MoO ₃ N.	47
Table 3-5: Atoms, Charge and MAPLE of an individual atom in an ordered structure.....	48
Table 3-6: Coordination number (CN), Effective Coordination Number (ECoN) and Mean Effective Ionic Radii (MEFIR) (Å) for Na ₃ MoO ₃ N.....	49
Table 3-7: Powder diffraction data of Na ₅ MoO ₄ N (d > 150.0 pm).....	51
Table 3-8: Crystallographic data and structure refinement for Na ₅ MoO ₄ N.	54
Table 3-9: Atomic co-ordinates and isotropic thermal parameters (pm ² ×10 ⁻¹) for Na ₅ MoO ₄ N.	55
Table 3-10: Anisotropic displacement parameters (pm ² ×10 ⁻¹). The anisotropic displacement factor exponent takes the form: -2π ² [h ² a × 2U ₁₁ + ... + 2 h k a × b × U ₁₂].	55

Table 3-11: Atoms, Charge and MAPLE of an individual atom in Na ₅ MoO ₄ N.	56
Table 3-12: Coordination number (CN), Effective Coordination Number (ECoN) and Mean Effective Ionic Radii (MEFIR) (Å) for Na ₅ MoO ₄ N.	57
Table 3-13: Selective bond lengths of Na ₅ MoO ₄ N.	59
Table 4-1: Crystallographic data and structure refinement of the HT and RT- K ₃ Na(WO ₄) ₂	68
Table 4-2: Positional and isotropic displacement parameters for the HT-K ₃ Na(WO ₄) ₂ at 275 °C.	74
Table 4-3: Selected interatomic distances in HT- K ₃ Na(WO ₄) ₂	74
Table 4-4: Atomic parameters for RT-K ₃ Na(WO ₄) ₂	77
Table 4-5: Anisotropic displacement parameters for RT-K ₃ Na(WO ₄) ₂ . (Å ²).....	78
Table 4-6: Selective interatomic bond distances of atoms in RT-K ₃ Na(WO ₄) ₂	78
Table 4-7: Coordination number (CN), Effective Coordination Number (ECoN) and Mean Effective Ionic Radii (MEFIR) (Å) for RT-K ₃ Na(WO ₄) ₂ using MAPLE calculations.	79
Table 4-8: Coordination number (CN), Effective Coordination Number (ECoN) and Mean Effective Ionic Radii (MEFIR) (Å) for HT-K ₃ Na(WO ₄) ₂ using MAPLE calculations.	80
Table 4-9: M-O bond lengths at room temperature and phase transition temperatures of some glaserite compounds.	85
Table 5-1: Crystallographic data and Structure Refinement of K ₆ Mo ₁₀ O ₃₃	89
Table 5-2: Atomic co-ordinates of K ₆ Mo ₁₀ O ₃₃	90
Table 5-3: Anisotropic displacement parameters of K ₆ Mo ₁₀ O ₃₃ . (Å ²).....	91
Table 5-4: Crystallographic data and Structure Refinement of K ₃ MoO ₃ N.	110

Table 5-5: Positional and isotropic displacement parameters for
K₃MoO₃N. 110

Table 5-6: Anisotropic displacement parameters of K₃MoO₃N in (Å²). 111

Table 5-7: Different cubic oxynitrides with their lattice constants. 116

1. Chapter-1

1.1 Introduction

Solid state chemistry is the study of solid materials, which may be either molecular, supramolecular or extended solids, including their syntheses, structures and the physical properties. As with other branches of the physical sciences, solid state chemistry also extends to related areas that furnish concepts and explanations of those phenomena, which are more characteristic of the subject. It is mainly concerned with the synthesis, structure, properties and applications of solid materials. For the preparation of solids, several methods are available e.g. solid state reaction, precipitation or electrochemical methods. One of the most common methods of preparing solid materials is by reacting solid components at elevated temperatures. The advantages of solid state reaction are the ready availability of precursors and low costs for production on an industrial scale. There are few important factors that influence the rate of the reaction between solids [1]. The reaction rate depends on

- Particle size of the reactants (smaller the better)
- Degree of homogenization achieved on mixing
- Intimacy of contact between the grains
- Temperature at which the reaction is carried out
- Rate of nucleation of the product phase
- Rates of diffusion of ions through the various phases especially the product phase

The rate is also promoted by performing the solid state reactions in molten fluxes or high temperature solvents (e.g. Bi, Sn, alkaline metals etc) and also by grinding the sample periodically.

The physical techniques and methods that are used to analyze solids are also quite often different from those that are used in other branches of chemistry. Thus, there is much less emphasis on spectroscopic methods and, instead, more emphasis on a variety of diffraction, e.g. X-ray diffraction, and microscopic techniques, e.g. electron microscopy. X-ray diffraction has two principal uses in solid state chemistry. Firstly, almost all crystal structures are solved by using X-ray diffraction, especially by single crystal methods. Secondly, crystalline solids have their own characteristic X-ray powder diffraction pattern which may be used as a means of “fingerprinting”. So, the powder X-ray diffraction pattern plays the main role in phase analysis.

By using solid state reactions, new oxides and oxynitrides have been synthesized in the course of this work. The forthcoming part of this chapter gives a brief history about the compounds known in alkali transition metal oxides, in particular the oxides of molybdenum and tungsten (ternary and quaternary systems), alkali bronzes of molybdenum and tungsten, and alkali oxynitrides of molybdenum.

Alkali transition metal oxides, in short ATMO, can be prepared by the solid state reaction of transition metal oxides and alkali metal oxides. Ternary oxides of the transition metals exhibit various interesting structural, chemical and physical characteristics. In these ternary systems, the oxidation state of the central metal atom can be varied by changing the composition of the starting materials as well as the reaction conditions. According to the oxidation states of the central metal atom, unusual coordination geometry, higher and lower coordination numbers are possible. Very few fully oxidized molybdates and tungstates are known in comparison to the number of molybdenum and tungsten bronzes. In the anions, the molybdenum and tungsten atoms occupy the centers of MO_4 tetrahedra (where $M = \text{Mo}$ or W). Since the ionic radii of Mo^{6+} and W^{6+} are nearly equal, a compound A_2MoO_4 (where $A = \text{Alkali metal}$) may be isomorphous with A_2WO_4 . The common molybdates and tungstates of the alkali metals consist of MoO_4^{2-} and WO_4^{2-} anions. In the $\text{Na}_2\text{O}-\text{MoO}_3$ system, $\text{Na}_2\text{Mo}_2\text{O}_7$ [2] and $\text{Na}_6\text{Mo}_{10}\text{O}_{33}$ [3] are crystallographically characterized until the late 1990's, while the existence of many other phases with different compositions was postulated [4]. $\text{Na}_2\text{Mo}_2\text{O}_7$ contains chains of corner

sharing distorted MoO_6 octahedra, which are linked together via MoO_4 tetrahedra by common corners [5,6]. $\text{Na}_6\text{Mo}_{10}\text{O}_{33}$ contains a three dimensional network from two different chains of molybdenum polyhedra. The first chain consists of edge- and corner- sharing distorted MoO_6 octahedra. In the second chain, corner- sharing pairs of octahedra share edges with pairs of MoO_5 square pyramids, which are inverted with respect to each other [3]. Recently two more compounds have been added in the $\text{Na}_2\text{O}-\text{MoO}_3$ system, namely the sodium rich molybdate Na_4MoO_5 [7], and the molybdenum rich compound, $\text{Na}_6\text{Mo}_{11}\text{O}_{36}$ [8]. Na_4MoO_5 crystallizes in the Na_4SeO_5 structure [7], where the molybdenum atoms have a square pyramidal environment. The crystal structure of $\text{Na}_6\text{Mo}_{11}\text{O}_{36}$ consists of a three dimensional network of highly distorted edge sharing MoO_6 octahedra similar to the anatase structure [9].

Na_2MoO_4 exists in four different modifications (α -, β -, γ - and δ - Na_2MoO_4 phases) between RT and 670 °C. α - Na_2MoO_4 crystallizes with a spinel type structure where molybdenum atoms occupy the tetrahedral positions in the close packing of oxygen atoms, while sodium atoms are situated in the octahedral interstitials. The structure of β - Na_2MoO_4 is not well understood. In γ - Na_2MoO_4 , molybdenum atoms remain tetrahedrally coordinated while the arrangement of sodium atoms differs from that of α -phase. In δ - Na_2MoO_4 , the MoO_4 groups are disordered and two partly occupied oxygen sites are associated with the molybdenum atom corresponding to the three different oriented MoO_4 tetrahedra. In short, α - Na_2MoO_4 phase is isostructural with Na_2WO_4 , the γ -phase with thenardite, Na_2SO_4 (V), and the δ -phase with Na_2SO_4 (I). Table 1-1 gives the list of some of the sodium molybdenum oxides including sodium molybdenum bronzes reported so far along with their lattice constants.

There are several reports on the synthesis and characterization of potassium molybdates. A short overview on potassium molybdates is mentioned here. Addition of alkali superoxide (KO_2) to the pure metal molybdenum yields alkali molybdates, K_2MoO_4 and KMo_4O_6 [10]. The latter is a mixed valence compound in which the oxidation state of Mo is found to be +2 and +3. The structure of KMo_4O_6 consists of double strings of edge sharing Mo_6 octahedra (each octahedron sharing four edges with four other octahedra). These double strings are interconnected via corner

sharing of oxygen atoms. Potassium is coordinated to eight oxygen atoms in a distorted square prismatic arrangement.

Table 1-1: Crystallographic data for the few reported sodium molybdenum oxides*.

S.No	Compound	Space group	a (Å)	b (Å)	c (Å)	α (°)	β (°)	γ (°)	Volume (Å ³)
1	Na ₂ MoO ₄ [11]	<i>Pnam</i>	7.76	10.05	5.60	90	90	90	436.7
2	Na ₄ MoO ₅ [12]	<i>P$\bar{1}$</i>	9.995	10.02	5.65	96.54	96.29	113.35	508.8
3	Na ₄ MoO ₅ [13]	-	17.93	18.27	12.16	90	90	90	3983.3
4	Na ₂ Mo ₂ O ₇ [6]	<i>Cmca</i>	7.164	11.837	14.714	90	90	90	623.8
5	Na ₆ Mo ₁₀ O ₃₃ [3]	<i>P$\bar{1}$</i>	8.049	12.18	7.576	99.96	100.74	109.88	663.4
6	Na _{0.88} Mo ₆ O ₁₇ [14]	-	9.557	5.518	12.964	90	90.02	90	683.6
7	Na _{0.9} Mo ₆ O ₁₇ [15]	-	5.50	5.50	12.91	90	90	120	338.2
8	Na _{0.93} Mo ₆ O ₁₇ [16]	<i>P$\bar{3}m1$</i>	5.51	5.51	12.95	90	90	90	340.4
9	Na _{0.9} Mo ₂ O ₄ [17]	<i>C</i>	12.438	2.884	4.925	90	103.95	90	85.7
10	Na ₂ Mo ₃ O ₆ [18]	-	-	-	-	-	-	-	-
11	NaMoO ₂ [19]	<i>R$\bar{3}m$</i>	2.92	2.92	17.12	90	90	120	42.1

* arranged in the descending order of Mo oxidation state.

The other known molybdenum rich potassium molybdate, K₃Mo₁₄O₂₂ [20], is prepared by reacting a mixture of K₂MoO₄, MoO₂ and Mo in a mole ratio of 3:11:8 in an evacuated and sealed molybdenum tube, fired at 1250 °C for 8 days. The structure consists of molybdenum oxide cluster framework built from the condensation of three Mo₆O₁₈ units along trans- edges. All exterior edges of the metal–metal bonded octahedra in the trimeric clusters are bridged by oxygen atoms. The waist molybdenum atoms at the ends of the cluster and also apical molybdenum atoms have terminal bonds to oxygen atom. The coordination number of potassium is ten and eleven. The compounds A₆Mo₂O₉ (A = K, Rb, Cs) were obtained by the solid state reaction between A₂O and A₂MoO₄. Their polymorphism was studied by DTA and HT X-ray diffraction. Three phases were observed for K₆Mo₂O₉ [21], a room temperature orthorhombic up to 448 °C, a hexagonal up to 750 °C and a face

centered cubic elpasolite type one. The structures of these compounds were not characterized sufficiently. Table 1-2 gives the list of potassium molybdates reported along with their crystallographic data.

Table 1-2: Crystallographic data of some reported potassium molybdenum oxides*.

S.No	Compound	Space group	a (Å)	b (Å)	c (Å)	α (°)	β (°)	γ (°)	Volume (Å ³)
1	K ₂ MoO ₄ [22, 23]	$P\bar{3}m1$	6.26	6.26	7.89	90	90	120	267.7
2	K ₂ MoO ₄ [45]	$C2/m$	12.348	6.081	7.538	90	115.74	90	509.85
3	K ₄ MoO ₅ [24]	$P\bar{1}$	16.903	10.195	6.258	96.151	92.635	94.223	1067.7
4	K ₆ Mo ₂ O ₉ [21]	-	8.56	8.56	8.56	90	90	90	156.8
5	K ₆ Mo ₂ O ₉ [21]	-	12.17	12.17	7.63	90	90	120	978.6
6	K ₂ Mo ₂ O ₇ [48]	$P\bar{1}$	7.51	7.24	6.95	92	112	82.5	347
7	K ₂ Mo ₃ O ₁₀ [49]	$C2/c$	13.95	7.58	9.02	90	99.2	90	481.5
8	K _{0.26} MoO ₃ [25]	$C2/m$	14.278	7.723	6.387	90	92.34	90	351.7
9	K _{0.28} MoO ₃ [26]	$C2/m$	18.249	7.56	9.855	90	117.32	90	602.8
10	K _{0.3} MoO ₃ [27]	$C2/m$	18.211	7.56	9.834	90	117.51	90	600
11	K _{0.33} MoO ₃ [28]	$C2/m$	14.299	7.737	6.394	90	92.62	90	353.3
12	K _{0.9} Mo ₆ O ₁₇ [29]	$P\bar{3}$	5.538	5.538	13.656	90	90	120	362.7
13	K ₂ Mo ₇ O ₂₀ [30]	$Pbcm$	4.0176	17.891	21.825	90	90	90	1568.7
14	K ₂ Mo ₈ O ₁₆ [31]	$P2/n$	10.232	10.286	5.758	90	90	90.14	606
15	K _{0.5} Mo ₄ O ₆ [10]	$Pbam$	9.794	9.476	2.873	90	90	90	266.6
16	K(Mo ₄ O ₆) [10]	$P4/mbm$	9.61	9.61	2.95	90	90	90	272.5

* arranged in the descending order of Mo atom oxidation state.

Similar to the alkali molybdates, alkali tungstates were synthesized and characterized. Sodium tungstate, Na₂WO₄, is of spinel type having Na atoms in octahedral and W atoms in tetrahedral sites. Pentasodium tetradecatungsten tetratetracontaoxide, Na₅W₁₄O₄₄ [32], was synthesized by electrolyzing fused mixtures of Na₂WO₄ and WO₃ in the molar ratio 3:5. The structure of this compound

is built up by groups of four layers of WO_6 octahedra similar to those found in hexagonal tungsten bronzes, but relatively displaced to each other to form the tunnels of trigonal and hexagonal sections. These groups are linked together through a layer of isolated WO_5 trigonal bipyramids. Sodium atoms are being coordinated with eight oxygen atoms forming a hexagonal bipyramidal arrangement. $\text{Na}_2\text{W}_2\text{O}_7$ (I) was reported to be isostructural to $\text{Na}_2\text{Mo}_2\text{O}_7$ while $\text{Na}_2\text{W}_2\text{O}_7$ (II) synthesized under high pressure [33] consists of distorted perovskite type slabs composed of WO_6 octahedra and sodium atoms situated between the slabs in seven fold coordination with oxygen. Crystals of $\text{K}_2\text{W}_4\text{O}_{13}$ [34] were synthesized by heating an intimate mixture of K_2CO_3 and WO_3 in a molar ratio of 1:4 in a Pt crucible at 750°C for 2 weeks. The structure is formed by the layers of ${}_{\infty}^2[(\text{W}_4\text{O}_{13})^{2-}]$. The structure is built up of highly distorted WO_6 octahedra, and KO_{14} and KO_{18} coordination polyhedra. $\text{K}_2\text{W}_3\text{O}_{10}$ [35] was synthesized in the same way as mentioned above but with different molar ratios. This structure is built up of distorted WO_6 octahedra, and KO_{13} and KO_9 coordination polyhedra. Four WO_6 octahedra are linked to form W_4O_{18} group by sharing edges, and five WO_6 to form W_5O_{24} group by sharing corners. These kinds of groups are further linked by sharing corners constructing a framework of the ${}_{\infty}^2[(\text{W}_4\text{O}_{13})^{2-}]$ anion. Table 1-3 gives the list of few reported sodium and potassium tungstates including bronzes.

The polymolybdate compounds of univalent Mo ions with general formula, $\text{A}_2^+ \text{Mo}_n^{+6} \text{O}_{3n+1}^{-2}$ were studied extensively in the 1970's. Table 1-4 contains the cell parameters of the structures reported. Studies have shown that the structures of these compounds depend on the number of Mo atoms, n , and the size of the counter ion (the potassium compounds being taken as structural models). With $n = 1$, the structure contains isolated tetrahedral MoO_4 ions. The compounds with $n = 2$ comprise of infinite chains built with two blocks of octahedra sharing an edge, each block being connected through corners by two tetrahedra. The building block of the chain of the $n = 3$ compounds consists of two trigonal bipyramids connected by an octahedron, each polyhedron sharing edges.

Table 1-3: List of few sodium and potassium tungstate compounds*.

S.No	Compound	Space group	a (Å)	b (Å)	c (Å)	α (°)	β (°)	γ (°)	Volume (Å ³)
1	Na ₂ WO ₄ [36]	<i>Fd</i> $\bar{3}m$	9.1297	9.1297	9.1297	90	90	90	190.2
2	K ₂ WO ₄ [22, 23]	<i>P</i> $\bar{3}m1$	6.3	6.3	7.92	90	90	120	272.2
3	Na ₄ WO ₅ [37]	<i>P</i> $\bar{1}$	5.694	8.477	5.657	101.29	102.25	109.2	241.3
4	K ₄ WO ₅ [24]	<i>P</i> $\bar{1}$	16.9218	10.2119	6.2639	96.139	92.611	94.239	1071.7
5	Na ₂ W ₂ O ₇ [38]	<i>Cmc</i> 21	3.7777	26.6067	5.429	90	90	90	272.8
6	Na ₂ W ₂ O ₇ [39]	<i>Cmca</i>	7.216	11.899	14.716	90	90	90	631.7
7	Na ₆ WO ₆ [13]	-	8.49	10.15	15.14	90	90	90	1304.6
8	K ₆ W ₂ O ₉ [21, 40]	-	12.22	12.22	7.62	90	90	120	985.4
9	K ₂ W ₃ O ₁₀ [35]	<i>P</i> 2/c	10.947	3.864	31.955	90	108.44	90	1282.2
10	K ₂ W ₄ O ₁₃ [34]	<i>P</i> $\bar{3}$	15.566	15.566	3.846	90	90	120	807
11	Na ₅ W ₁₄ O ₄₄ [32]	<i>P</i> $\bar{1}$	7.274	7.2911	18.551	96.375	90.714	119.66	847.1
12	Na _{0.1} WO ₃ [41]	<i>P</i> 4/nmm	5.255	5.255	3.890	90	90	90	107.4
13	Na _{0.3} WO ₃ [42]	<i>P</i> 6 ₃ 22	7.411	7.411	7.619	90	90	120	362.3
14	Na _{0.33} WO ₃ [43]	<i>P</i> $\bar{4}$ 21 <i>m</i>	12.097	12.097	3.754	90	90	90	549.3
15	K _{0.33} WO ₃ [44]	<i>I</i> 2/m	16.2312	7.5502	9.8614	90	94.895	90	1204.1
16	Na _{0.48} WO ₃ [43]	<i>P</i> 4/mbm	12.14	12.14	3.767	90	90	90	555.1

* arranged in the descending order of Mo atom oxidation state.

With $n = 4$, the chain starts to widen and when n is greater than 4, compounds with odd number of n were prepared only with heavy alkaline atoms. The structure consists of double sheets of MoO₆ octahedra sharing edges.

Table 1-4: Crystallographic data for univalent metal polymolybdates.

S.No	Compound	Space group	a (Å)	b (Å)	c (Å)	α (°)	β (°)	γ (°)	Volume (Å ³)
1	K ₂ MoO ₄ [45]	<i>C2/m</i>	12.348	6.081	7.538	90	115.74	90	509
2	Rb ₂ MoO ₄ [46]	<i>C2/m</i>	12.821	6.253	7.842	90	115.64	90	566
3	Cs ₂ MoO ₄ [47]	<i>Pnma</i>	11.608	6.562	8.510	90	90	90	648
4	Na ₂ Mo ₂ O ₇ [2, 6]	<i>Cmca</i>	7.164	11.837	14.714	90	90	90	623.8
5	K ₂ Mo ₂ O ₇ [48]	<i>P$\bar{1}$</i>	7.51	7.24	6.95	92	112	82.5	347
6	K ₂ Mo ₃ O ₁₀ [49, 50]	<i>C2/c</i>	13.952	7.757	9.015	90	98.84	90	961.03
7	Cs ₂ Mo ₃ O ₁₀ [49, 51]	<i>C2/c</i>	14.465	8.3997	9.4614	90	97.74	90	1139.1
8	Rb ₂ Mo ₃ O ₁₀ [52]	<i>C2/c</i>	14.14	8.085	9.151	90	98.4	90	1035
9	Li ₂ Mo ₄ O ₁₃ [53, 54]	<i>P$\bar{1}$</i>	8.612	11.562	8.213	94.457	96.38	111.25	751.36
10	K ₂ Mo ₄ O ₁₃ [55]	<i>P$\bar{1}$</i>	7.972	8.352	10.994	119.4	62.7	109.8	560.5
11	Rb ₂ Mo ₄ O ₁₃ [55]	<i>P$\bar{1}$</i>	8.41	10.274	8.24	103.71	109.7	107.19	593
12	Cs ₂ Mo ₄ O ₁₃ [56]	<i>C2/c</i>	45.92	10.418	7.923	90	92.94	90	3784
13	Tl ₂ Mo ₄ O ₁₃ [57, 58]	<i>Pbca</i>	7.583	15.409	18.798	90	90	90	2196.4
14	Cs ₂ Mo ₅ O ₁₆ [59]	<i>C2/c</i>	21.44	5.559	14.338	90	122.74	90	1437.4
15	Cs ₂ Mo ₇ O ₂₂ [59, 59]	<i>C2/c</i>	21.54	5.537	18.91	90	122.7	90	1897
16	Rb ₂ Mo ₇ O ₂₂ [59]	<i>C2/c</i>	20.73	5.553	18.56	90	120.79	90	1836
17	Tl ₂ Mo ₇ O ₂₂ [60]	<i>C2/c</i>	20.512	5.526	19.46	90	125.23	90	1802

The term bronze was coined by Wöhler [61] in 1825 and is used as a trivial name to describe a class of transition metal oxides incorporating variable amounts of a third element, usually an alkali metal. Partial reduction of molten sodium molybdates or tungstates by hydrogen, zinc, molybdenum or tungsten, or by electric current, leads to intensely colored mixed compounds which are valued as pigments. Transition metal bronzes are a class of compounds having the general formula, A_xTO_n , where A is an alkali, alkali earth, rare earth, group 11, group 12, NH₄⁺, H⁺ or some metal

ions and T is a transition metal atom such as Ti, V, Mn, Nb, Ta, Mo, W or Re. The alkali tungsten bronzes, A_xWO_3 ($0.0 < x < 1.0$, in practice x usually varies from 0.3 to 0.9), have been studied most intensively and reviewed in the past [62-65]. These alkali transition metal bronzes have wide variety of crystal structures and an enormous amount of data was accumulated on their structures [66,67], and consequently a variety of physical properties. Tungsten bronzes have technological applications such as electrochemical devices, humidity sensors, solid fuel cells, secondary batteries, ion sensitive electrodes, etc. [68,69]. Wold *et al.* (1964) describes the first synthesis of the alkali metal molybdenum bronze [70]. In the early 1980's, most of the interest was focused on the study of molybdenum bronzes and especially on the so called "blue bronzes", $A_{0.3}MoO_3$ ($A = K, Rb$ and Tl). The interest in the study of alkali molybdenum bronzes is primarily concerned with the structural and physical properties unique to some of these bronzes, and also due to their quasi low dimensional properties, which include highly anisotropic transport properties [71-73], and, super conductivity as described in several reviews [74-77]. The ternary tungsten bronzes, characterized by their non stoichiometric compositions, have three dimensional structures built up of corner sharing WO_6 octahedra [78,79]. The ternary molybdenum bronzes, on the other hand, are typically layered compounds with edge/corner sharing MoO_6 octahedra. Interestingly, the high pressure prepared alkali molybdenum bronzes A_xMoO_3 ($A = K$ and Rb) are known to be isostructural with their tungsten analogues [80].

Molybdenum bronzes may be classified on the basis of similarity of color, stoichiometry, and structure as

- Blue bronzes $A_{0.3}MoO_3$ ($A = K, Rb, Cs$ and Tl) [26,81]
- Red bronzes $A_{0.33}MoO_3$ ($A = Li, K, Rb, Cs$ and Tl) [25] and
- Purple bronzes $A_{0.9}Mo_6O_{17}$ ($A = Li, Na, K$ and Tl) [82,83].

The structures of the blue and red bronzes have similar sheet structures consisting of clusters of edge sharing MoO_6 octahedra while the structure of purple bronze consists of ReO_3 - type slabs of corner sharing MoO_6 octahedra, having MoO_4

tetrahedra at the surfaces of these slabs. The ideal structure of the purple bronze, $A\text{Mo}_6\text{O}_{17}$ can be described in terms of slabs of Mo-O corner sharing polyhedra. Each slab of Mo-O polyhedra consists of four layers of corner sharing MoO_6 octahedra, which are terminated on either side by a layer of MoO_4 tetrahedra sharing corners with adjacent MoO_6 octahedra in the same layer. These slabs are perpendicular to the *c*- direction and are separated from each other by a layer of monovalent metal ions in a KO_{12} icosahedral environment of oxygen [29,84]. The monoclinic structure of red bronze, determined by Stephenson *et al.* [25] is built up of infinite sheets of corner/edge-sharing distorted MoO_6 octahedra joined together by the K^+ ions which are in an irregular eightfold coordination. The blue bronze exhibits a metal to semiconductor transition at 180 K with the formation of the CDW. The purple bronze is a quasi two dimensional conductor which undergoes a CDW at about 120 K due to the nesting of hidden Fermi surfaces. The red bronze acts as a semiconductor at all temperatures.

Despite the rich chemistry of ternary oxides and ternary bronzes, little is revealed about the quaternary oxides of type $A_n\text{B}_x\text{M}_y\text{O}_z$ where A and B = alkali or rare earth metals and M = W, Mo. Several tungsten oxide bronzes $A_x\text{B}_y\text{MO}_3$ (A = Li, Na, K, Rb and B = Li, K) in polycrystalline form have been proposed for application as ion selective electrodes by Dobson *et al.* [85]. The study of structures of alkali metal polytungstates and mixed alkali tungstates has seen considerable progress only in the recent years. Only three compounds of mixed alkali (Na and K) molybdates and two tungstates are reported. $\text{K}_3\text{Na}(\text{MoO}_4)_2$, $\text{K}_{2.5}\text{Na}_{1.5}(\text{MoO}_4)_2$ [86] and KNaMoO_4 are the only known molybdenum compounds with potassium and sodium. These compounds were prepared by heating the mixture of Na_2MoO_4 and K_2MoO_4 in a Pt crucible. The RT phase of $\text{K}_3\text{Na}(\text{MoO}_4)_2$ and $\text{K}_{2.5}\text{Na}_{1.5}(\text{MoO}_4)_2$ are isostructural with the monoclinic low temperature phases of $\text{K}_3\text{Na}(\text{SeO}_4)_2$ and $\text{K}_3\text{Na}(\text{CrO}_4)_2$. There exists a phase transition from monoclinic to trigonal phase above RT. The structure of molybdates slightly differs from that of the sulphate, chromate and selenate. The structure consists of isolated MoO_4 tetrahedra connected by alkali cations. The coordination number of potassium was found to be 9 and 10. Few other compounds of molybdenum are reported with rubidium and sodium, namely $\text{NaRbMo}_3\text{O}_{10}$,

$\text{Na}_{0.67}\text{Rb}_{1.33}\text{MoO}_4$ and $\text{Na}_{0.5}\text{Rb}_{1.5}\text{MoO}_4$ [87]. Rubidium sodium molybdate was synthesized by the reaction of the sodium molybdate along with RbNO_3 and MoO_3 and also by heating the mixture of corresponding alkali carbonates with MoO_3 . Among tungstates, $\text{K}_{0.39}\text{Na}_{0.27}\text{WO}_3$ [88] phase was reported by Li *et al.* which was prepared by fused salt electrolysis. Hoppe *et al.* synthesized a compound containing a larger amount of sodium than potassium, KNa_3WO_5 [89]. The compound was prepared by reacting Na_4WO_5 with K_2O (Na:K:W = 4:3:1) for 35 days at 750 °C. This part of research is open for the discovery of new mixed alkali tungstates.

The most common methods of synthesizing ternary or quaternary oxides/bronzes involves the reaction between the transition metal oxide (Mo) and the hydroxides, nitrates, carbonates or the oxides of the corresponding alkali metals, under the flow of argon as well as of oxygen. For the preparation of ternary oxides, various starting materials were well mixed in appropriate stoichiometric ratios. Several methods of syntheses of bronzes are known [90-92]. The bronzes are formed by electrolytic reduction of $\text{A}_2\text{MoO}_4\text{-MoO}_3$ melts [93], or by decomposition of alkali iodide with metal oxide mixtures [94], while the reaction of WO_3 , MoO_3 and V_2O_5 with alcohols or glycols yields hydrogen bronzes [95]. Sol-gel synthesis has also been employed to synthesize tungsten bronzes [96]. But these methods are quite tedious and take about 24 to 160 h for the completion of the reactions. In recent years, a wide variety of inorganic solids have been prepared using microwave irradiation and the reactions have been found to require much shorter reaction times [97-99]. Recently (in 2005), for the synthesis of tungsten bronzes, a green route has been reported by Guo *et al.* [100]. This route is a modification of the route of Rao *et al.* [97,98].

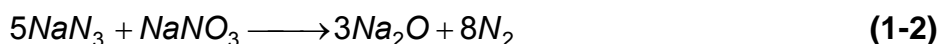
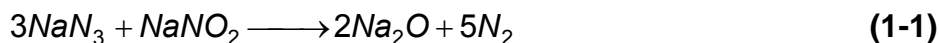
Non-oxide solids or those which contain another anion apart from oxide include nitrides, sulphides, carbides and the intermediate oxynitrides and oxysulphides. Transition metal carbides, nitrides and oxynitrides have considerable attention during the past few years because of their unique physical properties and numerous technological applications. Nitrides containing N^{3-} ion exhibit a wide range of structures and properties somewhat different from those of the more familiar oxides, as the nitrogen atom is less electronegative than oxygen. Not more than one

compound in the field of ternary nitride system, Na_3MN_3 (M= Mo or W) is known [101]. Oxynitrides offer a chance to explore the region between oxides and the more covalent nitrides. The interesting fundamental and technological properties of oxides and nitrides [102,103] have led to a recent upsurge of interest in the synthesis of mixed anion oxynitride solids [104].

The possibilities for property enhancement arising from the development of this synthetic chemistry are illustrated by the new oxynitrides, CaTaO_2N and LaTaO_2N red pigments [105]. New applications in catalysis for oxynitrides have been found. It is now considered to control the acidic–basic properties of a catalyst for successful applications. Galloaluminophosphate oxynitrides [106] and Zirconophosphate oxynitrides [107,108] offer this possibility. Adjusting the nitrogen content of the oxynitrides allow to tune their acidic–basic properties. With the increasing nitrogen content, their surface basicity increases. Non-oxide materials are less stable than oxides and therefore their preparation has to be carried out using synthetic techniques different from the conventional ones used to prepare oxides. The use of oxide precursors has been well renowned as an experimentally simple and inexpensive method for the synthesis of a wide variety of nitride and oxynitride products. Oxynitrides are produced by incorporation of nitrogen. Oxynitrides, in general were prepared by the ammonolysis of the respective ternary metal oxide precursors. There are many reports in the literature on the preparation of oxynitrides by heating ternary oxides along with alkali nitrites or alkali hydroxides under the flow of ammonia gas [109]. Although, tetrahedral oxide nitride anions are well established for the second and third transition series e.g. $\text{OsO}_3\text{N}^{3-}$, $\text{ReO}_3\text{N}^{2-}$, WO_3N^{3-} [110-112], while the $\text{MoO}_3\text{N}^{3-}$ ion is not yet known. Only a few oxynitrides of molybdenum and tungsten compounds are reported. The molybdenum oxynitrides are always isostructural to the corresponding compounds of tungsten. In most of the oxynitrides, the transition metals are fully oxidized and hence these compounds are usually insulating.

The alkali oxides are the strongest oxide bases available and are used in the synthesis of ternary oxides. Hoppe *et al.* has revealed that cations in such ternary

alkali oxometallates exhibit an extraordinary and wide variety of valence (common oxidation state to unusual oxidation state of the central metal atom). Few compounds which come under this category, are $K_6Co_2O_7$ [113], K_3FeO_2 [114], Cs_3AuO [115], $KCoO_2$ [116] etc. However the synthesis of these compounds is rather tedious and complicated. The new technique so called “azide–nitrate/nitrite route” provides a facile access for synthesizing such kind of oxides. This route is applicable to prepare alkali oxometallates and it is based on the reaction of sodium azide with sodium nitrate or sodium nitrite, first described by Zintl *et al.* [117]. The following equations explain how the reaction proceeds.



The reaction proceeds in a controlled manner only if the heating rate is slow. Rapid heating of the reactants may end up with an explosion. Thus for synthesis of alkali oxometallates, oxides of the transition metal were mixed along with azide-nitrate mixtures and the reactions were performed in sealed containers. In our group, many alkali oxocobaltate such as $Na_9Co_2O_7$ [118], $Na_6Co_2O_6$ [119], and $Rb_2Co_2O_3$ [120] and alkali oxocuprate namely Na_3CuO_2 [121] and $Na_3Cu_2O_4$ [121] were prepared by using this azide-nitrate route. Details about the container and reaction procedures are explained in Chapter 2 (under 2.2 subheading).

Scope of the present investigation/Motivation for the present work

Several reasons could be attributed as motivating factor to carry out the present investigation, namely;

- Alkali oxometallates is a well established field and in particular, alkali bronzes. Very few +6 oxidation compounds of molybdenum are known. The scope of this present thesis is to synthesize and characterize new alkali molybdenum oxides in which the molybdenum exhibits usual oxidation state of +6.
- The syntheses of these alkali oxometallates of the transition metals is quite complex. At first, the alkali metals are prepared and they are converted to oxides, peroxides or hyperoxides by reacting them with molecular oxygen. All the work procedures are accomplished in the inert gas atmosphere. The whole process is tedious and so we have tried to adopt a new technique to synthesize molybdates/tungstates. The recent development of the azide-nitrate/nitrite route makes the synthesis process easy as the starting materials are handled in the room atmosphere. So, in the present thesis, we have employed the azide nitrate route for preparing molybdates and tungstates in which molybdenum and tungsten are fully oxidized.
- Many oxynitrides have been prepared by gas-solid reactions. Solid state reactions are commonly used for synthesizing oxides of several transition metals. As this method is simple in comparison to gas-solid reactions, one can think about using solid state reactions for preparing such oxynitrides. The present work deals with the implementation of solid state technique for synthesizing the oxynitrides of transition metals.
- Many alkali molybdenum oxides are known. The chemistry of non-oxide compounds is very much less explored and represents a promising area for the discovery of new materials with interesting properties. The effect of substitution in the anion sublattice of alkali molybdenum oxides has not been studied effectively. The area of alkali molybdenum oxynitride is not well

explored. In order to explore this area and to synthesize new oxynitrides, the following research work has been done.

- The crystal structures of some molybdenum oxides have not been solved yet. Hence, the characterization of those oxides seems to be an important task, so that one can understand more about the material. The aim of this present work is to synthesize and characterize these materials.
- Though ternary tungsten oxides/bronzes have many interesting properties, less has been studied about the mixed alkali tungsten oxides (quaternary systems) while some mixed alkali molybdenum oxides are already reported. This work is also performed to discover new mixed alkali tungsten oxides.

2. Chapter-2

2.1 Equipments and Work Techniques

Since most of the alkali oxometallates compounds obtained from the reactions are extremely sensitive to humidity and/or oxygen, handling of these materials under inert atmosphere becomes important. For these purposes, a glass apparatus is specially designed in which the flow of argon is continuously maintained. The sensitive compounds obtained as reaction products were handled in the glass apparatus which are mentioned in this chapter or they can be handled in a glove box. For most of the reactions, the reactants itself were more sensitive to moisture and/or oxygen. In such cases, the reaction mixtures were prepared in the glove box, where grinding and pelleting of the reactants were carried out under inert atmosphere.

2.1.1 Working under Inert Atmosphere

2.1.1.1 Vacuum and Inert Gas Glass Apparatus

This apparatus can be either filled with argon or oxygen. Argon was supplied by the low temperature service department (Max-Planck-Institute, Stuttgart, Germany) through copper tubes. Before using the argon, the gas was passed through four drying towers, which contain successively blue gel, potassium hydroxide, molecular sieve (mesh size 3 Å) and phosphorous pentoxide on an inert substrate (Sicapent, Merck). This arrangement removes humidity traces from the inert gas argon. The rate of argon flow can be controlled and can be visualized by using a flow control. The apparatus shown in figure 2-1 was made from Duran glass, attached to a rotary valve oil pump (Type: RD4, Vacuubrand). The quality of vacuum was controlled by a Pirani manometer (Thermovac TM 20, Leybold) with the measuring range 10^{-3} - 10^3 mbar. To search for the leakage in the glass tubes, a high frequency vacuum examiner (VP 201, G. Lauer) was used. Glass apparatus were connected by L-

shaped angled glasses. Equipments that were connected by glass spirals or angled glasses can be evacuated and flooded with argon by opening the valve to which it has been attached. The joints are usually sealed with silicone grease (Wacker).

Before using the necessary glass wares, they were subjected to heating under vacuum with the flame of a natural gas burner. Then the setup was immediately rinsed with thoroughly dried argon. The process of evacuating, heating and refilling with argon was repeated for 3 times to ensure that the apparatus was completely dried and cleaned.

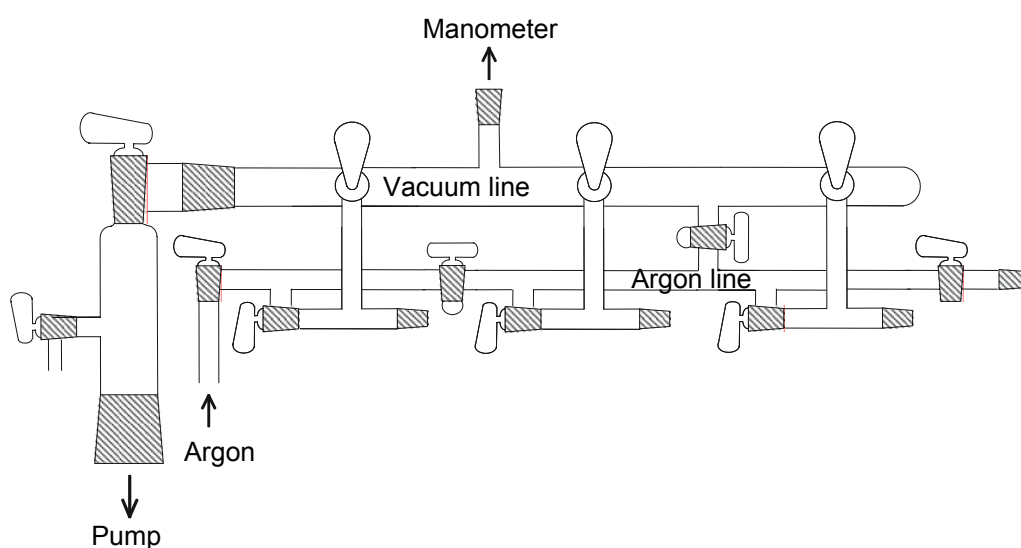


Figure 2-1: Vacuum and argon line system for handling air/moisture sensitive compounds.

The most important work on inert conditions was accomplished by using the apparatus shown in figure 2-2 or the drying pipes (Figure 2-3). These are based on the technology developed by Schlenk [122] for the handling of sensitive substances. This equipment favors the homogenization of the substances present in it by crushing them to powder using a dried glass rod. This glass apparatus also privileges the filling of glass capillaries of various diameters with the substances (under the flow of argon), which are further used for having the radiographs. The sealing of remaining substances in small glass ampoules (5-10 mm in diameter) is also possible by this setup.

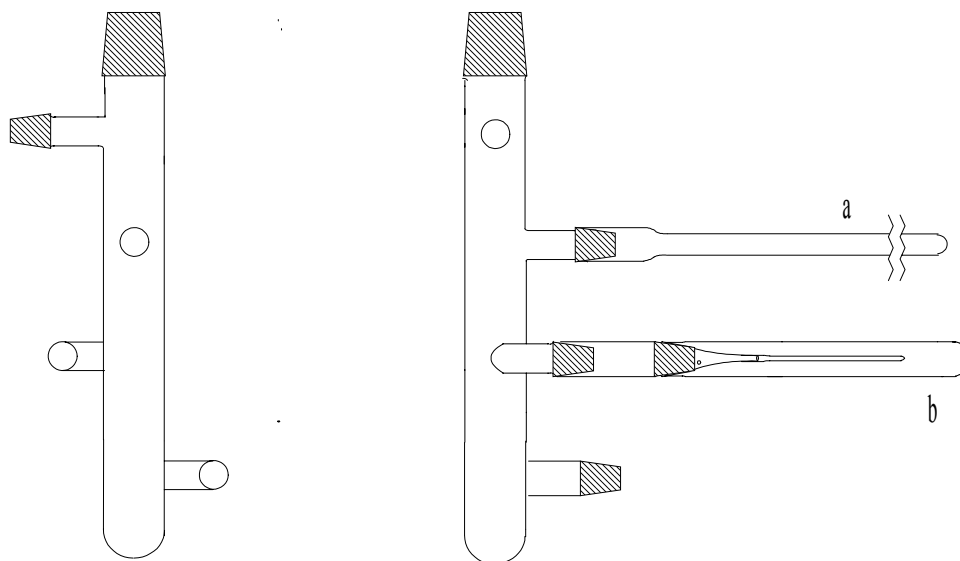


Figure 2-2: Schlenk apparatus (upper cross sections: LV of 29, remaining cross sections LV 14.5) (a) Ampoules sealing part, (b) Capillary filling part.

If the reaction mixtures are to be dried, one uses the drying pipes (Figure 2-3) under vacuum. All the work was generally performed under the flow of dried argon when these apparatus was open.

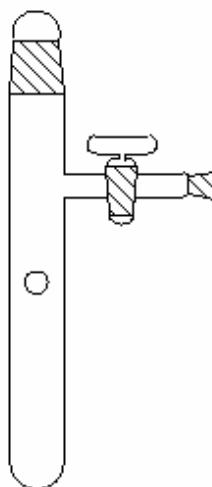


Figure 2-3: Drying tube (upper cross sections: LV of 29, remaining cross sections LV 14.5).

2.1.1.2 Glove Box

The glove box apparatus is normally used for picking single crystals, preparing KBr pellets for infrared (IR) spectroscopy and also for preparing the reaction mixtures when the reactants are sensitive to moisture and/or oxygen. Pellets of such reaction mixture can also be pressed inside the glove box. These things are not possible with the inert gas setup shown in figure 2-1 while they can be mastered in the glove box compartment (MT 200 - M. Braun). The cleaning of the inert gas is done by passing it over the molecular sieve. The quality of the inert gas can be judged over gas analyzers. The water content inside the glove box compartment is maintained below 0.2 ppm and the oxygen content below 0.5 ppm. Apparatus or samples can be taken inside or outside the glove box compartment through airtight evacuation chambers (big and small). The big chamber is evacuated for about 15 minutes and then filled with argon. The process of evacuation and refilling with argon is repeated for two more times to make sure that the atmosphere inside the chamber is completely inert. Same process is repeated with the small evacuation chamber with the evacuation time of about 3 minutes.

2.1.2 Azide-Nitrate/Nitrite Route

Azide-Nitrate route is a very promising route to synthesize ternary oxides and nitrides of alkali metals. In all the cases, the experimental procedure remains the same. The weighed reactants: alkali metal azide, nitrate, nitrite or even peroxide is blended carefully with the oxides of the metals. Then they were finely ground in a ball-mill, pressed as a pellet (6-13 mm diameter) under 10^5 N, dried under vacuum (10^{-3} mbar) at 150 °C for 10-20 h, and placed under argon in a tightly closed steel container provided with a silver/molybdenum inlay. This reaction crucible is shown in figure 2-4.

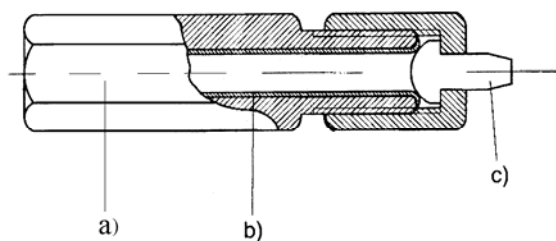
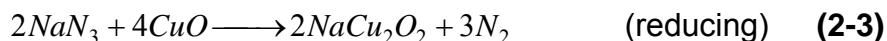
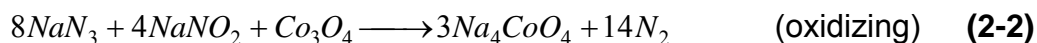
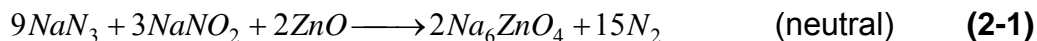


Figure 2-4: Reaction crucible. (a) Crucible (hexagonal, steel 9S29-K), (b) Inlays (Mo, Ag), (c) Inlay lid (Mo, Ag).

Special temperature regime was applied for the reactants that are kept in the crucibles. Rapid heating of the mixture may cause some explosion as the nitrogen pressure shoots up inside the crucible because of presence of azide in it. It was found to be safe when the temperature was increased at the rate of 5 °C/h till the decomposition of the corresponding alkali azide. After the decomposition of the azide, the rate of temperature can be varied.

Silver inlays can be used for the reactions in which the final temperature does not exceed 700 °C. Above this temperature, there may be a possibility of these silver inlays getting damaged. Molybdenum or platinum crucibles were used for carrying out the reactions above 700 °C.

The main advantage of this route is the simplification of the preparative work and wide variety of systems that can be tackled. In addition to the acid-base reactions, it is possible to perform redox reactions with simultaneous reduction or oxidation of the counter cation which is as shown in the following equations.



Exploration of oxides, bronzes and oxynitrides by using a novel method “Azide-Nitrite/Nitrate route” makes the synthesis easy and also seems to be very promising with other transition elements such as Co, Ti, Mo, W, Zn, Ni and Cu [123].

2.1.3 Crystal Growing

Crystals were grown by annealing pressed pellets of powder sample sealed in silver crucibles designed for annealing. (For the air sensitive sample, pellets were prepared inside the glove box). This silver crucible was then transferred into a quartz tube, which was melted further in the form of ampoules under the flow of argon. It was then annealed between 400 and 2000 h at a selected temperature. Suitable crystals were separated in the glove box compartment under the microscope using a 0.1 mm sharp edged glass capillary and inserted into a 0.3 mm capillary, which is then sealed under dry argon.

2.2 Analyzing Techniques

2.2.1 Powder X-ray Diffraction

The radiographic investigations of the sample have now become automatic. The X-ray investigation of the powder sample was performed on a STOE Stadi P diffractometer at room temperature using a position sensitive detector and a curved germanium monochromator in Debye-Scherrer geometry (for air sensitive substances) or transmission geometry (for air insensitive substances). This diffractometer is equipped with a copper anode with Cu-K $_{\alpha 1}$ radiation ($\lambda = 1.5406 \text{ \AA}$) and possesses three detectors with different resolutions and different angle ranges:

- a) Curved PSD1 [(Position Sensitive Detector), angle range 35° , $\Delta 2\theta$ resolution = 0.15°]
- b) Linear PSD2 [angle range 6° , $\Delta 2\theta$ resolution = 0.08°], and
- c) IP-PSD [(Image Plate Position Sensitive Detector), angle range 140° , $\Delta 2\theta$ resolution = 0.10°]

The second diffractometer is equipped with Co anode ($\lambda = 1.7890 \text{ \AA}$) and/or Mo anode ($\lambda = 0.7093 \text{ \AA}$) and possesses two detectors: a curved PSD1 and a linear PSD2. This equipment was used for obtaining the X-ray diffraction pattern for the

powders containing elements like Co, Nb and W etc. Because of the higher intensities with the same exposure time, PSD1 and IP-PSD are particularly suitable for the fast routine measurements, i.e. for the phase analyses of the samples. The PSD2 is used for the precision measurements. Here, elementary silicon (cubic, $Fd\bar{3}m$, $a = 543.08(8)$ pm) serves as an external standard for the correction of 2θ values. The obtained powder X-ray pattern was analyzed by using the software provided by STOE [124]. The products were identified by comparing them with the well known substances, whose crystallographic data are provided by the data base bank (e.g. PCPDFWIN [125]). Air sensitive samples were sealed in the glass capillaries whose outside diameter is 0.1 and 0.3 mm respectively (glass number: 14, Hilgenberg). Air insensitive compounds were stuck by means of silicone grease on plastic foils for the recording of the radiographs.

2.2.2 Heating-Guinier Method

This measurement was done for the samples that are expected to undergo phase transitions as a function of temperature. Such transitions as well as decompose reactions were monitored using the Guinier-Chamber (FR553, Enraf-Nonius). Temperatures between room temperature and 1100 °C can be achieved by blowing hot air, and samples can be measured between these regions. Powder samples were melted in glass/quartz capillaries (outer diameter ranges between 0.1 and 0.5 mm) under argon. For the temperature above 350 °C, quartz capillaries are preferred and glass capillaries were used for the temperature within the range of RT to 350 °C. The photographs/X-ray radiographs were made both continuously and also at regular intervals of temperature. Silicon serves as an external standard for the correction of 2θ values. The data collection took place on the image plates and were further processed and analyzed by using the software AIDA (Version 2.1).

2.2.3 Structure Solution and Refinement from Powder Diffraction

Scattering of the powder samples gives one-dimensional projections of the reciprocal lattice. Because of the limited resolution of the involved detectors at the

recording of powder patterns, the information about the intensity of some reflections can be lost due to the overlapping of closely situated reflections. The overlapping of symmetrically non-equivalent reflections occurs particularly in the structures with low symmetry or with large lattice constants. Owing to this, methods of structure refinement that are ground on the calculation of structure factors based on powder data intensities are usually not used for solution of complex structures. However, if a structure model exists, the problem of overlapping of reflections can be circumvented by a method developed by Rietveld [126,127]. This procedure is suitable for neutron, synchrotron and X-ray powder data. Here, not only the integrated intensities, but also the single data points of the measurement are used in the calculations. The refinement is based on the variation of profile parameters, background coefficients and structure parameters with the least squares method until the calculated profile matches with the observed powder pattern as exact as possible. In this work, the program FullProf [128,129] was used for the *Rietveld* refinement of X-ray data. Structure models can be found with the program Endeavour [130,131] (Crystal Impact) by a combined optimization (Pareto optimization [132]). By using this program, the difference between calculated and measured powder diffractogram as well as the potential energy of the considered systems were optimized. The combined cost function, C , [131] was calculated by

$$C = \alpha E_{pot} + (1 - \alpha) R_B \quad (2-4)$$

Where E_{pot} is the potential energy of the atomic arrangement, R_B denotes R -Values frequently used for the comparison of calculated and experimental diffraction patterns and α is the Pareto parameter which weights the contributions of the two parts of the cost function.

2.2.4 X-ray Diffraction on Single Crystals

2.2.4.1 Precession Technique

In this method, a crystal has to be initially fixed and then adjusted on the precession camera goniometer in a way that a reciprocal crystal axis is oriented parallel to the

rotation axis of the camera. A constant orientation of the crystal relative to the film plane during the precession round the X-ray beam is achieved by a mechanical coupling. By this way one can obtain an undistorted image of the reciprocal lattice. By taking several layers, it is possible to determine metric, type of lattice (integral extinction), and diffraction symbol (serial and zonal extinction) of the compound, definitely. For the measurements Mo-K α radiation ($\lambda = 0.7107 \text{ \AA}$, zirconium filter) was applied. An image plate system was used for data collection.

2.2.4.2 Four and Three Axes Diffractometers

For collecting single crystal intensities, an automatic four axes diffractometer with Euler geometry (STADI4, STOE), a three axes diffractometer with a CCD detector (AXS, Bruker), and a STOE Imaging Plate diffractometer (IPDS-2) were used. A fine focusing tube with Mo anode ($\lambda = 0.71073 \text{ \AA}$) served as a X-ray radiation source. The radiation was monochromatized by using a graphite monochromator. The controlling, data processing and backup of the diffractometer was performed by computer-assisted tools/programs [133].

Direct methods were used for the structure solutions (SHELXS-97 [134]). The refinement of the obtained structure model was carried out using the method of least squares by the SHELXL-97 [135] program.

2.2.5 Thermal Analysis

The thermal analysis comprises the methods, by which physical and/or chemical properties of a substance are measured as a function of temperature. In this work thermogravimetric analysis (TGA), differential thermal analysis (DTA), and differential scanning calorimetry (DSC) were used. TGA and DTA curves were measured simultaneously on a STA 429 thermal analysis device (Netzsch). Using a Skimmer coupling (Netzsch) the volatile decomposition products can be directed to a quadruple mass spectrometer (QMS 421, Balzers) and their mass up to 1024 m/e can be measured.

A differential scanning calorimeter (DTA 404, Netzsch) equipped with a NiCr/NiCu-thermoelement (type E, Argon) was used. As a sample holder, cylindrical Pt/Rh/Al crucibles (external diameter 7 mm, height 2.5 mm) with lid were applied.

2.2.6 Measurement of the Specific Heat

For the measurement of the specific heat, the samples were taken in cylindrical Al crucibles which are sealed by using a Al lid. The measurements were carried out in a PPMS device (Quantum Design).

2.2.7 IR-Spectroscopy

IR spectra were obtained using a Fourier transformation spectrometer IFS 113v (Bruker) equipped with vacuum optic and Genzel interferometer. A silicon carbide globar as the radiation source and a DTGS detector (**d**euterated **t**riglycine **s**ulphate) for the detection were applied. The resolution of the spectra is 2 cm^{-1} for this measurement. The samples for the measurements were prepared in form of pellets (ca. 1 mg substance to 500 mg KBr).

2.2.8 Measurements of Electrical Properties

In general, the total conductivity of a solid sample contains of anionic, cationic and electronic parts. The ionic conductivity can be calculated by subtracting electronic conductivity from the total one. The conductivity measuring device allows the alternate recording of DC (for ion blocking but electron conducting electrodes: electronic conductivity) or AC (total conductivity) data in the temperature range up to $700\text{ }^{\circ}\text{C}$. The program Sigma-Messung [136] was used for a central computer-assisted controlling of all the components. An impedance analyzer (HP 4192A LF, Hewlett-Packard) generates the AC voltages of 5 Hz to 10 MHz needed for recording impedance spectra.

A programmable DC voltage source (TR 6142, Advantest Corporation) was used for collecting DC conductivity data. The current was measured by a digital multimeter

(195 A, Keithley) serving as a serial switched ampere meter. The voltage was measured by another digital multimeter (HM 8112-2, Hameg Instruments) which was parallelly switched as a voltmeter.

The measuring cell [137] consists of a quartz tube provided with openings for an electrode arrangement, gas flow connection, and quartz duct for thermoelements. The screened lines were connected inside the cell by the platinum wires to the platinum electrodes, between which the sample is located. For carrying out the temperature dependent measurements, the measuring cell was put into a furnace. The furnace temperature was measured using a Ni/Cr-Ni thermoelement and controlled by a computer. The measuring cell can be evacuated by a rotation pump (pKD 4, Saskia, Saugleistung 3.7 m³/h) and can be filled with dried argon. The samples were pressed in the form of pellets (0.35 GPa, diameter 6 mm, height ca. 0.5 mm). The data processing was performed by the program Sigma-Auswertung [136].

For the measurement of the specific resistance in the temperature range of 2-300 K, among four points method a self constructed device (Chemical service, MPI FKF Stuttgart) was applied. The sample was cooled in a cryostat (Keithley). The current was measured using a digital multimeter (Kryovac, Keithley) and the voltage using a nano voltmeter (HP 4208, Hewlett Packard).

2.2.9 Measurements of Magnetic Properties

The temperature dependence of the magnetic susceptibility was measured on a SQUID magnetometer (Superconducting Quantum Interference device) MPMS 5.5, (Company: Quantum Design, San Diego, CA, USA). This device allows investigations in the temperature range of 1.7-800 K in a homogeneous magnetic field up to 7 T. The samples were sealed in ampoules in super pure quartz under helium atmosphere. Diamagnetic correction was applied using tabulated values [138]. The representation of the results measured and data matching for different models were performed using Microcalc Origin [139] program.

3. Chapter-3

3.1 Alkali Oxynitrides of Molybdenum

There are plenty of reports in the literature on the preparation of ternary nitrides or oxynitrides from ternary oxides and ammonia gas [140-142]. These new materials have been studied to determine the presence of order or disorder in the anionic sites [143], to understand their dielectric properties [144] and to compare the electrical properties of reduced oxynitrides to reduced oxides [145]. Among these, a few oxynitrides of molybdenum and tungsten compounds were reported. Jacobs and Pinkowski (1993) [146] synthesized many ternary nitrides by reacting the oxides of the metal with the corresponding alkali amide in autoclaves. To synthesize the oxynitride of Mo and W, they adopted the same technique of reacting the oxides of Mo or W (MoO_3 and WO_3) with an excess of NaNH_2 in autoclaves at the temperature ranging from 250 °C to 750 °C. In 1994, S. H. Elder and F. J. DiSalvo synthesized and characterized a new oxynitride compound of tungsten, $\text{Na}_3\text{WO}_3\text{N}$ [147]. This compound was first synthesized by heating Na_2WO_4 in an alumina boat from room temperature to 700 °C and holding at this temperature for 12 h in a flow of NH_3 gas. In order to avoid the presence of impurities such as (W_2N), a small amount of Na_2O was added to get the pure yellow compound, $\text{Na}_3\text{WO}_3\text{N}$. The structure of this compound is based on an ordered wurtzite superlattice. Locating the atomic positions of nitrogen and oxygen with X-ray diffraction will be a difficult task because of the small X-ray scattering factors of these atoms compared to that of tungsten. So, neutron powder diffraction experiments were performed and with the help of it, the order and disorder of nitrogen and oxygen was found. So far, only two alkali oxynitride compounds of molybdenum $\text{Na}_4\text{Mo}(\text{O},\text{N})_4$ and $\text{Na}_4(\text{MoO}_2\text{N}_2)$ [148] have been reported. These compounds were prepared by the reaction of MoO_3 and NaNH_2 in autoclaves. Commonly, oxynitrides are accessible by nitridation of different composition of oxide precursors in flowing NH_3 for various times in various temperature ranges [149-151]. The incorporation of alkali metal is achieved either by

using alkali metal monoxide (A_2O), alkali hydroxide $[A(OH)]$ or alkali carbonates (A_2CO_3) as a starting material along with other reactants. General preparation methods for this class of compounds were given in references [148-152]. Among these, the most versatile route seems to be the reaction between the metal oxides, and oxides, hydroxides or amides of alkali metals under a flow of N_2 or NH_3 . The use of oxide precursors has been well known as an experimentally simple and inexpensive method to the synthesis of nitrides and oxynitrides.

The oxidation state of the molybdenum atom in the known alkali oxynitrides is found to be +6 as this state is more stable than any other possible oxidation states.

Many oxynitrides are obtained by the reaction of MO_3 ($M= Mo, W$) with the corresponding alkali metal amide and liquid ammonia in between the temperature range between 500 °C and 600 °C. The reactions were carried out in autoclaves for salt melts in order to prevent the earlier decomposition of ANH_2 to A , N_2 and H_2 . Now two new compounds in the system $Na/Mo/O/N$ are found, their synthesis and characterization are reported here.

3.2 Synthesis and Structure of Na_3MoO_3N

3.2.1 Synthesis

The new oxynitride compound of molybdenum, Na_3MoO_3N was prepared via the azide route from the solid state reaction between MoO_3 (Merck 99.5 %) and NaN_3 (Aldrich 99.5 %). The reactants were initially dried under vacuum for about 15 h. Then they are sealed in a glass tube in the form of small ampoules. The dried starting materials, MoO_3 and NaN_3 were mixed in the ratio of 1:4. Then they were ground in a ball-mill, pressed as a pellet under 10^5 N, dried under vacuum (10^{-3} mbar) at 150 °C for 12 h, and placed under argon in a tightly closed steel container provided with a silver inlay. In a flow of dry argon, the following temperature treatment was applied: 25 °C \rightarrow 260 °C (150 °C/h) \rightarrow 380 °C (5 °C/h) \rightarrow 650 °C (70 °C/h, 72 h) \rightarrow 30 °C (80 °C/h).

The obtained colorless hygroscopic product was sealed in glass ampoules under argon and kept for further investigations. All the analyses have been performed in an atmosphere of dry argon.

3.2.2 Thermal Analysis

The thermal behavior of the sample, $\text{Na}_3\text{MoO}_3\text{N}$ was investigated by using the device DTA/TGA (STA 409, Netzsch, Selb) coupled with a quadruple mass spectrometer. The sample was heated at the rate of $10\text{ }^\circ\text{C}/\text{min}$ in a corundum crucible under a flow of dry argon. The oxynitride decomposes at around $850\text{ }^\circ\text{C}$ to form Na_2MoO_4 as the sole solid residue.

3.2.3 Powder Diffraction Analysis

X-ray powder diffraction analysis of $\text{Na}_3\text{MoO}_3\text{N}$ was effected on a STOE StadiP diffractometer with $\text{Cu-K}_{\alpha 1}$ radiation ($\lambda = 1.5406\text{ \AA}$) at room temperature using a position sensitive detector (angle range 6°) and a curved monochromator in Debye-Scherrer geometry. The powder diffraction data were collected in the 2θ range of 5 and 90° . The sample was stored under argon in a 0.3 mm capillary. Silicon (cubic, $Fd\bar{3}m$, $a = 5.43.08(8)\text{ \AA}$) was used as an external standard. The orthorhombic indexing ($a = 7.2463(1)\text{ \AA}$, $b = 6.2498(1)\text{ \AA}$, $c = 5.6386(1)\text{ \AA}$) was performed with the program WinXPOW [153]. A small amount of metallic silver, which derives from the container inlay, can be detected in the diffraction pattern and was considered in the refinement.

$\text{Na}_3\text{MoO}_3\text{N}$ is a lower symmetry derivative of the Cu_3AsS_4 [154] structure, which can be derived from the well-known wurtzite type of structure as aristotype. The XRD pattern is similar to the tungsten analogue, $\text{Na}_3\text{WO}_3\text{N}$ [147], and the new oxynitride is isostructural to $\text{Na}_3\text{WO}_3\text{N}$.

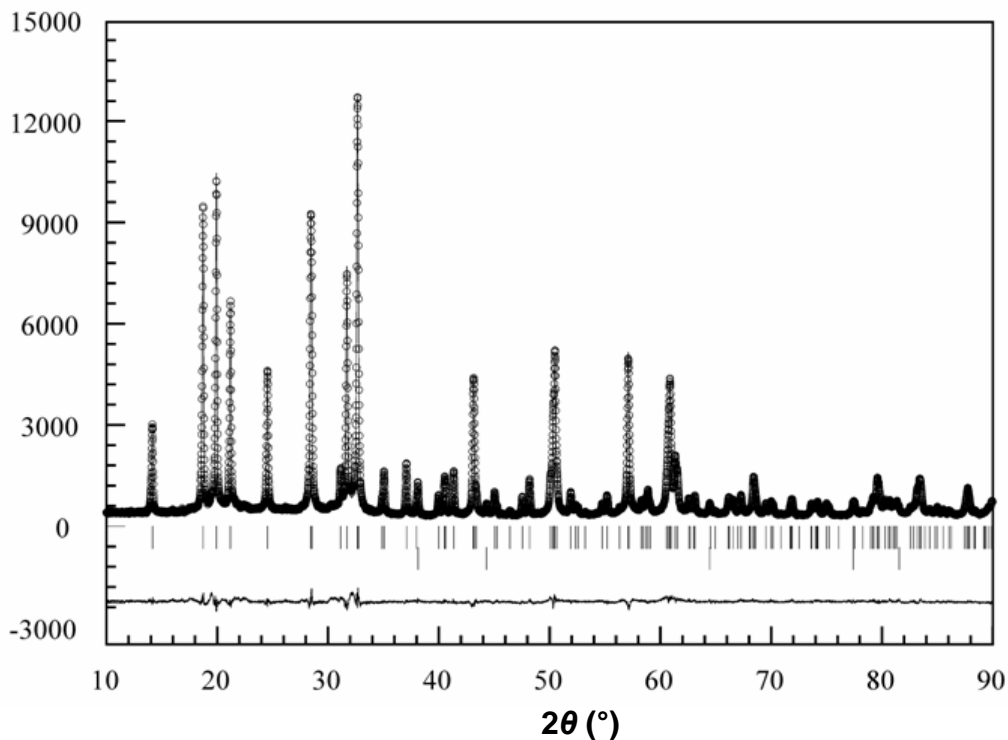


Figure 3-1: *Rietveld*-plot of $\text{Na}_3\text{MoO}_3\text{N}$. Shown is the observed pattern (circles), the best *Rietveld* plot (line), the Bragg Positions of $\text{Na}_3\text{MoO}_3\text{N}$ and Ag and the difference plot (Ag was used as a container material and is observed in a very small amount in the powder pattern and hence considered in the refinement).

Both oxynitride compounds of tungsten and molybdenum crystallize orthorhombic in the acentric space group $Pmn2_1$ which has been confirmed by SHG measurements (explained in detail in § 3.2.5). As a starting model for the *Rietveld* refinement, the atomic co-ordinates of the iso-structural compound, $\text{Na}_3\text{WO}_3\text{N}$, were used. The refinement was performed with the program FullProf [128]. Figure 3-1 shows the *Rietveld* fit of the XRD pattern of the sample. Details of the crystal data and refinement are given in table 3-1. In table 3-2, the atomic co-ordinates and the isotropic displacement parameters are listed. The displacement parameters for both sodium sites are constrained to be equal and the same is with the three anionic sites.

Table 3-1: Crystallographic data and Structure Refinement of Na₃MoO₃N.

Empirical Formula	Na ₃ MoO ₃ N
Formula weight /g mol ⁻¹	226.9143
Crystal system	Orthorhombic
Space group	<i>Pmn</i> 2 ₁ (No. 31)
Lattice parameters /Å	<i>a</i> = 7.2463(1) <i>b</i> = 6.2498(1) <i>c</i> = 5.6386(1)
Cell Volume /Å ³	255.36(7)
Z	2
Density calc. /g·cm ⁻³	2.951
X-rays/ Monochromator	Cu-K _{α1} / Germanium
Temperature /K	295
2θ range /°	4.985 to 89.965
No. of data points	8500
No. of reflections	134
No. of constrains / restrains	0
Refined parameters	29
R-Values	<i>R_p</i> : 9.04 %; <i>R_{wp}</i> : 9.83 %; <i>R_{exp}</i> : 6.25 %

Table 3-2: Positional and isotropic displacement parameters for Na₃MoO₃N.

Atom	Site	<i>x</i>	<i>y</i>	<i>z</i>	<i>U</i> _{eq} /pm ²
Mo	2 <i>a</i>	0	0.8257(1)	0	100(2)
Na1	2 <i>a</i>	½	0.8386(5)	0.981(1)	105(5)
Na2	4 <i>b</i>	0.2440(3)	0.3277(4)	0.984(1)	105(5)
O/N1	2 <i>a</i>	0	0.101(1)	0.8975(9)	156(10)
O/N2	2 <i>a</i>	½	0.173(1)	0.8194(8)	156(10)
O/N3	4 <i>b</i>	0.2056(5)	0.6902(7)	0.8975(6)	156(10)

3.2.4 Structural Discussion

The structure can be described as a distorted hexagonal close packing of oxide, together with nitride anions in a ratio of 3:1, with the cations in half of the tetrahedral cavities (Figure 3-2). The cations are ordered, whereas from the X-ray powder diffraction data no ordering can be deduced for nitrogen and oxygen. Because of the small difference in the scattering lengths of nitrogen and oxygen, we were unable to distinguish between fully ordered, fully disordered, or partially ordered anions. As in ZnS, both, the anions and cations are tetrahedrally coordinated. The metal centered tetrahedra are linked via corners in a manner, that the MoO₃N complex anions are isolated and solely linked with NaO₃N tetrahedra. It is clear that NaO₃N tetrahedra chains form an alternate layer, while the other layer is comprised of NaO₃N - MoO₃N tetrahedral chains. Figure 3-3 shows the MoO₃N isolated tetrahedral in the crystal structure and in figure 3-4, a view along *a*- direction shows that all the tetrahedral are pointing in *c*- axis. Molybdenum occupies a twofold site, Na a twofold and fourfold site and the anions occupy two twofold sites and one fourfold site. An ordering of the anions is possible, if the nitride occupies one of the twofold positions which has been explained with MAPLE (explained in detail in § 3.2.6).

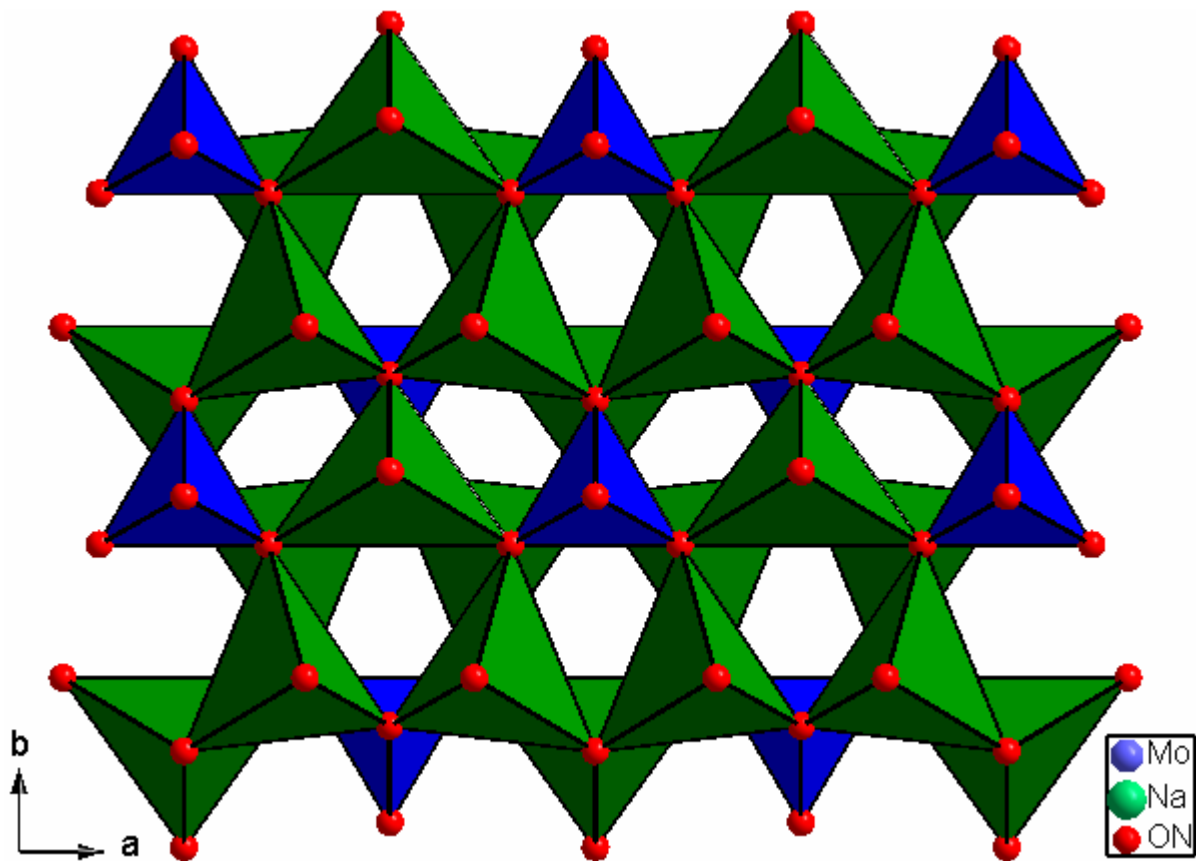


Figure 3-2: A view of a portion of $\text{Na}_3\text{MoO}_3\text{N}$ structure emphasizing the distorted hexagonal lattice network in 001 direction.

Taking into account that commonly N^{3-} -Na distances [155] are shorter than the corresponding O^{2-} -Na distances, the fact that O/N2 (see Table 3-3) exhibit shorter distances to the surrounding sodium cations than the other anions, leads to the assumption that the nitride occupies this site. Furthermore, calculations of the Madelung part of the lattice energy [156,157] shows a maximum for the ordered model with the nitride anion on this 2a site.

Table 3-3: Selected interatomic distances (Å) in Na₃MoO₃N.

Atoms	Atoms	Distance
Na1	O/N1	2.374(9) × 1
	O/N2	2.275(9) × 1
	O/N3	2.377(5) × 2
Na2	O/N1	2.315(5) × 1
	O/N2	2.287(5) × 1
	O/N3	2.364(8) × 1
	O/N3	2.327(6) × 1
Mo	O/N1	1.818(6) × 1
	O/N2	1.810(5) × 1
	O/N3	1.812(4) × 2

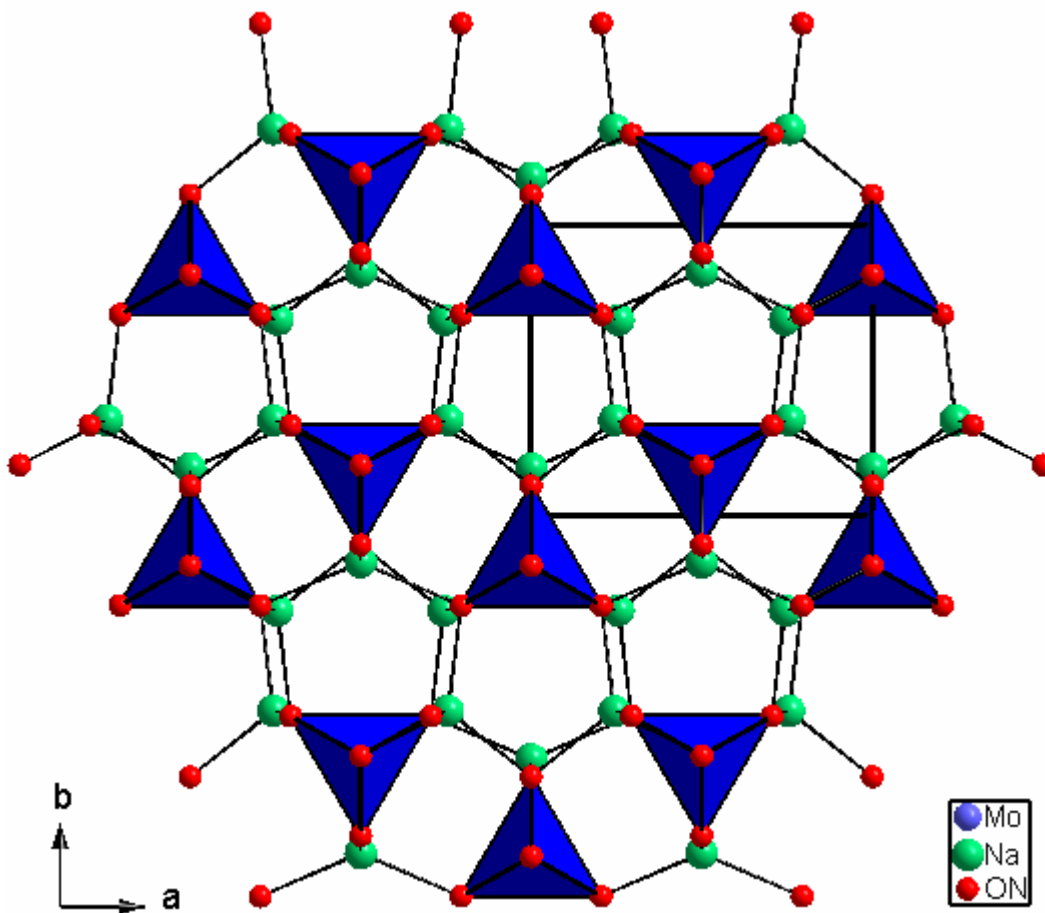


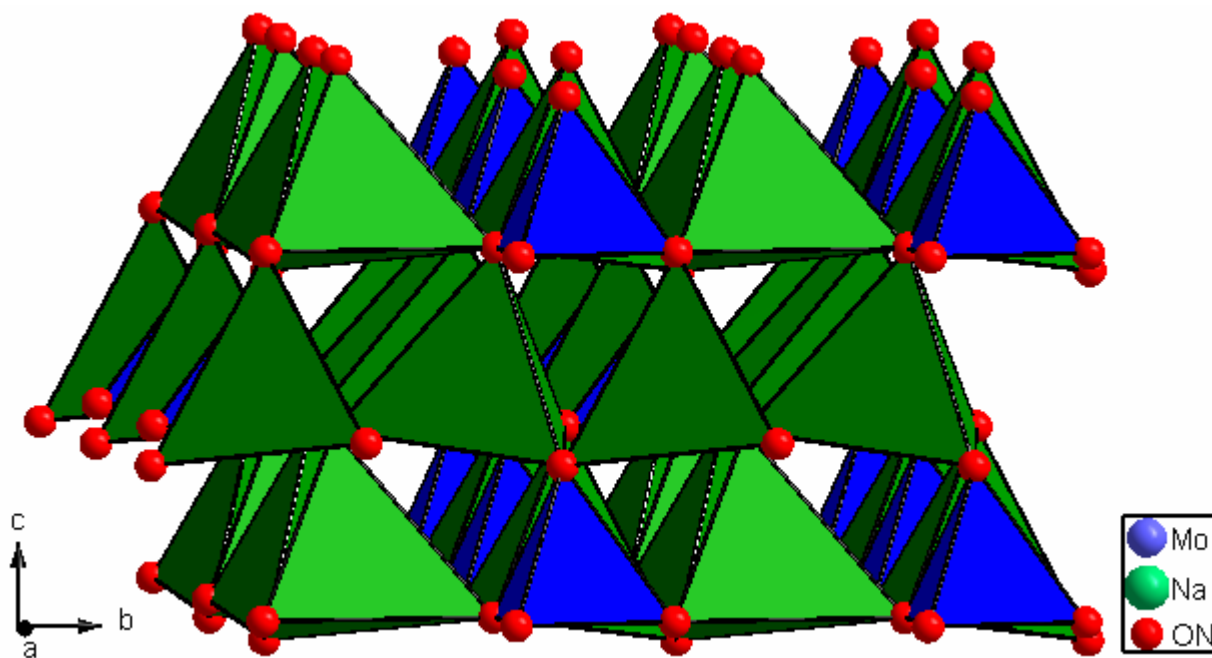
Figure 3-3: Crystal structure of $\text{Na}_3\text{MoO}_3\text{N}$ showing the isolated $[\text{MoO}_3\text{N}]$ tetrahedra.

3.2.5 Second Harmonic Generation

In order to confirm the acentricity of the oxynitride obtained, attempts have been made to observe Second Harmonic Generation, (SHG) [158]. As the source of the fundamental radiation, we used a diode-pumped Nd-YAG laser with the wavelength of $1.06 \mu\text{m}$. The scattered second-harmonic light was analyzed by a double monochromator equipped with photon counting detector system. The acentricity of the sample is confirmed from the qualitative results of SHG, which is shown in table 3-4.

Table 3-4: Second Harmonic Generation of $\text{Na}_3\text{MoO}_3\text{N}$.

Sample	Laser power in arb. Units	SHG from quartz tube in counts per second (cps)	SHG from the sample in counts per second (cps)
1	2.5	7	1.4×10^3
2	4.3	17	4.28×10^3
3	5.9	43	8.85×10^3
4	7.6	67	1.16×10^4
5	8.8	99	1.75×10^4

**Figure 3-4:** Arrangement of all $\text{NaO}_3\text{N-MoO}_3\text{N}$ tetrahedral in the crystal.

3.2.6 MAPLE Calculation

The Madelung part of lattice energy calculation helps us to predict the most probable structure of the oxynitride, $\text{Na}_3\text{MoO}_3\text{N}$. The structure can be explained in two ways; either all the anions are ordered or statistically distributed. Calculations have been done for the two possible structures which are listed below.

1. Nitrogen atoms occupying the $2a$ site while the other $2a$ and $4b$ sites are occupied by oxygen atoms.
2. Both nitrogen and oxygen atom are distributed statistically in all the anionic sites.

Table 3-5 gives the MAPLE* values of the ordered anion structure, and from the table, the coulomb part of lattice energy are calculated by using the formula.

Table 3-5: Atoms, Charge and MAPLE of an individual atom in an ordered structure.

Atom	Charge	Shortest interatomic distances (pm)	MAPLE*
Mo	+6	180.08	112.38
Na1	+1	227.99	155.34
Na2	+1	228.73	158.50
O1	-2	181.77	155.43
N2	-3	180.08	132.61
O3	-2	180.85	154.64

$$\text{MAPLE}^* = \text{MAPLE} / (\text{Charge})^2 \text{ in kcal/mole}$$

Coulomb part of lattice energy = 3785.71 kcal/mol

Coulomb part of lattice energy in kJ/mol is 15844.31

The coulomb part of lattice energy for the case (1) is found to be greater than the coulomb part of the lattice energy for the case (2) which is 3748.61 kcal/mole. The larger the lattice energy, the more stable the structure model should be. So, case (1)

is found to be the most probable structure for this oxynitride. Table 3-6 shows the coordination number of atoms and effective coordination number for this case obtained from the program MAPLE. MEFIR values are also mentioned in the table.

Table 3-6: Coordination number (CN), Effective Coordination Number (ECoN) and Mean Effective Ionic Radii (MEFIR) (Å) for Na₃MoO₃N.

Atoms	CN	ECoN	MEFIR
Mo	4	3.9986	0.40
Na1	4	3.9610	0.95
Na2	4	3.9823	0.92
O1	4	3.9971	1.40
N2	4	3.9902	1.38
O3	4	3.9966	1.41

From the results of MAPLE one can believe that the anions in the structure are ordered. But the results from MAPLE calculations are not enough to prove the order and disorder of the system. So, the question of order/disorder in the anionic sublattice of Na₃MoO₃N is not yet answered unambiguously.

3.3 Synthesis and Structure of Na₅MoO₄N

3.3.1 Synthesis

Na₅MoO₄N was synthesized starting from MoO₂ (Alfa Aesar[®], 99%), Na₂O₂ (Riedel-de Hën, 95%) and NaN₃ (Sigma, 99.5%). The reactants are dried and weighed according to the ratio of 1:1:4. These reactants were mixed together and dried under vacuum (10⁻³ mbar) at 150 °C for 12 h, after they were finely ground and pressed as a pellet (Φ =13 mm) under 10⁵ N. Then they were placed under argon in a tightly closed steel container provided with a Mo inlay. In a flow of dry argon, the following

temperature treatment was applied: 25 °C → 260 °C (20 °C/h) → 380 °C (5 °C/h) → 500 °C (80 °C/h, 48 h) → 30 °C (20 °C/h). The light green crystals obtained were sealed in glass ampoules under argon atmosphere. All the preparation work of the reaction mixture was carried out in the glove box.

3.3.2 Thermal Analyses

The thermal behavior of $\text{Na}_5\text{MoO}_4\text{N}$ was investigated by using the device DTA/TGA (STA 409, Netzsch, Selb) coupled with a quadruple mass spectrometer. The sample was heated at the rate of 10 °C/min in a corundum crucible under a flow of dry argon. According to the TGA/DTA, run in a corundum crucible, the decomposition temperature of the oxynitride was found to be 600 °C. Thermal analyses of this sample did not give us much information about the phase formed. This is because, on the decomposition of the sample, the nitrogen present in it gushes out and blocks the mass spectrometer. In order to identify the phase formed, high temperature X-ray measurement was performed.

3.3.3 Powder Diffraction Analysis

The X-ray investigation on powder was performed on a STOE Stadi P diffractometer with $\text{Cu-K}_{\alpha 1}$ radiation ($\lambda = 1.5406$) at room temperature using a position sensitive detector and a curved germanium monochromator in Debye-Scherrer geometry. The powder diffraction data are given in Table 3-7. Figure 3-5 shows the powder diffraction of the sample obtained at room temperature.

Table 3-7: Powder diffraction data of Na₅MoO₄N (*d* > 150.0 pm).

No.	<i>h</i>	<i>k</i>	<i>l</i>	<i>d</i> (pm)	<i>I</i> / <i>I</i> ₀
1	0	0	2	535.31	33.0
2	2	0	0	492.57	9.1
3	1	1	1	451.88	100.0
4	1	1	2	364.79	5.8
5	2	0	2	362.48	22.7
6	1	1	3	290.16	6.6
7	0	2	0	288.93	4.0
8	3	1	0	285.51	0.8
9	0	2	1	278.95	4.0
10	3	1	1	275.87	18.7
11	0	0	4	267.66	18.5
12	0	2	2	254.26	26.9
13	3	1	2	251.91	37.3
14	2	2	0	249.22	7.4
15	4	0	0	246.29	2.7
16	1	1	4	235.81	3.4
17	2	0	4	235.18	7.3
18	2	2	2	225.94	4.8
19	0	2	3	224.56	8.1
20	4	0	2	223.75	4.3
21	3	1	3	222.94	33.2
22	1	1	5	196.74	2.3
23	0	2	4	196.35	1.4
24	3	1	4	195.27	0.8
25	5	1	0	186.49	0.5

No.	<i>h</i>	<i>k</i>	<i>l</i>	<i>d</i> (pm)	<i>I</i> / <i>I</i> ₀
26	1	3	1	186.16	8.3
27	4	2	1	184.63	3.2
28	5	1	1	183.72	1.2
29	2	2	4	182.39	6.6
30	4	0	4	181.24	13.4
31	0	0	6	178.44	1.3
32	1	3	2	178.25	1.8
33	4	2	2	176.90	7.9
34	0	2	5	172.03	4.6
35	3	1	5	171.30	16.6
36	1	1	6	168.00	0.6
37	2	0	6	167.77	2.4
38	1	3	3	167.05	3.1
39	3	3	0	166.15	11.4
40	5	1	3	165.28	3.0
41	6	0	0	164.20	6.9
42	3	3	1	164.18	1.0
43	3	3	2	158.68	1.4
44	6	0	2	156.98	1.9
45	1	3	4	154.41	3.4
46	4	2	4	153.53	4.2
47	0	2	6	151.82	5.0
48	3	1	6	151.31	5.8
49	3	3	3	150.62	2.5

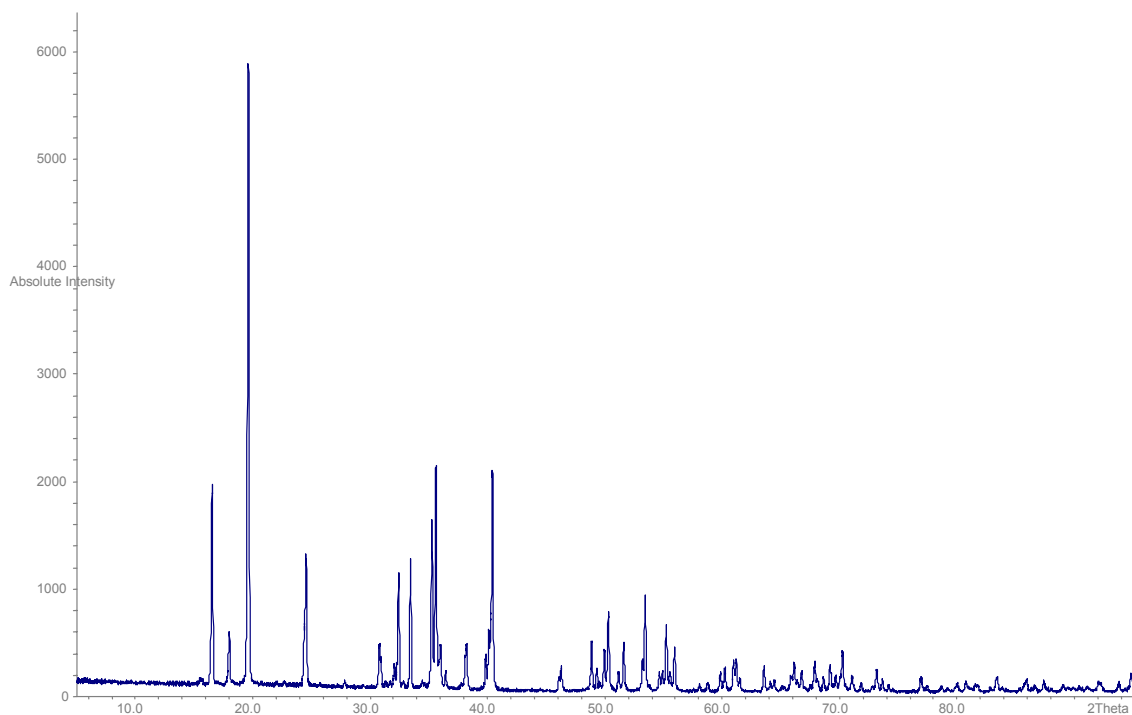


Figure 3-5: Obtained powder diffraction pattern of $\text{Na}_5\text{MoO}_4\text{N}$ with $\text{Cu-K}\alpha_1$ radiation ($\lambda = 1.5406$) at room temperature.

3.3.4 Single Crystal Data

Single crystals of $\text{Na}_5\text{MoO}_4\text{N}$ were picked in the glove box using 0.1 mm glass capillary and are inserted into a 0.3 mm capillary which was then sealed under dry argon. Single crystal diffraction analysis was effected on a STOE STADI 4 diffractometer coupled with a CCD Oxford instrument detector, at room temperature after mounting the crystals. The crystallographic details are given in table 3-8. Table 3-9 contains the atomic co-ordinates and the isotropic displacement parameters, and the anisotropic displacement parameters are listed in table 3-10.

3.3.5 High Temperature X-ray Analysis

High temperature X-ray analysis was also performed on a sample to find out the product obtained at high temperature. From the results of the high temperature X-ray measurements, it follows that the sample decomposes at 300 °C to form $\text{Na}_3\text{MoO}_3\text{N}$ [159], as Na_2O is extracted from the oxynitride while reacting with the quartz capillary during the measurement. High temperature X-ray diffraction pattern is shown in figure 3-6 and the profiles obtained are shown in figure 3-7.

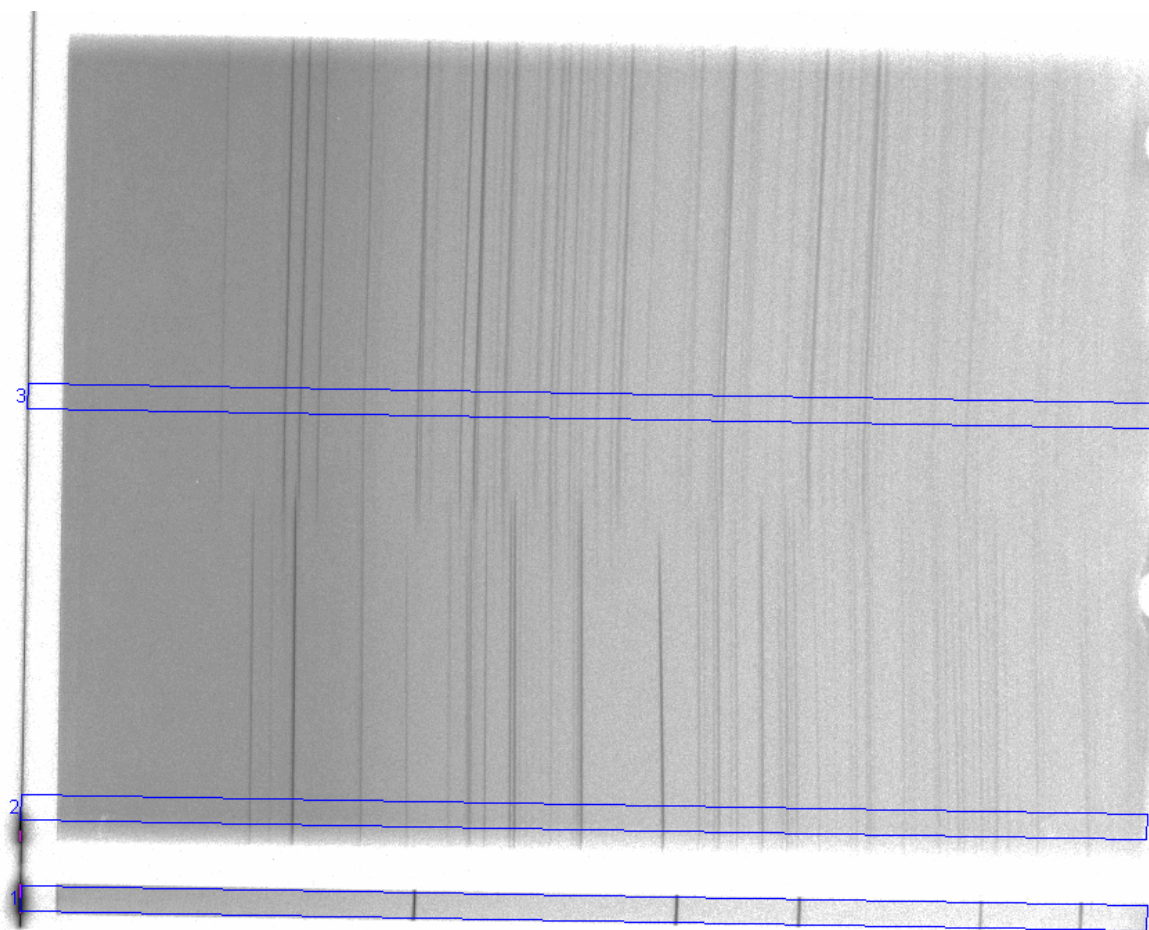


Figure 3-6: HT X-ray pattern of $\text{Na}_5\text{MoO}_4\text{N}$. Region 1 indicates the silicon standard pattern obtained at RT. Region 2 indicates the pattern obtained at around 50 °C. Region 3 indicates the pattern obtained at 480 °C.

Table 3-8: Crystallographic data and structure refinement for Na₅MoO₄N.

Crystal system	Orthorhombic
Space group	<i>Cmcm</i> (No. 63)
Lattice parameters /Å (from X-ray powder data)	<i>a</i> = 9.911(2), <i>b</i> = 5.743(1) <i>c</i> = 10.677(2)
Z	4
Cell Volume /Å ³	607.7(2)
Formula weight /g mol ⁻¹	288.90
Density calc. /mg·m ⁻³	3.158
Crystal color	Light green
Crystal size, mm	0.08 × 0.1 × 0.12
Method of the refinement	Full-matrix least-squares on <i>F</i> ²
Parameters refined	34
<i>R</i> -Values	<i>R</i> ₁ = 0.0157, <i>wR</i> ₂ = 0.0429
Weight	$W = 1/(\sigma^2(F_o^2) + (0.0267 \times P)^2 + 0.57 \times P)$, where $P = (\max(F_o^2, 0) + 2 \times F_c^2)/3$
$\Delta\rho_{\min}, \rho_{\max}$ (e ⁻ /Å ³)	-0.84, 0.54
Diffractometer	STOE STADI 4, CCD Oxford instrument
Monochromator	Graphite
Mo-K _α Radiation, λ	0.71073 Å
2θ range for data collection	4.10 to 36.92°.
Range of <i>h, k, l</i>	-13 ≤ <i>h</i> ≤ 14, -8 ≤ <i>k</i> ≤ 7, -14 ≤ <i>l</i> ≤ 14
Reflections collected	2669
Independent reflections	529 [R(int) = 0.0264]
Absorption coefficient mm ⁻¹	2.455
F(000)	544
Temperature in K	293

Table 3-9: Atomic co-ordinates and isotropic thermal parameters ($\text{pm}^2 \times 10^{-1}$) for Na₅MoO₄N.

Atom	Wyckoff Position	x	y	z	U(eq)
Mo1	4c	0	0.2086(1)	1/4	8(1)
Na1	8e	0.1904(1)	0	0	19(1)
Na2	8g	0.1893(1)	0.6419(2)	1/4	14(1)
Na3	4b	0	1/2	0	33(1)
O	16h	0.1366(1)	0.3030(2)	0.3723(1)	11(1)
N	4c	0	0.0907(5)	1/4	24(1)

Table 3-10: Anisotropic displacement parameters ($\text{pm}^2 \times 10^{-1}$). The anisotropic displacement factor exponent takes the form: $-2\pi^2 [h^2 a \times 2U_{11} + \dots + 2 h k a \times b \times U_{12}]$.

Atoms	U_{11}	U_{22}	U_{33}	U_{23}	U_{13}	U_{12}
Mo1	7(1)	7(1)	10(1)	0	0	0
Na1	23(1)	16(1)	18(1)	-6(1)	0	0
Na2	13(1)	13(1)	16(1)	0	0	2(1)
Na3	12(1)	57(1)	31(1)	32(1)	0	0
O	10(1)	14(1)	9(1)	0(1)	-1(1)	0(1)
N	14(1)	10(1)	49(2)	0	0	0

3.3.6 MAPLE Calculation

The Madelung part of lattice energy calculation was performed for the new oxynitride, Na₅MoO₄N. Table 3-11 gives the MAPLE* values of the structure, and from the table, the coulomb part of lattice energy were calculated by using the formula.

Table 3-11: Atoms, Charge and MAPLE of an individual atom in Na₅MoO₄N.

Atom	Charge	Shortest interatomic distances (pm)	MAPLE*
Mo	+6	171.82	113.55
Na1	+1	229.82	143.89
Na2	+1	235.77	144.43
Na3	+1	224.61	141.42
O1	-2	195.52	144.14
N1	-3	171.82	136.24

MAPLE* = MAPLE/ (Charge)² in kcal/mole

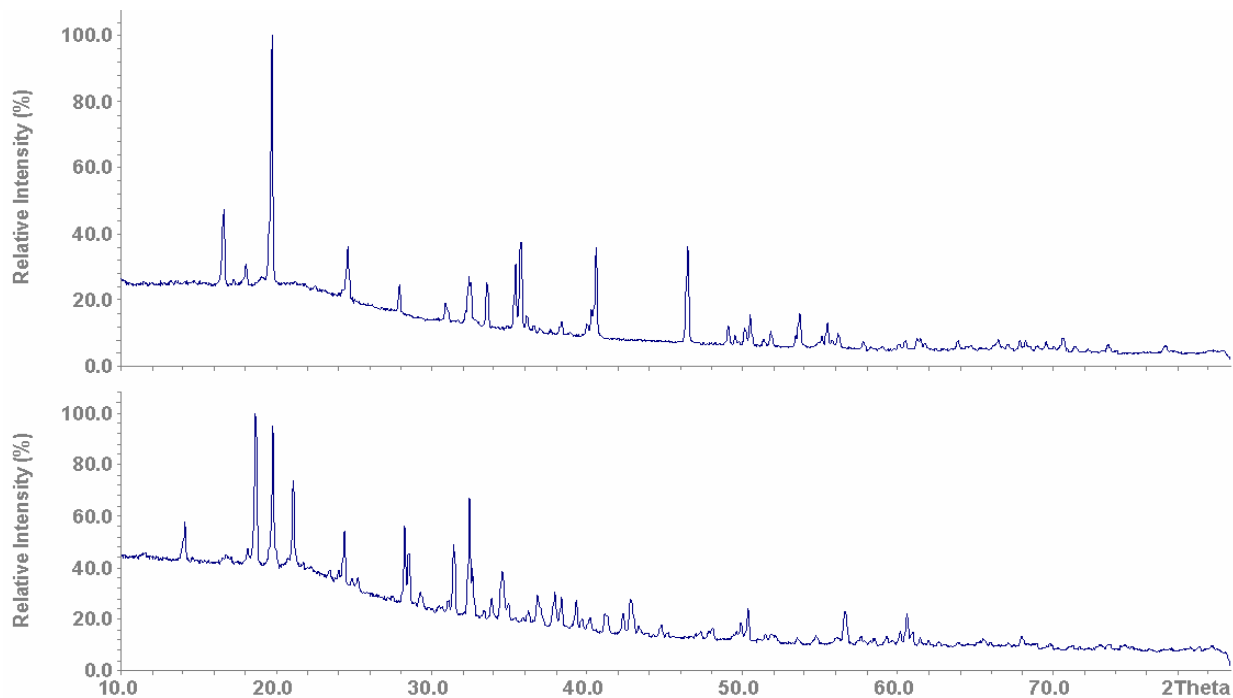
Coulomb part of lattice energy = 8338.40 kcal/mol

Coulomb part of lattice energy in kJ/mol is 34904.53

The coordination number of atoms and effective coordination number for this sample obtained from the program MAPLE are given in table 3-12. MEFIR values are also mentioned in the table.

Table 3-12: Coordination number (CN), Effective Coordination Number (ECoN) and Mean Effective Ionic Radii (MEFIR) (Å) for $\text{Na}_5\text{MoO}_4\text{N}$.

Atoms	CN	ECoN	MEFIR
Mo	5	4.5240	0.46
Na1	4	3.8515	0.96
Na2	5	4.9886	0.98
Na3	4	4.0000	0.85
O1	6	5.8364	1.41
N1	3	2.8149	1.37

**Figure 3-7:** X-ray profiles obtained at region 2 (50 °C) which is shown above and at region 3 (480 °C) shown below.

3.3.7 Structural Discussion

$\text{Na}_5\text{MoO}_4\text{N}$ has been obtained as highly hygroscopic pale green color crystals. This molybdenum oxynitride is nearly iso-structural to sodium tungsten oxynitride, $\text{Na}_5\text{WO}_4\text{N}$ [160], which has been reported to crystallize in space group, $Cmc2_1$, an acentric subgroup of $Cmcm$ found by us.

In $\text{Na}_5\text{MoO}_4\text{N}$, the molybdenum atom is co-ordinated with four O-atoms and with one N-atom forming an isolated rectangular (almost square) pyramidal polyhedron. One half of the polyhedra is oriented in $[0\ 1\ 0]$ direction while the other is oriented in the opposite direction, which is shown in figure 3-8. The Mo atom is located above the plane formed by the four oxygen atoms and the nitrogen atom occupies the apex of the square pyramid. The bond distance Mo-N (1.719 Å) is significantly shorter than Mo-O (1.958 Å), cf. Table 3-13.

The three crystallographic independent sodium atoms present exhibit different coordination spheres by oxygen. Four oxygen atoms form an approximate tetrahedron around the sodium atom Na1, while Na2 atom is co-ordinated by four oxygen atoms forming the plane, and one nitrogen atom at the apex, of a rectangular pyramid. The Na3 atom is co-ordinated to four oxygen atoms forming a rectangular plane. The potential experienced by this sodium atom is flat in the direction perpendicular to the plane. This explains the enhanced thermal motion as reflected by the slightly increased U_{22} of Na3.

Table 3-13: Selective bond lengths of $\text{Na}_5\text{MoO}_4\text{N}$.

Atom	Atom	Dist. in Å
Mo1	N	1.719
	O	1.958 (4×)
Na1	O	2.274 (2×)
	O	2.465 (2×)
Na2	O	2.354 (2×)
	O	2.401 (2×)
	N	2.42.4
Na3	O	2.230 (4×)

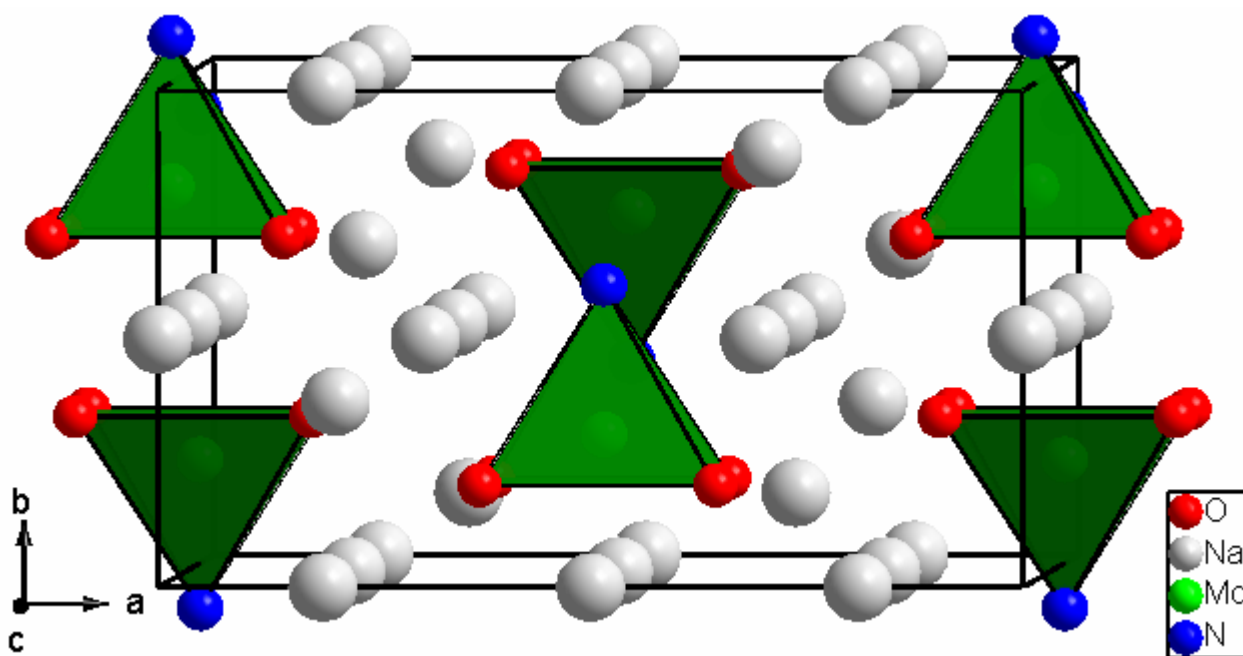


Figure 3-8: Perspective view of the crystal structure of $\text{Na}_5\text{MoO}_4\text{N}$.

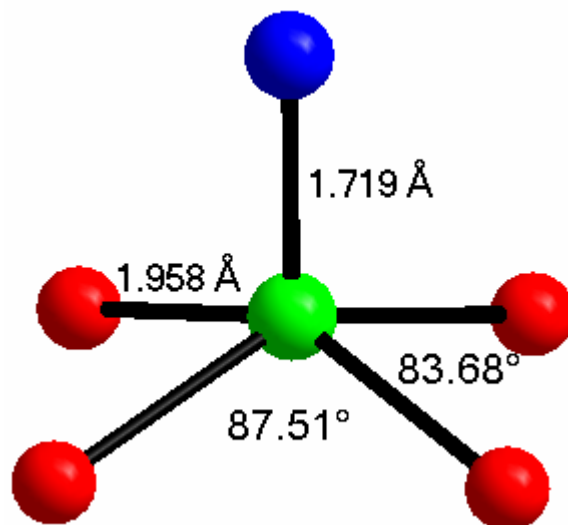


Figure 3-9: The complex anion $[\text{MoO}_4\text{N}]^{5-}$.

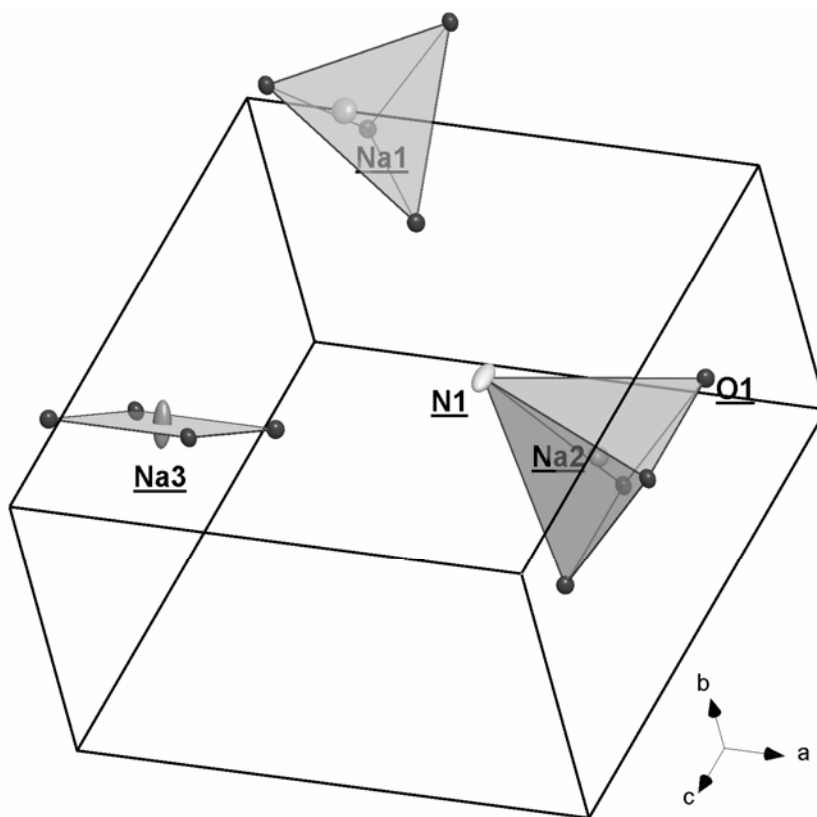


Figure 3-10: Elongated Na(3) atom along with selected Na, N and O atoms in the unit cell. The oxide and nitride anions are represented by black and white spheres respectively.

These obtained oxynitrides, Na₃MoO₃N and Na₅MoO₄N, contains molybdenum in hexavalent state and due to this are diamagnetic. As most characteristical structure units the complex Mo anions, tetrahedral [MoO₃N]³⁻ and square pyramidal [MoO₄N]⁵⁻ complex anions have been found. The two compounds are formally differing by one mole of Na₂O per formula unit. The difference in Mo surrounding is mainly due to the fact that all anions strive to coordinate the highest charge cations.

4. Chapter-4

4.1 Tripotassium Sodium Tungstate, $K_3Na(WO_4)_2$

Alkali tungstates as well as alkali molybdates form crystals with structures based on polymerized $[M_nO_{3n+1}]^{2-}$ anions when they crystallized from melts. The anions forming an isolated tetrahedron of $[WO_4]^{2-}$ are found in Li_2WO_4 [161] (hexagonal phenacite structure), Na_2WO_4 [36] (spinel structure), K_2WO_4 , Rb_2WO_4 [162] etc. Also infinite chains, layers or frameworks built up of WO_4 tetrahedra and/or WO_6 octahedra as in the case of $Na_2W_2O_7$ [33] are also common. Often the tungstates show strong similarities to the corresponding molybdates. Nevertheless, sometimes alkali tungstates show a tendency to adopt structures different from the corresponding molybdates, as it is found for $K_2Mo_3O_{10}$ [49,50] and $K_2W_3O_{10}$ [35].

Tungstates or molybdates with more than one kind of alkali metal cations are explored very rarely, and only a very small number of potassium sodium tungstates are known until today. In 1989, Li and Wang reported a phase named $K_{0.39}Na_{0.27}WO_3$ [88] which they prepared by fused salt electrolysis. In the same year, Hoffmann and Hoppe published a compound containing a larger amount of sodium than of potassium, KNa_3WO_5 [89]. This compound was synthesized by a solid state reaction of K_2O with Na_4WO_5 [89] for 35 days at 750 °C. In 1977, Eysel and co-workers reported the lattice parameters of $K_3Na(WO_4)_2$ [163]. At room temperature, the pattern was indexed hexagonally and at 625 °C the compound was reported to have orthorhombic unit cell constants. Neither a method of synthesis nor any structural parameters are given in that publication.

In the present chapter, we discuss the synthesis part, characterization techniques adopted and also the crystal structures of $K_3Na(WO_4)_2$, both at room temperature and at elevated temperature with full elucidation of structures. Unlike previous report, the phase crystallizes in a monoclinic cell at room temperature and a hexagonal one at high temperature. The obtained solid tripotassium sodium

tungstate, $K_3Na(WO_4)_2$ belongs to a family of compounds with the common chemical formula $A_3B(CX_4)_2$ where A, B = Alkali metal ions like Li, Na, K, Cs, Rb, NH_4^+ ions and $CX_4 = SO_4, SeO_4, CrO_4, MoO_4$.

4.1.1 Synthesis

The new mixed alkali tungsten oxide, $K_3Na(WO_4)_2$, is prepared from the corresponding alkali tungstates. Stoichiometric amounts of anhydrous sodium tungstate and anhydrous potassium tungstate were ground intimately. The mixture is then heated in a silver crucible up to 600 °C. The sample was held at this temperature for 40 h and then cooled down to room temperature at the rate of 20 °C/h. The obtained colorless product was then sealed in a glass ampoule under the flow of dry argon in order to make sure that it has no contacts with atmospheric air or moisture.

4.1.2 Thermal Analysis

The investigation of the thermal behavior of $K_3Na(WO_4)_2$ gave us no information about the melting point. No decomposition was detected up to 1000 °C which is shown in figure 4-1.

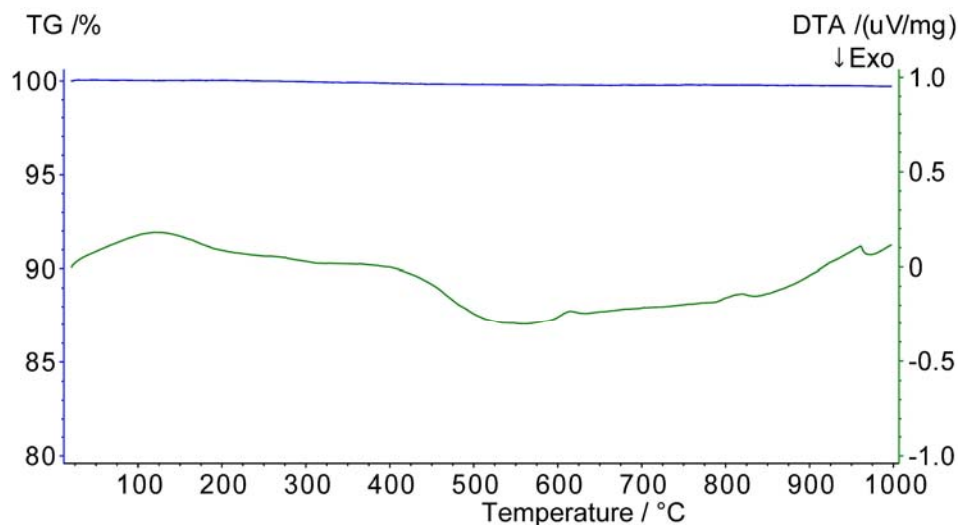


Figure 4-1: Thermal analysis of $K_3Na(WO_4)_2$. (TGA in blue and DTA in green)

4.1.3 X-ray Analyses

4.1.3.1 Powder Diffraction Analyses

To determine the crystal system and to refine the lattice constants, an X-ray powder pattern of a finely ground microcrystalline sample was measured at room temperature. The indexing of the obtained reflections gave a monoclinic unit cell with $a = 10.510 \text{ \AA}$, $b = 15.302 \text{ \AA}$, $c = 6.066 \text{ \AA}$ and $\beta = 90.09^\circ$ (see also Table 4-1). The analyses of the reflection positions in the 2θ range between 5° and 90° shows that $K_3Na(WO_4)_2$ is isotypic with the monoclinic phases of $K_3Na(CrO_4)_2$ and $K_3Na(MoO_4)_2$. The observed diffraction pattern of $K_3Na(WO_4)_2$ listed in the ICDD PDF2 data base [ref no: 28-802] was reported with hexagonal cell parameters which differ only slightly from the monoclinic. The complete X-ray profiles of the sample at high temperature as well as at room temperature (275°C) are shown in the figure 4-2 and figure 4-3, respectively. Nevertheless, additional reflections in the measured powder pattern as well as the indexing of the single crystal data prove the monoclinic setting unambiguously.

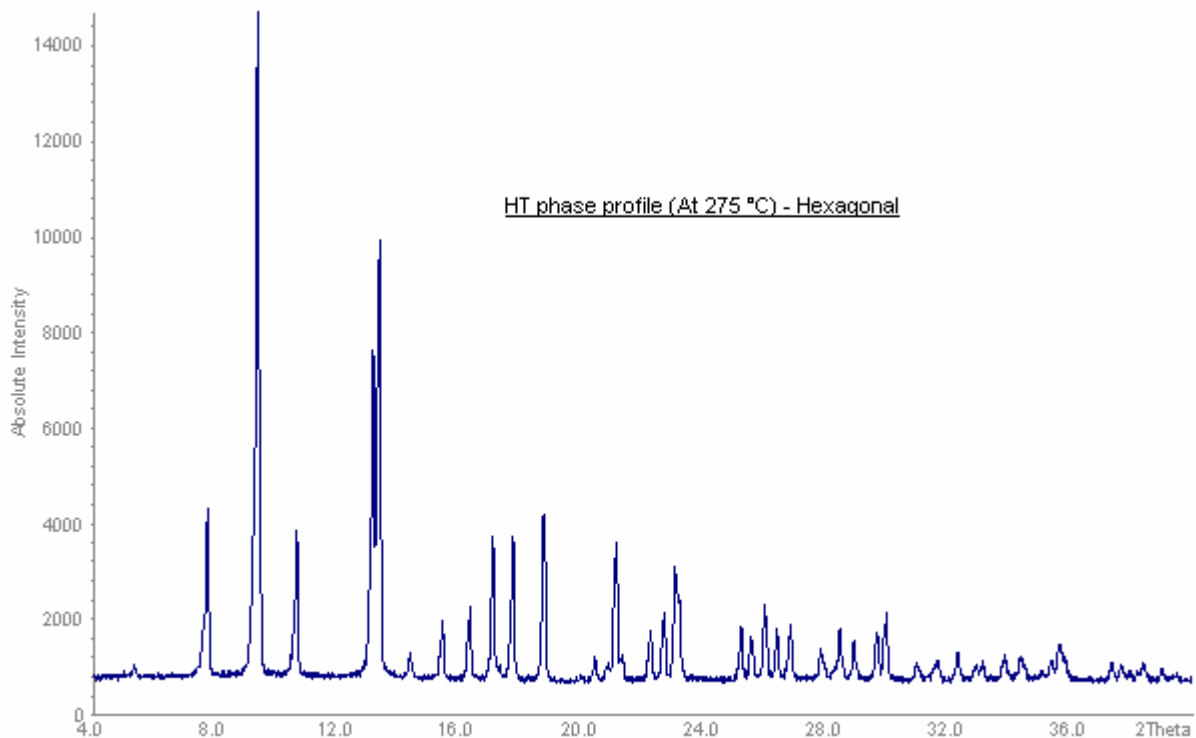


Figure 4-2: Measured X-ray pattern of HT- $K_3Na(WO_4)_2$, Mo- K_α , at 275 °C.

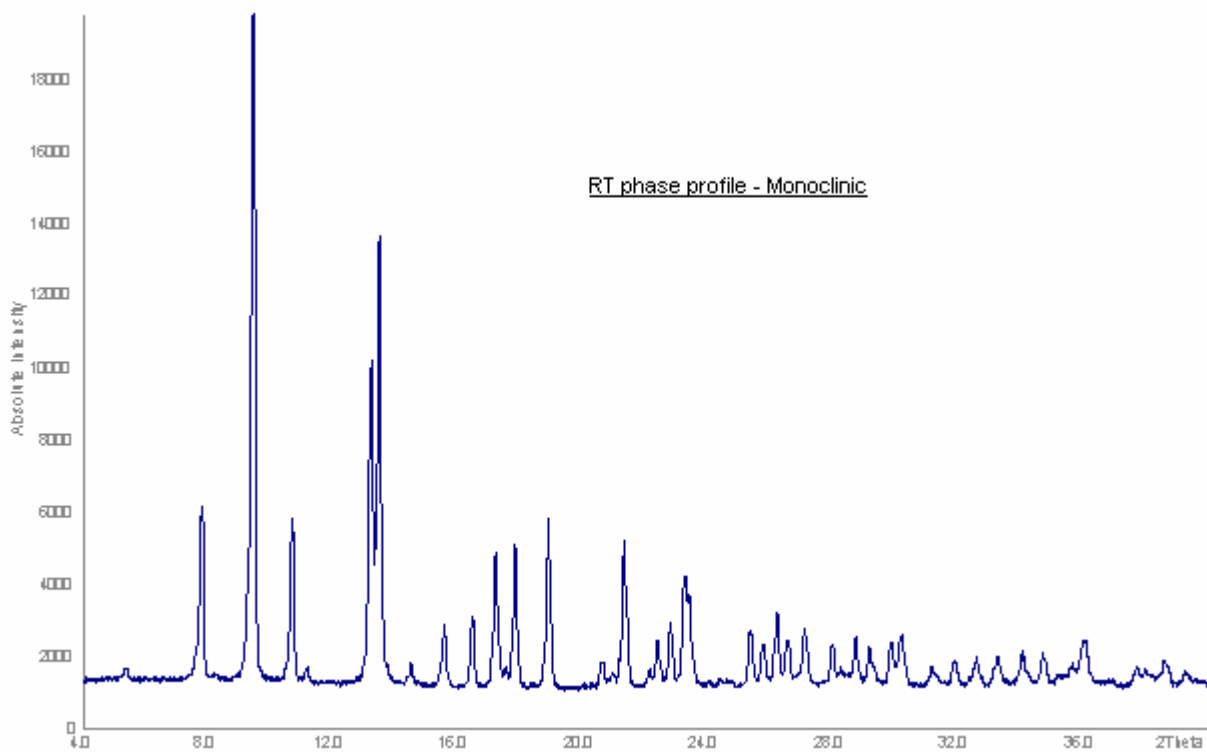


Figure 4-3: Measured X-ray pattern of RT- $K_3Na(WO_4)_2$, Mo- K_α , at 275 °C.

4.1.3.2 Single Crystal Diffraction Analyses

Single crystals of $K_3Na(WO_4)_2$ were picked from the bulk sample in the glove box using 0.1 mm glass capillary and are inserted into a 0.3 mm capillary which was then sealed under dry argon. To find the quality of the single crystal and for the basic indexing of the obtained product, $K_3Na(WO_4)_2$, few images were made by using the precession camera. Figure 4-4 shows the single crystal diffraction patterns (precession image) of the $[0 k l]$, $[h 0 l]$ and $[h k 0]$ plane of the $K_3Na(WO_4)_2$ of the monoclinic cell obtained at 25 °C. Single crystal diffraction analysis was effected on a STOE-IPDS 2 diffractometer at room temperature after mounting the crystals. The crystallographic details are given in table 4-1.

4.1.4 Phase Transition Analyses

The solution of the crystal structure of $K_3Na(WO_4)_2$ showed that the new compound is isostructural to $K_3Na(SO_4)_2$, known as glaserite, and some related compounds. For some members of this group, a phase transition from low temperature monoclinic (paraelastic) form to a ferroelastic trigonal high temperature form was observed. According to this and with respect to the lattice constants which are closely related to the hexagonal metrics, we expected a phase transition above room temperature.

4.1.4.1 Low Temperature DSC Measurement

Low temperature (LT) DSC measurements were carried out in order to find out the presence and the temperature of the expected phase transition of the compound. The measurement of the heat capacity by this LT-DSC measurement indicates that there are no phase transitions below 0 °C. So, high temperature (HT) DSC measurement was performed to find the presence of phase transition.

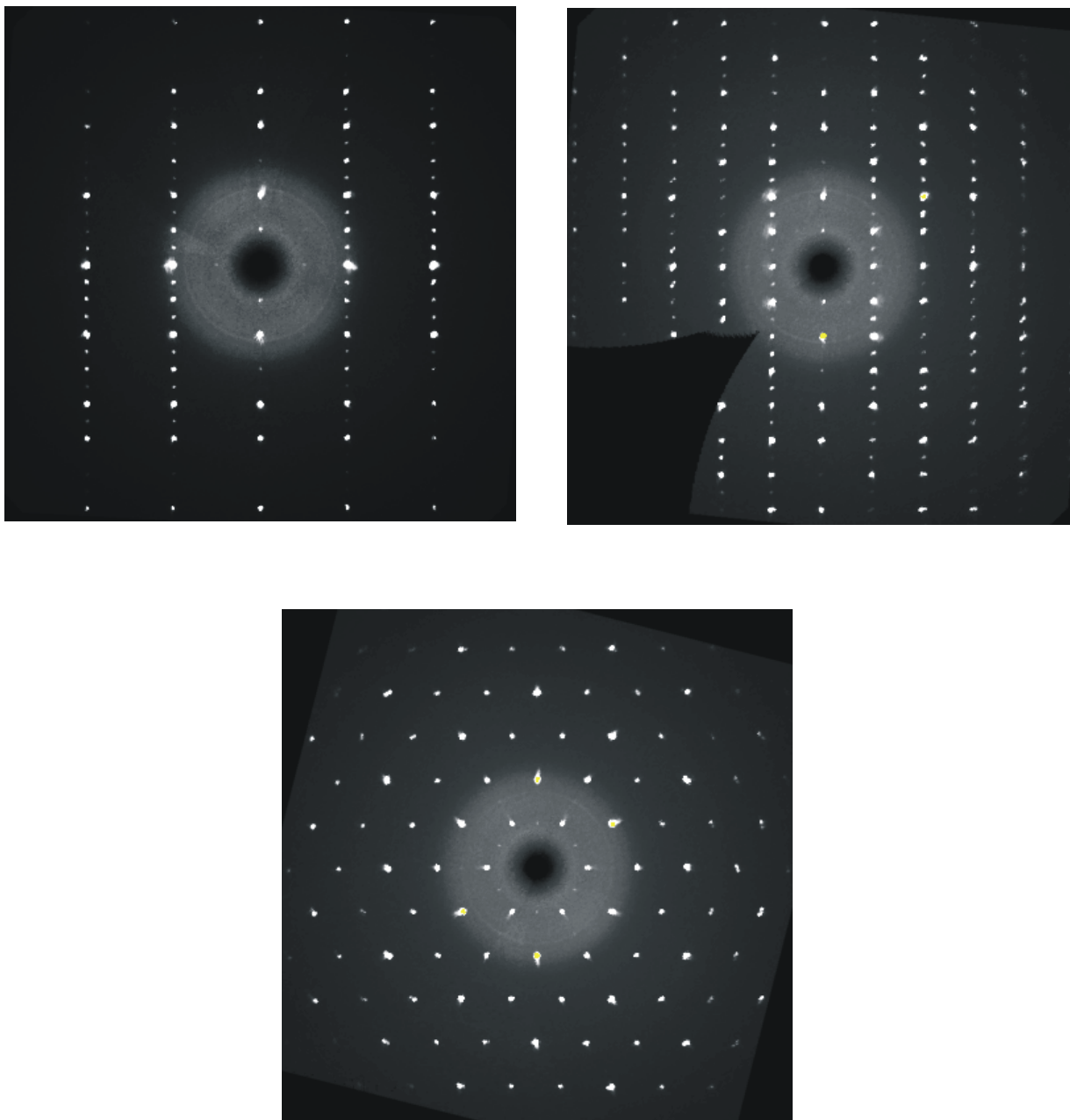


Figure 4-4: X-ray single crystal diffraction patterns of the $[0\ k\ l]$, $[h\ 0\ l]$ and $[h\ k\ 0]$ plane of the $K_3Na(WO_4)_2$ at room temperature (showing a monoclinic cell).

Table 4-1: Crystallographic data and structure refinement of the HT and RT- $K_3Na(WO_4)_2$.

Empirical Formula	$K_3Na(WO_4)_2$ (HT)	$K_3Na(WO_4)_2$ (RT)
Formula weight /g mol ⁻¹	1271.95	2543.92
Crystal system	Trigonal	Monoclinic
Space group	$P\bar{3}m1$ (No. 164)	$C2/c$ (No. 15)
Lattice parameters /Å	$a = 6.1305(1)$ $c = 7.6944(1)$	$a = 10.4928(1)$ $\beta = 90.087^\circ$ $b = 6.0693(1)$ $c = 15.2921(1)$
Cell Volume /Å ³	250.44(7)	986.83
Z	2	8
Density calc. /g·cm ⁻³	8.43324	4.28053
Obtained form	Powder	Single crystal
Diffractometer	STOE	STOE-IPDS 2
X-rays	Mo-K α_1	Mo-K α_1
Wavelength, λ / Å	0.7103	0.7103
Monochromator	Germanium	Graphite
Temperature, T / °C	275	25
2θ range /°	4 to 44.9	1.91 to 54.78
Range of h, k, l	-	$-13 \leq h \leq 13, -7 \leq k \leq 7, -19 \leq l \leq 19$
No. of data points	4100	-
No. of constrains / restrains	0	0
Refined parameters	22	37
R-Values / %	$R_p: 12.6; R_{wp}: 10.8$	$R_p: 6.01; R_{wp}: 5.76$ $R_p: 6.27; R_{wp}: 5.76$
F(000)	-	1120

4.1.4.2 High Temperature DSC Measurement

Measurements of the heat capacity by HT-DSC measurement should indicate clearly a phase transition. By plotting the specific heat ($J/g \times ^\circ C$) versus the temperature (T in $^\circ C$), we expected a sharp peak between the temperature range $200^\circ C$ and $275^\circ C$. For the measurement, a pure powdered sample was filled in an aluminum crucible, which was sealed afterwards. From the figure 4-5, no sharp peak was observed, but a heavily structured signal results upon gradually increasing the temperature. The structured signal could be the effect of special sample characteristics like e.g. grain size, which could not be eliminated. Also, the absence of sharp indicates that the phase transition is not rapid or it may be due to the fact that the energy change during the transition (from one phase to other phase) is negligibly small. Repeating the measurement with another batch of sample has lead to the same result. The nature of the phase transition observed thus has remained unexplored.

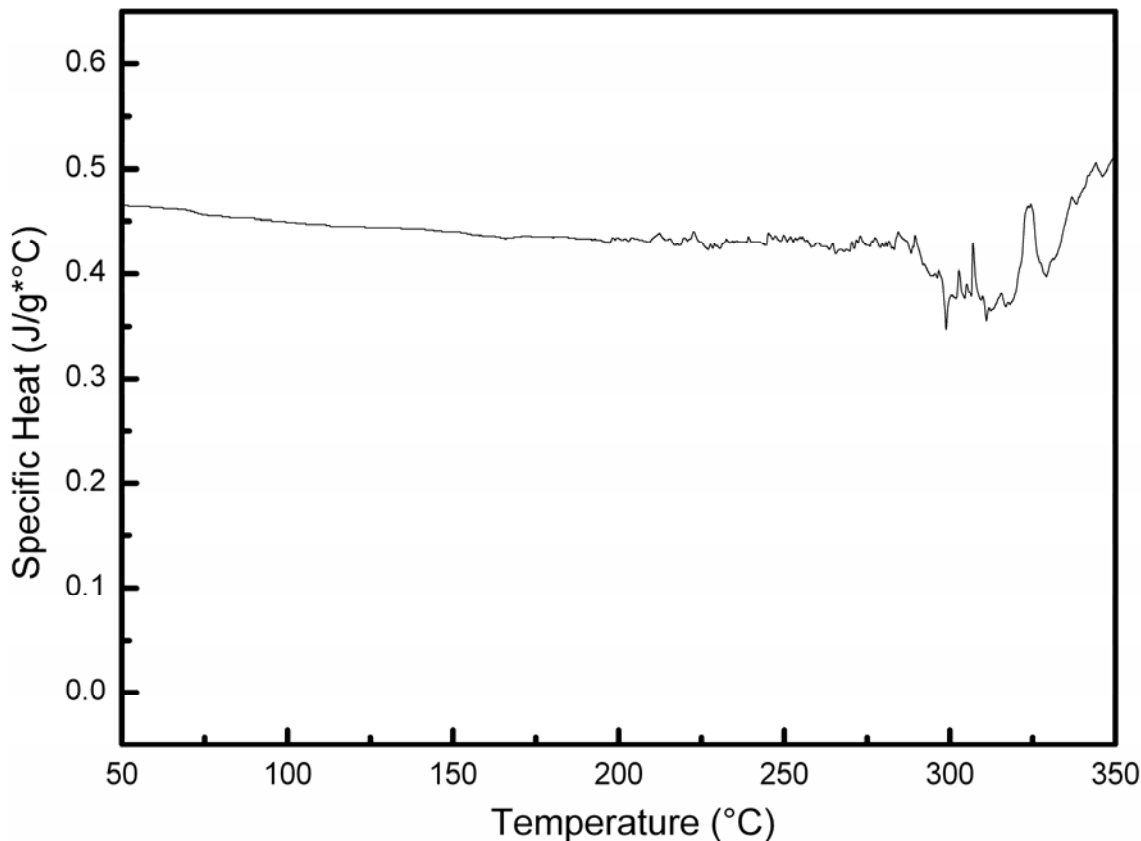


Figure 4-5: Heat capacity measurement of $K_3Na(WO_4)_2$ obtained. (powdered sample sealed in aluminum crucible)

4.1.4.3 High Temperature X-ray Powder Diffraction

High temperature X-ray powder diffraction of this sample was performed in order to find out the temperature at which the phase transition occurs. The measurements were performed using a molybdenum source with a hot air blower. As in the case of $K_3Na(MoO_4)_2$, we expect the phase transition above 200 °C for $K_3Na(WO_4)_2$. Starting from 150 °C, the measurement was conducted with the regular intervals of 50 °C with one in between at 275 °C. The X-ray diffractogram at different temperatures is shown in figure 4-6 and figure 4-7.

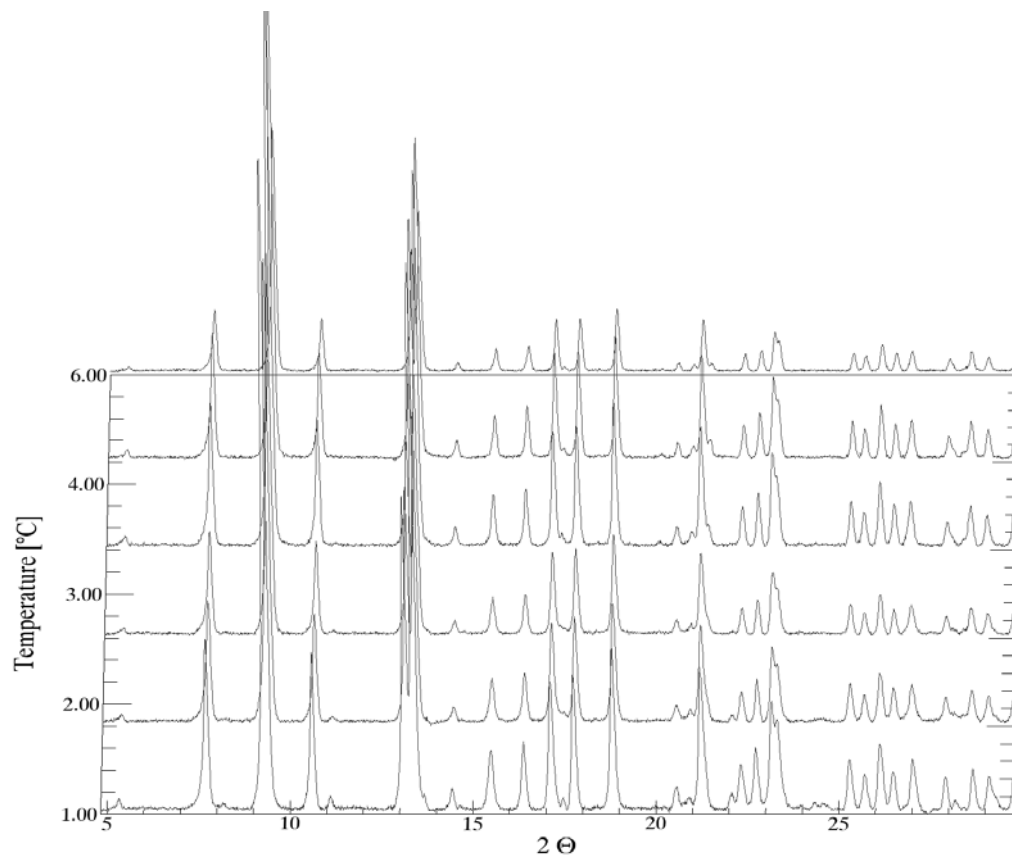


Figure 4-6: X-ray patterns obtained at different temperatures $K_3Na(WO_4)_2$ (from RT to 300 °C).

Figure 4-7 clearly shows that some of the reflections (at $2\theta = 11.1, 13.7$) are getting minimized upon the increase in the temperature of the sample from RT to 300 °C. Between the temperature region 250 and 275 °C, these reflections were completely disappeared. Thus, this measurement gave an idea of the temperature at which the phase transition is taking place.

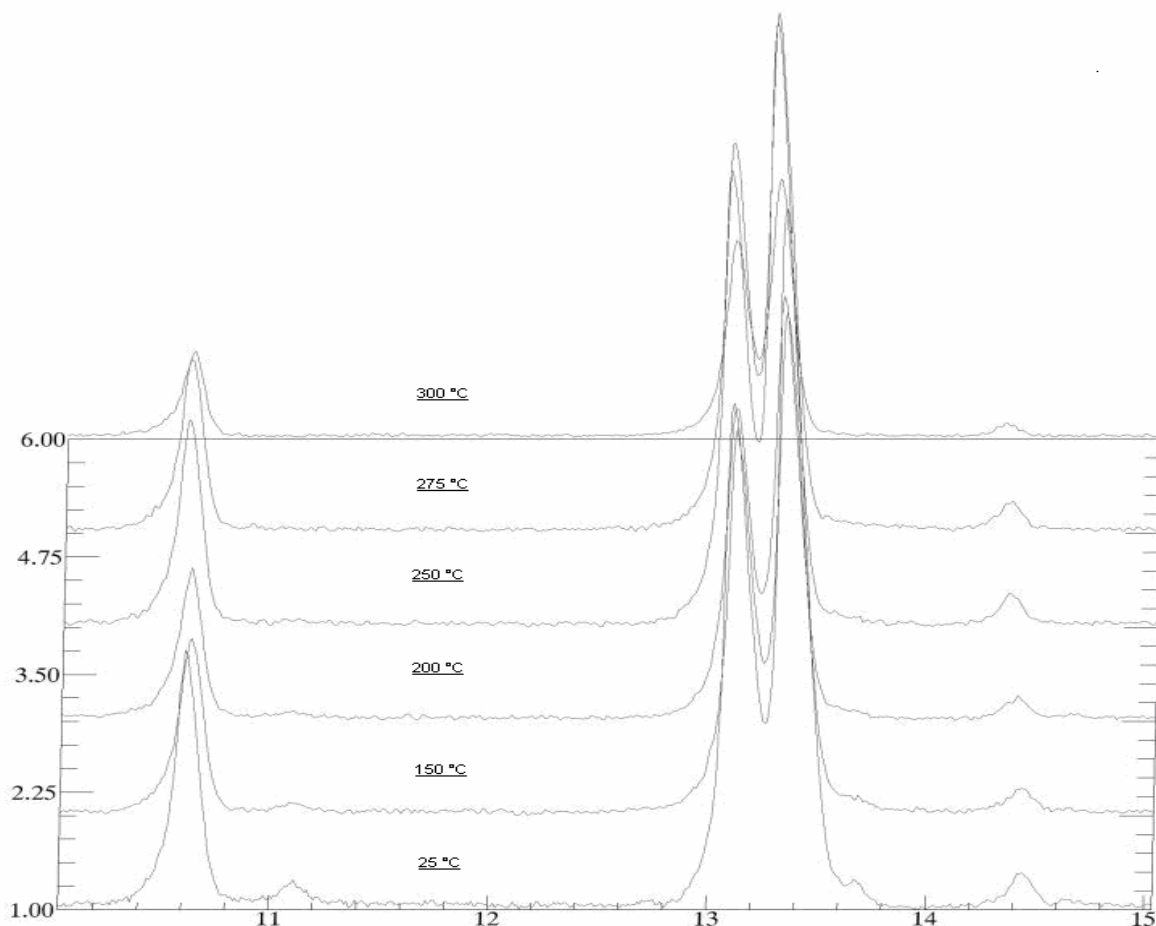


Figure 4-7: X-ray patterns obtained at different temperatures of $K_3Na(WO_4)_2$ (from RT to 300 °C and 2θ between 10 and 15).

4.1.5 Crystal Structure Description

In order to show the very closely related crystal structures of the high-temperature and low-temperature phases of $K_3Na(WO_4)_2$, the simpler HT-structure is explained firstly followed by the LT-structure, where only the main differences between both forms are described.

4.1.5.1 High-Temperature Phase

HT- $K_3Na(WO_4)_2$ crystallizes in the trigonal space group $P\bar{3}m1$. The structure was refined via the *Rietveld* method using the program FULLPROF [128] taking the

structural parameters of $K_3Na(MoO_4)_2$ as the starting model. Figure 4-8 shows the profile fit of the XRD pattern of $K_3Na(WO_4)_2$ recorded at 275 °C. The crystallographic details of the refinement are listed in table 4-1, the positional and isotropic displacement parameters in table 4-2.

Hexagonal phase

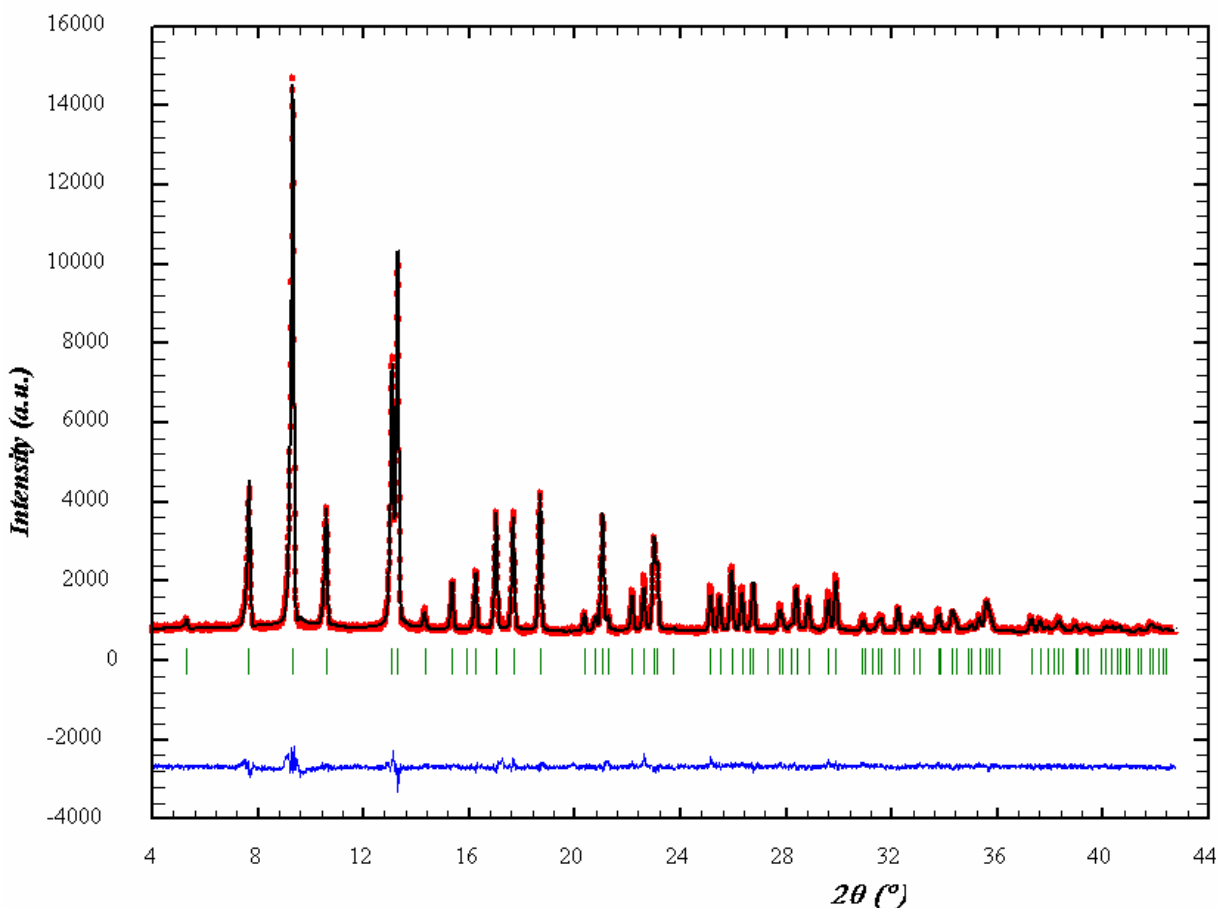


Figure 4-8: *Reitveld* plot of HT- $K_3Na(WO_4)_2$. Shown is the observed pattern (red circles), the best Rietveld plot (line), the Bragg Positions of the HT- $K_3Na(WO_4)_2$.

The main building units of the crystal structure are WO_4 tetrahedra, which are linked by sodium and potassium cations (see Figure 4-9). The W-O distances are in the average of 1.727 Å. The bond parallel to the c -axis is distinctly shorter (see Table 4-3), but are within the known ranges as observed in other tetrahedral tungstates. As shown in figure 4-10, sodium is coordinated by six oxygen atoms in the form of an octahedron which is compressed along $[001]$. The two crystallographically

independent potassium ions are surrounded by ten (K(1)) and twelve (K(2)) oxygen atoms, respectively.

Table 4-2: Positional and isotropic displacement parameters for the HT- $K_3Na(WO_4)_2$ at 275 °C.

Atom	Site	<i>x</i>	<i>y</i>	<i>z</i>	$U_{eq} / \text{Å}^2$
W	2 <i>d</i>	1/3	2/3	0.2190(6)	0.0368
K1	2 <i>d</i>	1/3	2/3	0.4152(7)	0.0634
K2	1 <i>a</i>	0	0	0	0.0623
Na1	1 <i>b</i>	0	0	½	0.0583
O1	6 <i>i</i>	-0.8198	0.8198	0.2998(2)	0.0702
O2	2 <i>d</i>	1/3	2/3	0.0001(3)	0.0187

Table 4-3: Selected interatomic distances in HT- $K_3Na(WO_4)_2$.

Atom	Atom	Distance (Å)
Na1	O1	2.4563 × 1
K1	O2	2.5367 × 1
	O1	3.0771 × 6
	O1	3.2828 × 3
K2	O1	2.9972 × 6
	O2	3.5394 × 6
W1	O2	1.6845 × 1
	O1	1.7407 × 3

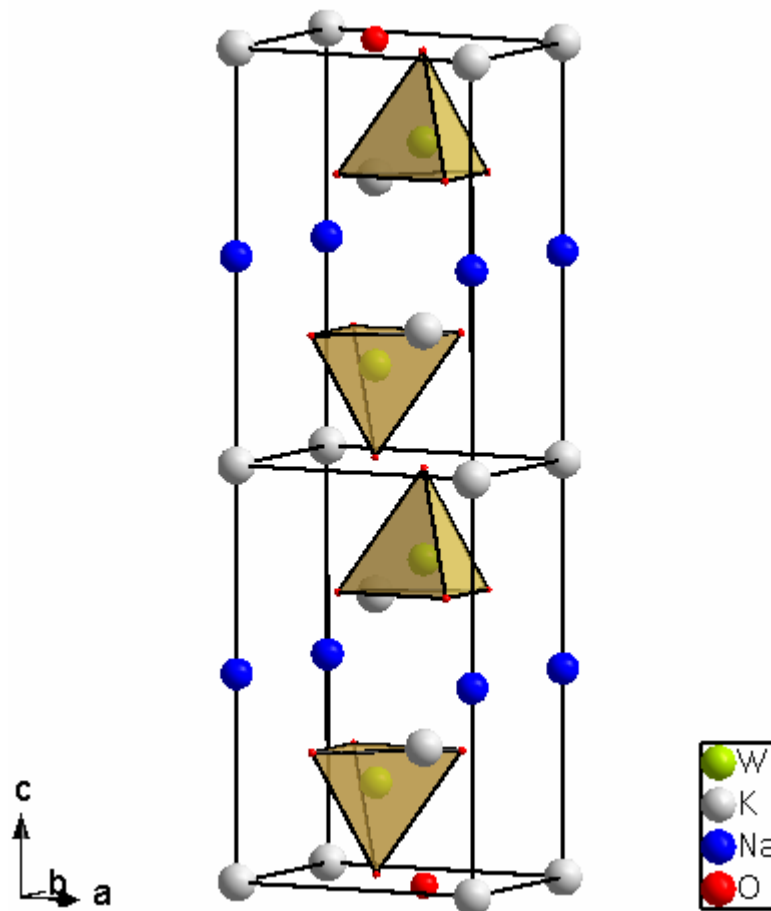


Figure 4-9: Two hexagonal unit cells of HT- $K_3Na(WO_4)_2$ showing the opposite facing apices of WO_4 tetrahedra.

For each KO_x polyhedron, six oxygen atoms are in plane with the center cation forming a regular hexagon which is capped by one single oxygen atom and a triangle of oxygen atoms or by two triangles forming an elongated trigonal anti-prism, in the second case resulting in a distorted cuboctahedron. The twelve fold coordinated potassium atom with its relatively remote oxygen neighbors seems to be “under-bonded”. Edge-sharing tetrahedral WO_4 groups around the cuboctahedron are forming a pinwheel where the apical oxygen atoms point alternately up and down (Figure 4-10). All oxygen atoms are bound to tungsten.

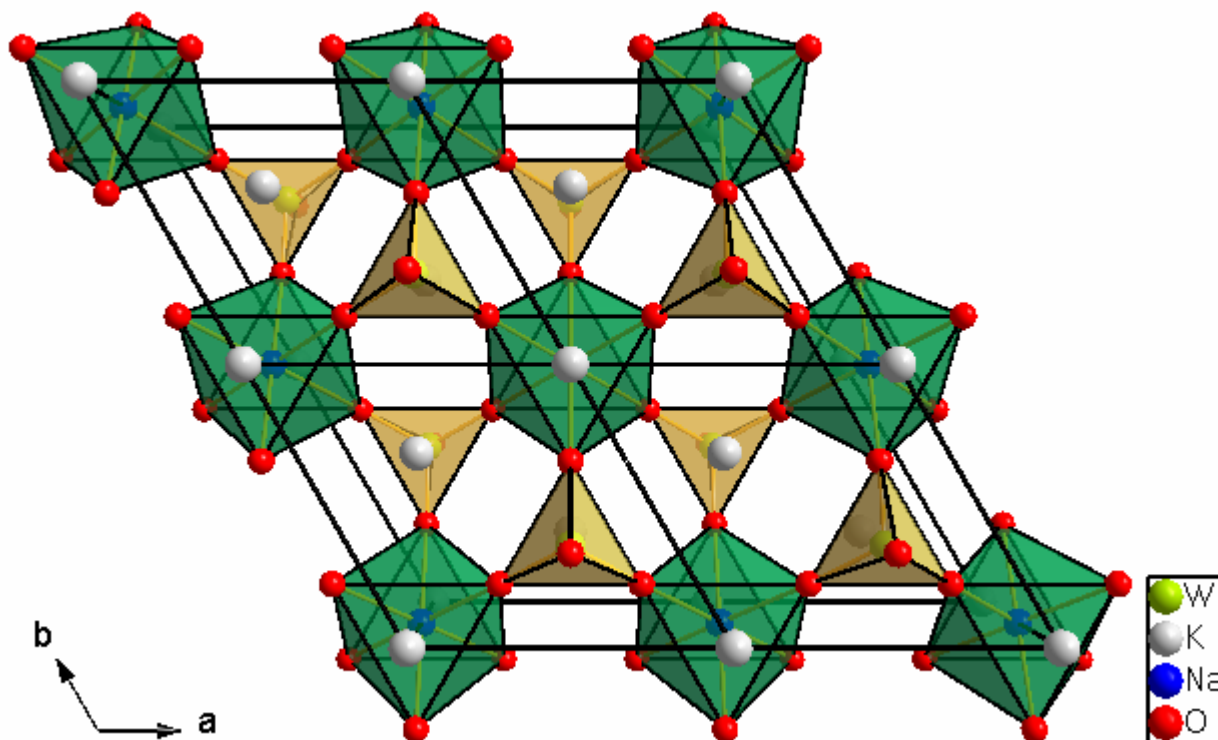


Figure 4-10: Perspective view along $[0\ 0\ 1]$ of the crystal structure of HT- $K_3Na(WO_4)_2$. Drawn are potassium atoms and the coordination polyhedra of tungsten (yellow tetrahedra) and sodium (green octahedra).

Beneath the shorter W-O bond mentioned above, another striking short distance of 2.537 Å is found between K(1) and O(2). Both the shorter bonds are parallel to the *c*-axis and are a part of the first coordination sphere of the same oxygen atom O(2), so the W-O(2)-K(1) angle is 180°. To expand both bonds, the respective cations have to shift in direction to each other, to approximate below a present value of 3.473 Å, or the *c*-axis has to be elongated. At lower temperatures, actually with decreasing lattice parameters, a third possibility to avoid shorter distances, particular structure reorganization, takes place. Nevertheless, short K-O distances like the present one are known from other compounds, e. g. from potassium osmate, K_2OsO_5 [164].

The high-temperature phase of $K_3Na(WO_4)_2$ is isotypic to glaserite, $K_3Na(SO_4)_2$ [165-167] and related compounds like e.g. the HT-forms of $K_3Na(CrO_4)_2$ [168-170] and $K_3Na(MoO_4)_2$ [86].

4.1.5.2 Low-Temperature Phase (Room Temperature Phase)

At room temperature $K_3Na(WO_4)_2$ crystallizes monoclinic in space group $C2/c$. The symmetry decrease from the trigonal HT-phase is passing one *translationengleichen* transition of index 3 and one *klassengleichen* of index 2. Because the temperature of the synthesis lies above the phase transition temperature, all crystals of the LT-form are systematically twinned. Because of difficulties to find satisfying single crystals, the structure was initially refined from X-ray powder diffraction measurements with the *Rietveld* method. Later the structure refinement succeeded from a merohedral twin by refining three individual domains of the structure. Details of both refinements are listed in table 4-1. The positional and anisotropic parameters are given in the table 4-4 and table 4-5, respectively while the selected bond distances are listed in table 4-6.

Table 4-4: Atomic parameters for RT- $K_3Na(WO_4)_2$.

Atom	Site	x	y	z
W	8f	0.1629(0)	0.4795(3)	0.1397(4)
K1	8f	0.1714(5)	0.4759(8)	0.4151(7)
K2	4e	0	0.9449(1)	¼
Na1	4a	0	0	0
O1	8f	0.1722	0.5553	0.2516(7)
O2	8f	0.0822	0.6933	0.0806(1)
O3	8f	0.0792	0.2313	0.1209(1)
O4	8f	0.3152(1)	0.4554	0.0933(1)

Table 4-5: Anisotropic displacement parameters for RT- $K_3Na(WO_4)_2$. (\AA^2)

Atom	U_{11}	U_{22}	U_{33}	U_{12}	U_{13}	U_{23}
W1	0.0130(3)	0.0156(4)	0.01300(18)	-0.0010(4)	-0.0024(3)	0.0010(4)
K1	0.024(2)	0.032(3)	0.0222(14)	0.001(2)	-0.003(2)	-0.001(2)
K2	0.032(4)	0.027(3)	0.024(2)	0.00000	-0.001(3)	0.00000
Na1	0.012(5)	0.027(7)	0.018(3)	0.001(5)	-0.003(5)	0.000(5)
O1	0.058(12)	0.043(10)	0.020(5)	-0.003(8)	0.007(9)	-0.002(6)
O2	0.039(11)	0.031(10)	0.019(8)	0.003(8)	-0.002(8)	0.014(7)
O3	0.018(9)	0.033(10)	0.04(1)	-0.013(6)	-0.01(1)	0.005(8)
O4	0.022(8)	0.046(13)	0.034(11)	0.007(8)	0.005(7)	0.005(10)

Table 4-6: Selective interatomic bond distances of atoms in RT- $K_3Na(WO_4)_2$.

Atom	Atom	Distance (\AA)	Atom	Atom	Distance (\AA)
Na1	O2	2.4033×2	K2	O3	3.0844
	O4	2.4353×2		O3	3.1078
	O3	2.4739×2		O2	3.1217
W1	O4	1.7646		O4	3.1561
	O3	1.7772		O4	3.1781
	O1	1.7806		O3	2.7678×2
	O2	1.8010		O1	2.9889×2
K1	O1	2.5574		O4	3.0978×2
	O2	2.8984		O2	3.1414×2
	O4	2.9240	O1	3.5258×2	
	O2	2.9838			

4.1.5.3 MAPLE Calculation

Table 4-7 and table 4-8 shows the result obtained from MAPLE calculations. MAPLE calculations have been carried out for the binary oxides K_2O , Na_2O and WO_3 and the lattice energy values are listed below.

Coulomb part of lattice energy (LE) for K_2O = 599.93 kcal/mol

Coulomb part of lattice energy (LE) for Na_2O = 695.70 kcal/mol

Coulomb part of lattice energy (LE) for WO_3 = 5468.87 kcal/mol

In general,

$$\Sigma \{3/2 \text{ LE}(K_2O) + 1/2 \text{ LE}(Na_2O) + 2 \text{ LE}(WO_3)\} = \text{Value obtained for RT-}K_3Na(WO_4)_2$$

It is found that the summation of the lattice energy, $\Sigma \{(3/2) K_2O + (1/2) Na_2O + 2 WO_3\}$ is equal to 12185.49 kcal/mol and the lattice energy obtained for RT- $K_3Na(WO_4)_2$ is equal to 13320.99 kcal/mol. The difference in the lattice energy was found to be 1135.51 kcal/mol. This error is due to the presence of shorter bond length between tungsten and oxygen atom in the structure. Also, it may be due to the change in the coordination of the cations which are involved in the structure of $K_3Na(WO_4)_2$.

Table 4-7: Coordination number (CN), Effective Coordination Number (ECoN) and Mean Effective Ionic Radii (MEFIR) (Å) for RT- $K_3Na(WO_4)_2$ using MAPLE calculations.

Atoms	Charge	CN	ECoN	Shortest interatomic distances (Å)	MEFIR
W	+6	4	3.9931	1.7656	0.37
Na1	+1	6	5.9706	2.4021	1.02
K1	+1	9	7.8265	2.5566	1.33
K2	+1	10	8.1403	2.7704	1.48
O1	-2	4	3.0737	1.7820	1.44
O2	-2	6	4.9231	1.8006	1.50
O3	-2	5	3.7610	1.7744	1.45
O4	-2	6	4.4958	1.7656	1.50

Table 4-8: Coordination number (CN), Effective Coordination Number (ECoN) and Mean Effective Ionic Radii (MEFIR) (Å) for HT- $K_3Na(WO_4)_2$ using MAPLE calculations.

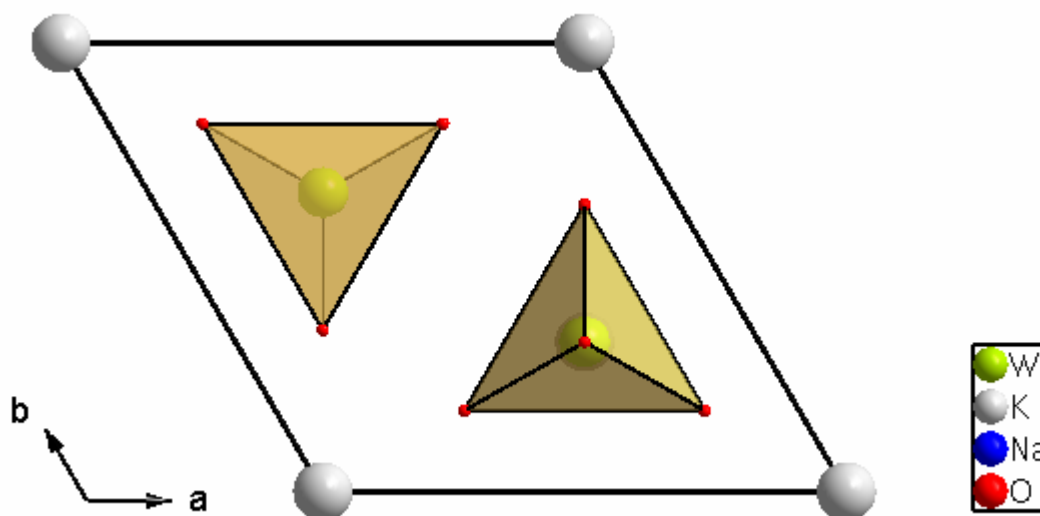
Atoms	Charge	CN	ECoN	Shortest interatomic distances (Å)	MEFIR
W	+6	4	3.9731	1.6845	0.32
Na1	+1	6	6.0000	2.4563	1.06
K1	+1	10	8.2540	2.5367	1.48
K2	+1	12	9.0937	2.9.72	1.69
O1	-2	6	5.0435	1.7407	1.44
O2	-2	5	3.0933	1.6845	1.45

MAPLE* = MAPLE/ (Charge)²

Coulomb part of lattice energy = 13689.82 kcal/mol

Coulomb part of lattice energy in kJ/mol is 57305.67

The setting of the monoclinic cell contains four formula units instead of one in the trigonal HT-solution. The volume per formula unit is decreased at ca. 2.9 % from 250.4 Å³ at 275°C to 423.5 Å³ at RT.

**Figure 4-11:** Unit cell of the crystal structure of HT- $K_3Na(WO_4)_2$ viewed along c-axis showing the two WO_4 tetrahedra inside.

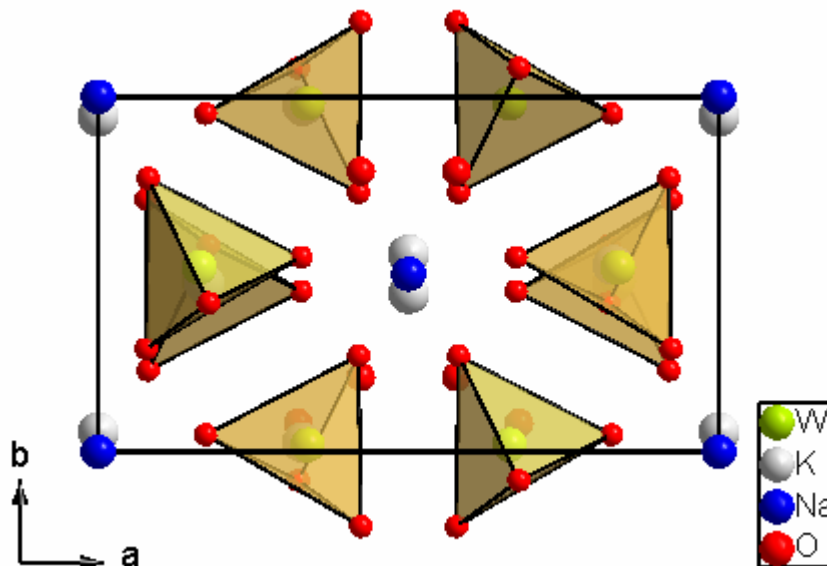


Figure 4-12: Unit cell of RT- $K_3Na(WO_4)_2$ viewed along c -axis showing the two tilted WO_4 tetrahedra.

The main structural difference to the trigonal structure, which can be seen in figure 4-15 and figure 4-16, is the tilting of the WO_4 tetrahedra, which are not parallel aligned to $[001]$ plane. Due to this, the threefold symmetry is destroyed and can be observed clearly by comparing figure 4-11 and figure 4-12 (viewing along $[001]$ direction). Remarkably, all $W-O$ bonds are longer than in the HT-phase, although the volume is decreased. This should be mainly an effect of the larger vibrational parameters of atoms in the high temperature phase. As volume, the length of the c -axis is also decreased but only to 0.6%. This smaller effect compared to the volume decrease is mainly because of the elongation of the bonds formerly quite short and parallel to $[001]$, namely the $W-O(2)$ and the $K(1)-O(2)$ distances in the trigonal phase. The internal stress/tension caused by these shorter bonds could be one of the main driving forces for the transition symmetry decrease containing phase transition during cooling down to room temperature. Another significant difference between HT- and LT- phases are found by comparing the coordination of the potassium ions. Both cations in the HT-phase are occupying the centers of high symmetric coordination polyhedra, while in the LT-phase, they are shifted away from the centers (Figure 4-13 to 4-14) resulting in smaller coordination numbers, 9

instead of 10 for K(1) and 8+2 instead of 12 for K(2). The rest of the formerly coordinating oxygen atoms are now situated in distances of 3.716 Å (K(1)) and 4.287 Å (K(2)) and have lost direct contact. As a result of the smaller coordination numbers, the weakly bound potassium atom K(2) in the HT-phase is strongly fixed which is also explained by the higher MAPLE energies (see Table 4-8). So, this could be another motivation for the observed phase transition.

4.1.5.4 Comparison of $K_3Na(WO_4)_2$ with Related Glaserites

As other sulphates, glaserite, $K_3Na(SO_4)_2$ [165-167], is the parent compound for many related compounds, which have been in the focus of intense work owing to their interesting crystal chemistry and importance in mineralogy. The structure of glaserite was investigated by Gossner [171] and later by Fischmeister [172]. Glaserites have the general formula $A_3B(MO_4)_2$, where A and B are cations of different sizes, A is significantly larger than B. Among others, $K_3Na(SeO_4)_2$ [173], $K_3V(VO_4)_2$ [174], $K_3Na(CrO_4)_2$ [168-170], and $K_3Na(MoO_4)_2$ [86] are crystallizing in the glaserite type of structure.

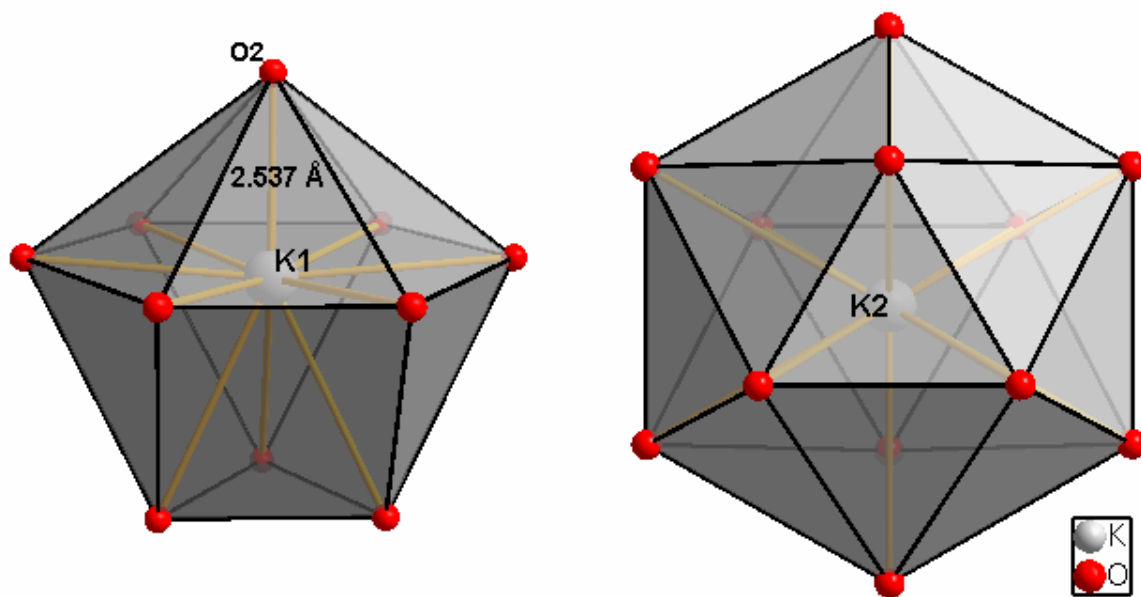


Figure 4-13: Coordination of K(1) and K(2) in HT-phase of $K_3Na(WO_4)_2$.

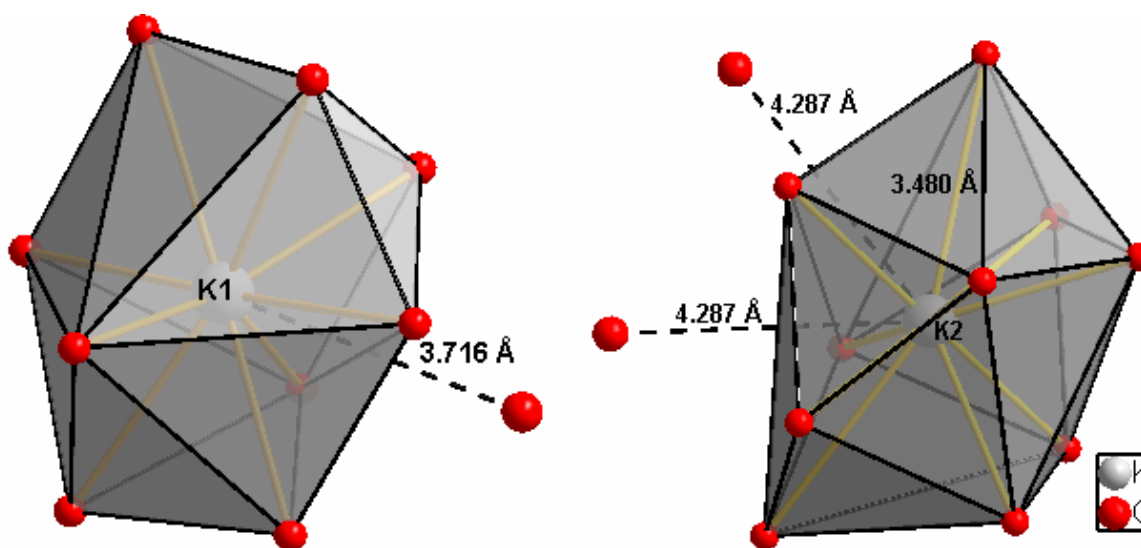


Figure 4-14: Coordination of K(1) and K(2) in LT-phase of $K_3Na(WO_4)_2$.

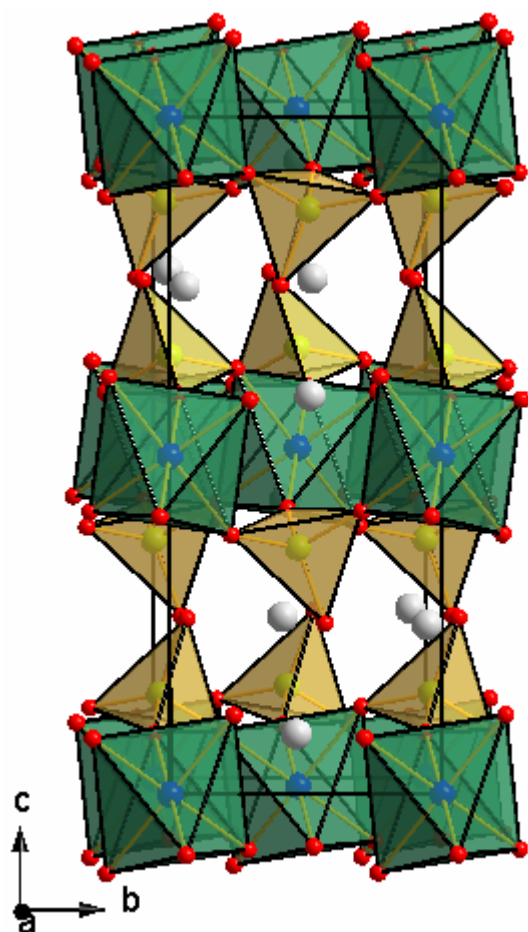


Figure 4-15: LT- $K_3Na(WO_4)_2$ with WO_4 tetrahedra and NaO_6 octahedra.

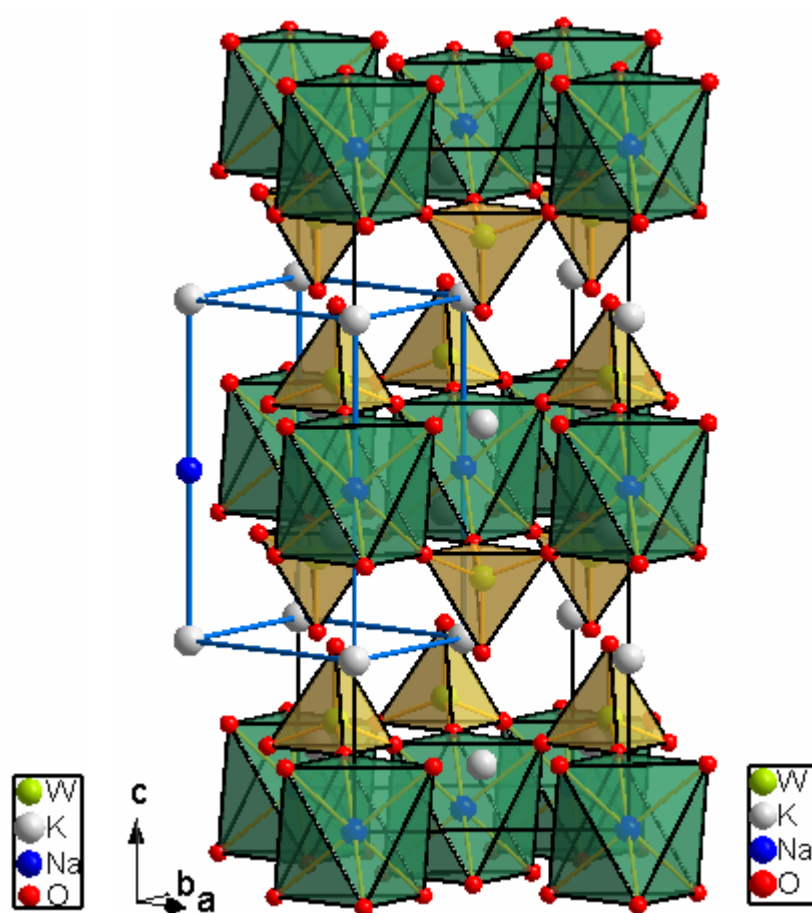


Figure 4-16: HT- $K_3Na(WO_4)_2$, drawn are WO_4 tetrahedra and NaO_6 octahedra. The hexagonal unit cell is drawn in blue, cell analogous to the monoclinic one in the LT-phase is drawn in red.

As many other members of the glaserite family, $K_3Na(WO_4)_2$ performs a phase transition from the trigonal form to a monoclinic form. With the tungstate the last missing member of the group 6, potassium sodium oxometallates is structurally characterized now, and the temperatures can be compared. The transition temperature seems to be mainly depending on the size of the MO_4 tetrahedron. While in $K_3Na(WO_4)_2$ the transition is finished at around $275\text{ }^\circ\text{C}$, the transition temperature in the corresponding molybdate, $K_3Na(MoO_4)_2$, with $240\text{ }^\circ\text{C}$ is in the

same range. The transition in the chromate, $K_3Na(CrO_4)_2$, is significantly lower, while in the sulphate glaserite, $K_3Na(SO_4)_2$, no phase transition could be detected at all.

Table 4-9: M-O bond lengths at room temperature and phase transition temperatures of some glaserite compounds.

Compound	M-O bond length [Å]	Phase transition temperature [°C]
$K_3Na(SO_4)_2$ [173]	1.472	-
$K_3Na(CrO_4)_2$ [170]	1.639	-34 °C
$K_3Na(MoO_4)_2$ [86]	1.773	240 °C
$K_3Na(WO_4)_2$	1.848	~250 °C

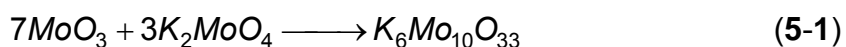
5. Chapter-5

5.1 Synthesis and Structure of $K_6Mo_{10}O_{33}$

As mentioned earlier, the family of alkali oxomolybdates is numerous and has been studied intensively. Among them, many molybdenum rich compounds are known, mainly belonging to the group of bronzes, but few of them are exhibiting singular crystal structures e.g. a three dimensional network of highly distorted edge sharing MoO_6 octahedra in $Na_6Mo_{11}O_{36}$ [175], a molybdenum oxide cluster framework built from the condensation of three Mo_6O_{18} units in $K_3Mo_{14}O_{22}$ [176], or double strings of edge sharing Mo_6 octahedra in KMo_4O_6 [10]. Because of these interesting structural properties, preparation of new molybdenum rich compounds became an important task. The most common methods of synthesizing such oxides involve the reaction between a molybdenum oxide and the hydroxide, nitrate, carbonate or the oxides of the corresponding alkali metals in argon as well as oxygen atmosphere. Here, the synthesis and characterization of one such new potassium molybdate is given in details. The idea of synthesizing low K/Mo ratio (i.e. molybdenum rich) resulted $K_6Mo_{10}O_{33}$ which can be related to the similar kind of silver, $Ag_6Mo_{10}O_{33}$ [177] and sodium phase, $Na_6Mo_{10}O_{33}$ [3].

5.1.1 Synthesis

The new potassium molybdate, $K_6Mo_{10}O_{33}$, was prepared from MoO_3 (Merck 99.5%) and K_2MoO_4 (Aldrich 99.5%). A mixture containing the stoichiometric amounts of the pre-dried reactants MoO_3 and K_2MoO_4 was thoroughly mixed, pressed as a pellet under 10^5 N, dried under vacuum (10^{-3} mbar) at 150 °C for 12 h, and placed under argon in a tightly closed steel container provided with a silver inlay. The reaction mixture was fired at 650 °C for 2 days and subsequently quenched to liquid nitrogen temperature.



Black needle like crystals were discovered in the silver inlay. The obtained black color product was sealed and stored in glass ampoules under argon for further investigations. All the analyses have been performed in an atmosphere of dry argon.

5.1.2 Thermal Analysis

Thermogravimetric measurements were performed with a Netzsch STA 409, Selb, coupled with a quadruple mass spectrometer. The container material for the thermal treatment (TGA and furnace) was of high purity Al_2O_3 . The sample was heated at the rate of 10 °C/min in a corundum crucible under a flow of dry argon. It was observed that the sample decomposes at around 950 °C and the residue left behind could not be traced out.

5.1.3 Powder Diffraction Analysis

The X-ray investigation on powder was performed on a STOE Stadi P diffractometer with Mo- $K\alpha_1$ radiation ($\lambda = 0.7103$) at room temperature using a position sensitive detector and a curved germanium monochromator in Debye-Scherrer geometry. Figure 5-1 shows the obtained powder diffractogram of the sample. On comparing the measured X-ray pattern with the data base [125], no proper match has been found out.

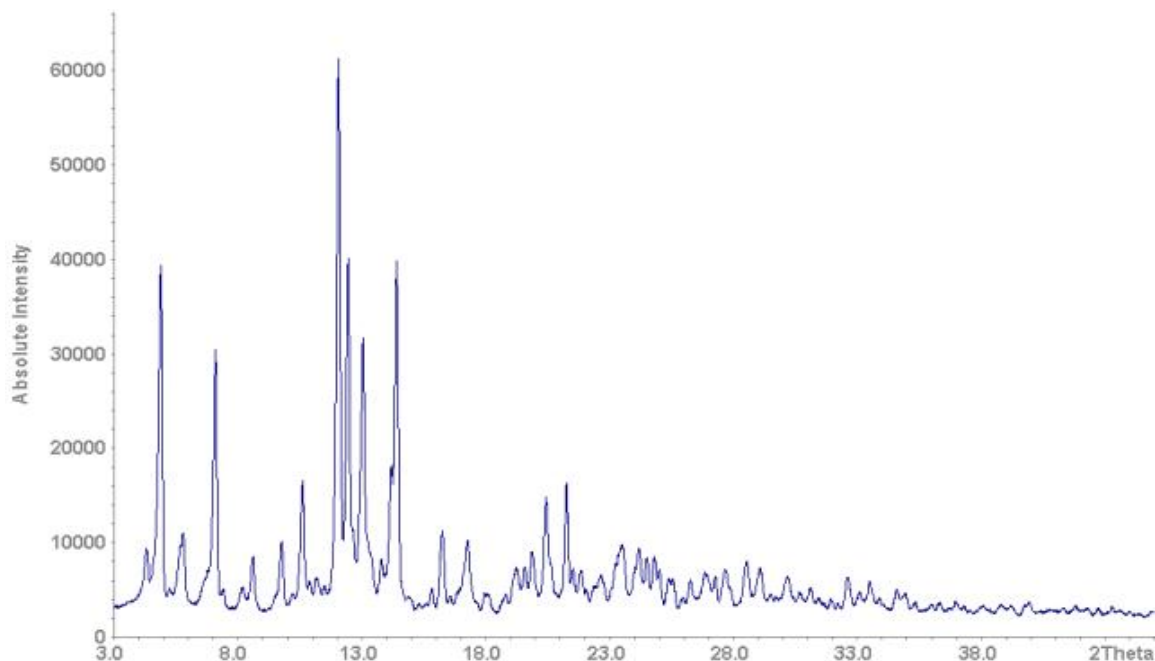


Figure 5-1: Measured X-ray powder diffractogram of $K_6Mo_{10}O_{33}$ with $Mo-K_{\alpha 1}$ radiation ($\lambda = 0.7103$) at room temperature.

5.1.4 Single Crystal Data

Single crystals of $K_6Mo_{10}O_{33}$ were selected in a glove box using a 0.1 mm glass capillary and were inserted into a 0.3 mm capillary which was then sealed under dry argon. Single crystal diffraction analysis was effected on a Bruker SMART-APEX CCD diffractometer at room temperature. $K_6Mo_{10}O_{33}$ crystallizes in the triclinic crystal system. All reflections were indexed with, $a = 7.7100 \text{ \AA}$, $b = 11.9659 \text{ \AA}$ and $c = 17.1321 \text{ \AA}$ with $\alpha = 86.42^\circ$, $\beta = 77.18^\circ$ and $\gamma = 74.14^\circ$. The structure has been solved in $P1$ and $P\bar{1}$. But, after the complete refinement, the quality factors in the non-centro symmetric space group R_1 and wR_2 , 6.81 % and 16.06 %, respectively (see Table 5-1), are significantly lower than those in $P\bar{1}$ ($R_1 = 8.64$ %, $wR_2 = 22.17$ %). Selected X-ray crystallographic data, with the better solution $P1$ of $K_6Mo_{10}O_{33}$ are presented in table 5-1. While all the atom parameters differ only slightly between both structure solutions, one significant structural change has been observed concerning the symmetrically created disorder of an oxygen atom, which will be

explained in the discussion part. The atomic parameters are listed in table 5-2, whereas the anisotropic thermal parameters are in table 5-3.

Table 5-1: Crystallographic data and Structure Refinement of $K_6Mo_{10}O_{33}$.

Empirical Formula	$K_6Mo_{10}O_{33}$
Formula weight /g mol ⁻¹	3443.94
Crystal system	Triclinic
Space group	$P 1$ (No. 1)
Lattice parameters /Å	$a = 7.7100(5)$ $\alpha = 86.42$ $b = 11.9659(8)$ $\beta = 77.18$ $c = 17.1321(1)$ $\gamma = 74.14$
Cell Volume /Å ³	1482.46
Z	2
Density calc. /g·cm ⁻³	3.8574
Crystal color and appearance	Black needles
Method of the refinement	Full-matrix least-squares on F^2
Parameters refined	554
R-Values	$R_1 = 6.76 \%$, $wR_2 = 16.06 \%$
Weight	$W = 1/(\sigma^2(F_o^2) + (0.0147 \times P)^2 + 76.19 \times P)$, where $P = (\max(F_o^2, 0) + 2 \times F_c^2)/3$
Diffractometer	Brucker SMART-APEX CCD
Monochromator	Graphite
Mo- K_α Radiation, λ	0.71073 Å
Maximum 2θ	69.965
Range of h, k, l	$-12 \leq h \leq 12$, $-19 \leq k \leq 18$, $-26 \leq l \leq 27$
Reflections collected	22776
Absorption coefficient mm ⁻¹	5.04
Independent reflections	20460
F(0 0 0)	1596
Temperature /K	295

Table 5-2: Atomic co-ordinates of $K_6Mo_{10}O_{33}$.

Atom	x	y	z	Atom	x	y	z
Mo1	0.67886	0.17153	0.49349	O4	0.78182	0.01077	0.41689
Mo2	0.82611	0.33016	0.99313	O5	0.69189	0.25187	0.40589
Mo3	0.78249	0.47193	0.38890	O6	0.46391	0.11323	0.49574
Mo4	1.24582	-0.01599	0.91231	O7	0.79742	0.48560	0.91175
Mo5	1.05186	0.50507	0.89268	O8	0.55794	0.38970	1.00172
Mo6	0.54875	0.50519	0.89258	O9	0.88538	0.23807	0.90662
Mo7	1.44207	0.00841	0.60738	O10	1.04327	0.38659	0.99227
Mo8	0.81880	0.03189	0.88615	O11	0.83567	0.23265	1.06766
Mo9	0.94409	0.00686	0.60579	O12	0.71636	0.48463	1.08407
Mo10	1.33510	0.51467	0.41657	O13	0.83955	0.42625	0.48760
Mo11	1.05722	-0.00751	0.39317	O14	0.94423	0.38398	0.32911
Mo12	0.55734	-0.00660	0.39257	O15	0.57767	0.49033	0.34510
Mo13	0.94819	0.49542	1.10661	O16	0.82811	0.60357	0.37225
Mo14	0.45002	0.49677	1.10701	O17	1.32968	-0.06729	1.01365
Mo15	1.17636	0.67618	1.00347	O18	1.29029	0.11505	0.90423
Mo16	1.31921	-0.17404	0.50994	O19	1.06479	0.01473	0.84244
Mo17	0.66022	0.48222	0.58619	O20	1.43046	-0.11012	0.85219
Mo18	0.75977	0.02201	1.08370	O21	1.16652	0.39992	0.81952
Mo19	1.20699	0.52399	0.61491	O22	0.59952	0.38980	0.83288
Mo20	1.18342	-0.02197	1.11044	O23	1.33021	0.12846	0.66539
K1	0.98398	0.26140	0.75253	O24	1.47885	-0.10828	0.67019
K2	0.49982	0.74187	0.27089	O25	0.71209	0.11679	0.81606
K3	1.12243	0.25570	0.52411	O26	1.21253	0.61226	0.35120
K4	1.26802	0.23706	0.24709	O27	1.29839	0.37795	0.41027
K5	1.35580	0.24644	1.00810	O28	0.99094	0.63831	0.84673
K6	0.22434	0.77284	0.75922	O29	0.91218	0.14008	0.65681
K7	0.73831	0.76672	0.75107	O30	0.94312	-0.08815	0.67960
K8	0.64891	-0.23956	0.98109	O31	0.79424	-0.09544	0.87468
K9	0.76587	0.24127	1.23988	O32	0.54424	0.61330	0.82502
K10	0.87349	0.74117	0.48207	O33	1.02396	-0.00276	1.01296
K11	0.49541	0.27393	0.73456	O34	1.53793	0.49225	0.48280
K12	1.01773	0.72806	0.24462	O35	0.97173	0.61334	1.00836
O1	0.93660	0.11432	0.49452	O36	1.27108	0.53061	0.91874
O2	0.69894	0.02433	0.58629	O37	1.05642	-0.10996	0.51035
O3	0.61106	0.27558	0.56911	O38	1.43521	0.61511	1.00009

Atom	x	y	z
O39	1.21809	-0.01265	0.58149
O40	1.30313	-0.02745	0.41473
O41	1.52932	-0.11542	0.50160
O42	1.39289	-0.27095	0.43332
O43	1.30763	-0.26087	0.59282
O44	1.17136	0.77693	0.92414
O45	1.07031	0.10195	0.32225
O46	1.10918	0.76052	1.08353
O47	0.20808	0.51799	1.08397
O48	0.41315	0.61285	1.16888
O49	1.01786	0.37514	1.15937
O50	0.66668	-0.12370	0.33201
O51	0.44844	0.37536	1.16498
O52	0.50959	0.10192	0.32781

Atom	x	y	z
O53	0.85270	0.59319	1.18012
O54	1.15011	0.57170	0.51665
O55	1.09263	-0.13348	0.34610
O56	1.42252	0.50501	0.65485
O57	0.69675	0.61231	0.59385
O58	0.77276	0.39939	0.64716
O59	1.29334	-0.11979	1.17224
O60	1.16372	0.38704	0.63130
O61	1.03354	0.62681	0.68185
O62	0.92344	0.00146	1.15268
O63	0.66748	0.08345	0.98805
O64	0.69063	-0.08486	1.09934
O65	1.21585	0.12022	1.12758
O66	0.59264	0.11062	1.14565

Table 5-3: Anisotropic displacement parameters of $K_6Mo_{10}O_{33}$. (\AA^2).

Atom	U_{11}	U_{22}	U_{33}	U_{12}	U_{13}	U_{23}
Mo1	0.01214	0.01162	0.01053	-0.00284	-0.00420	-0.00279
Mo2	0.01204	0.01089	0.02051	-0.00421	-0.00363	0.00210
Mo3	0.01940	0.02233	0.02282	-0.00328	-0.00542	-0.00023
Mo4	0.01496	0.02141	0.02080	-0.00443	-0.00093	-0.00423
Mo5	0.01039	0.01182	0.01284	-0.00418	-0.00242	-0.00180
Mo6	0.00858	0.01374	0.00951	-0.00368	-0.00424	-0.00001
Mo7	0.00987	0.01809	0.01255	-0.00464	-0.00124	0.00185
Mo8	0.02453	0.01401	0.03236	-0.00344	0.00135	0.00100
Mo9	0.01205	0.01697	0.00854	-0.00437	-0.00389	-0.00036
Mo10	0.01821	0.02155	0.02966	-0.00710	-0.01039	0.00765
Mo11	0.00585	0.00944	0.01360	-0.00157	-0.00128	-0.00100
Mo12	0.01044	0.01202	0.01005	-0.00507	-0.00431	-0.00166
Mo13	0.00930	0.01659	0.01024	-0.00474	-0.00329	0.00034
Mo14	0.01101	0.01286	0.01313	-0.00228	-0.00088	-0.00139
Mo15	0.01067	0.01194	0.00772	-0.00252	-0.00172	-0.00088
Mo16	0.01083	0.01214	0.01670	-0.00330	-0.00268	0.00470
Mo17	0.02407	0.02426	0.02406	-0.00898	-0.01436	0.00365

Atom	U_{11}	U_{22}	U_{33}	U_{12}	U_{13}	U_{23}
Mo18	0.01396	0.02382	0.02698	-0.00659	0.00330	-0.00029
Mo19	0.02622	0.02470	0.01923	0.00159	-0.00913	-0.00212
Mo20	0.01823	0.02724	0.01968	0.00171	-0.00034	0.00123
K1	0.02985	0.04293	0.03007	-0.02088	-0.00484	-0.00454
K2	0.02400	0.02877	0.02477	-0.00947	-0.00837	-0.01447
K3	0.02540	0.02458	0.02864	-0.00997	-0.00942	-0.00281
K4	0.01109	0.03891	0.02598	-0.00997	-0.00238	0.02145
K5	0.02168	0.01557	0.08422	-0.00770	-0.02101	0.00056
K6	0.03303	0.03519	0.01217	-0.01323	-0.00733	0.00191
K7	0.02337	0.01653	0.05125	-0.00237	-0.00447	-0.00137
K8	0.02291	0.02528	0.05563	-0.00808	-0.00803	0.00608
K9	0.04164	0.05367	0.04984	-0.02763	-0.01267	0.01083
K10	0.01872	0.01771	0.07054	-0.00451	-0.01472	0.00752
K11	0.03620	0.02508	0.02123	-0.00465	-0.00572	-0.00395
K12	0.02338	0.02364	0.01610	-0.00784	-0.00523	-0.00911
O1	0.01187	0.01029	0.02543	0.00216	-0.00741	-0.00931
O2	0.00390	0.03110	0.00889	-0.00806	-0.00881	0.00446
O3	0.02493	0.02436	0.01073	-0.00567	-0.00969	-0.01836
O4	0.00179	0.00386	0.01497	0.00057	0.00019	-0.00196
O5	0.02806	0.01685	0.03268	-0.01549	-0.00521	0.00455
O6	0.02197	0.01969	0.01448	-0.01401	-0.00710	0.01329
O7	0.00380	0.00831	0.01627	-0.00257	0.00032	0.00033
O8	0.02404	0.01857	0.03666	-0.01214	-0.02052	0.01399
O9	0.04254	0.02252	0.01288	-0.00205	-0.00895	-0.00152
O10	0.00989	0.00719	0.00663	-0.00318	-0.00018	-0.00074
O11	0.02609	0.00021	0.05530	-0.00804	0.00751	0.00574
O12	0.01171	0.01248	0.00765	-0.00276	-0.00173	-0.00197
O13	0.04100	0.03185	0.01130	-0.01167	0.00289	-0.00278
O14	0.01916	0.03487	0.02052	0.00001	0.00220	-0.00431
O15	0.00789	0.03735	0.06179	-0.00766	0.00874	-0.00683
O16	0.03833	0.03274	0.04988	-0.02754	-0.00975	0.01155
O17	0.03613	0.03134	0.02345	-0.01755	-0.00941	0.00557
O18	0.02897	0.00001	0.03442	0.00442	-0.00405	-0.00703
O19	0.02397	0.03064	0.05614	-0.00299	-0.03382	-0.00638
O20	0.01435	0.04597	0.02344	0.00558	0.01904	-0.00761
O21	0.01687	0.01135	0.02756	0.00222	0.00468	-0.00251
O22	0.01907	0.03407	0.00984	-0.00403	0.00111	-0.00929
O23	0.02369	0.02843	0.03014	-0.00505	-0.00490	0.01257

Atom	U_{11}	U_{22}	U_{33}	U_{12}	U_{13}	U_{23}
O24	0.03083	0.01995	0.02276	-0.01487	-0.00479	0.01960
O25	0.02960	0.05074	0.02617	0.00643	0.00326	0.01179
O26	0.01668	0.03943	0.04133	0.01509	-0.01603	-0.01120
O27	0.01135	0.03099	0.07953	-0.01315	-0.00185	-0.00177
O28	0.04448	0.00959	0.03368	-0.00262	-0.01684	-0.00494
O29	0.05705	0.02360	0.03177	-0.01001	-0.00488	0.00067
O30	0.03322	0.02607	0.01163	-0.01373	-0.00437	-0.01008
O31	0.02429	0.01836	0.03782	-0.00743	-0.00658	-0.00385
O32	0.02238	0.02193	0.02939	0.00626	-0.00436	0.00079
O33	0.01104	0.02205	0.03455	0.00619	-0.00267	-0.01223
O34	0.02657	0.01708	0.03753	-0.00324	-0.01734	0.00633
O35	0.01088	0.02397	0.02615	-0.00250	-0.01512	0.00332
O36	0.00638	0.01685	0.02683	0.00131	-0.00136	-0.01397
O37	0.00892	0.01960	0.00645	-0.00599	0.00024	0.00229
O38	0.00396	0.01039	0.00768	0.00271	0.00385	-0.00812
O39	0.02103	0.05463	0.01710	-0.01760	-0.00916	-0.00438
O40	0.01845	0.01630	0.03129	-0.00255	0.00365	0.00224
O41	0.00489	0.01359	0.01687	0.00284	-0.00519	-0.01120
O42	0.01830	0.01443	0.04900	0.00035	-0.00779	0.00845
O43	0.01618	0.01899	0.00954	0.00776	-0.00368	-0.00071
O44	0.01072	0.04179	0.00085	0.00374	-0.00515	0.00963
O45	0.01490	0.02328	0.03991	-0.01258	-0.00474	0.02722
O46	0.01241	0.01860	0.00835	-0.00180	-0.00380	-0.00393
O47	0.01906	0.04650	0.01714	-0.01123	-0.00714	-0.00050
O48	0.04050	0.01400	0.05234	-0.00587	-0.02203	-0.01687
O49	0.01832	0.02514	0.00971	-0.01334	-0.01192	0.01038
O50	0.01519	0.01803	0.03418	-0.00973	0.00856	-0.02687
O51	0.02378	0.02303	0.02017	-0.01476	-0.00291	0.00797
O52	0.02030	0.03723	0.02171	-0.00557	-0.01716	-0.00308
O53	0.00636	0.03563	0.02613	-0.00187	-0.00091	-0.02291
O54	0.03097	0.04676	0.02750	-0.00264	-0.00436	0.00385
O55	0.01076	0.01759	0.00826	0.00361	-0.00896	-0.01377
O56	0.02478	0.02293	0.04901	-0.00515	-0.01233	0.01242
O57	0.05797	0.01390	0.02116	-0.01741	-0.01444	-0.00123
O58	0.02543	0.01838	0.02034	-0.00722	-0.01096	0.00536
O59	0.04053	0.02507	0.02702	-0.00527	-0.01409	-0.00163
O60	0.04233	0.02713	0.04789	-0.00149	-0.00618	-0.00856
O61	0.03515	0.04798	0.02356	0.02167	0.00063	-0.02931

Atom	U_{11}	U_{22}	U_{33}	U_{12}	U_{13}	U_{23}
O62	0.03001	0.01730	0.04356	0.00399	-0.00566	0.00540
O63	0.04044	0.02491	0.02507	0.00290	-0.01289	-0.00666
O64	0.07217	0.23973	0.05087	-0.13027	-0.04965	0.09257
O65	0.03523	0.03792	0.05207	-0.02471	-0.00987	0.00480
O66	0.03082	0.01339	0.03750	-0.00630	-0.02147	-0.00392

5.1.5 Structure Description and Discussion

$K_6Mo_{10}O_{33}$ consists of sheets of MoO_6 octahedra lying in the crystallographic ab - plane and K^+ ions are connecting them. The sheets, one is shown in figure 5-2, are build from infinite chains of edge-sharing octahedra (drawn with close polyhedral faces) and groups of four octahedra (open polyhedra).

The chains running parallel to $[100]$ are formed by edge sharing octahedra with a translational period of six different (and symmetrically independent) Mo centers. The distortions present in the MoO_6 octahedra are shown by the Mo-O distances listed in table A of appendix. In all cases the molybdenum atoms are displaced from the ideal positions in the centre of the octahedra, resulting in two short (Mo-O range from 1.647-1.802 Å), two medium (1.909-2.044 Å), and two long Mo-O distances (2.091-2.341 Å). Such coordinations are frequently observed in molybdenum oxides like e. g. MoO_3 [178], $K_2Mo_3O_{10}$ [50], $K_6Mo_7O_{24} \cdot 4 H_2O$ [179], or $Na_2Mo_2O_7$ [6].

The chains are linked in the second dimension by Mo_4O_{17} groups via common vertices. These units can be described as four strongly distorted MoO_6 octahedra connected by common edges and altogether sharing one central oxygen atom as shown in figure 5-3 and figure 5-4. The molybdenum atoms are not forming a square, but a rhombus with angles of 78° and 102° , the dihedral angles are below 1° , so the four molybdenum atoms are in plane.

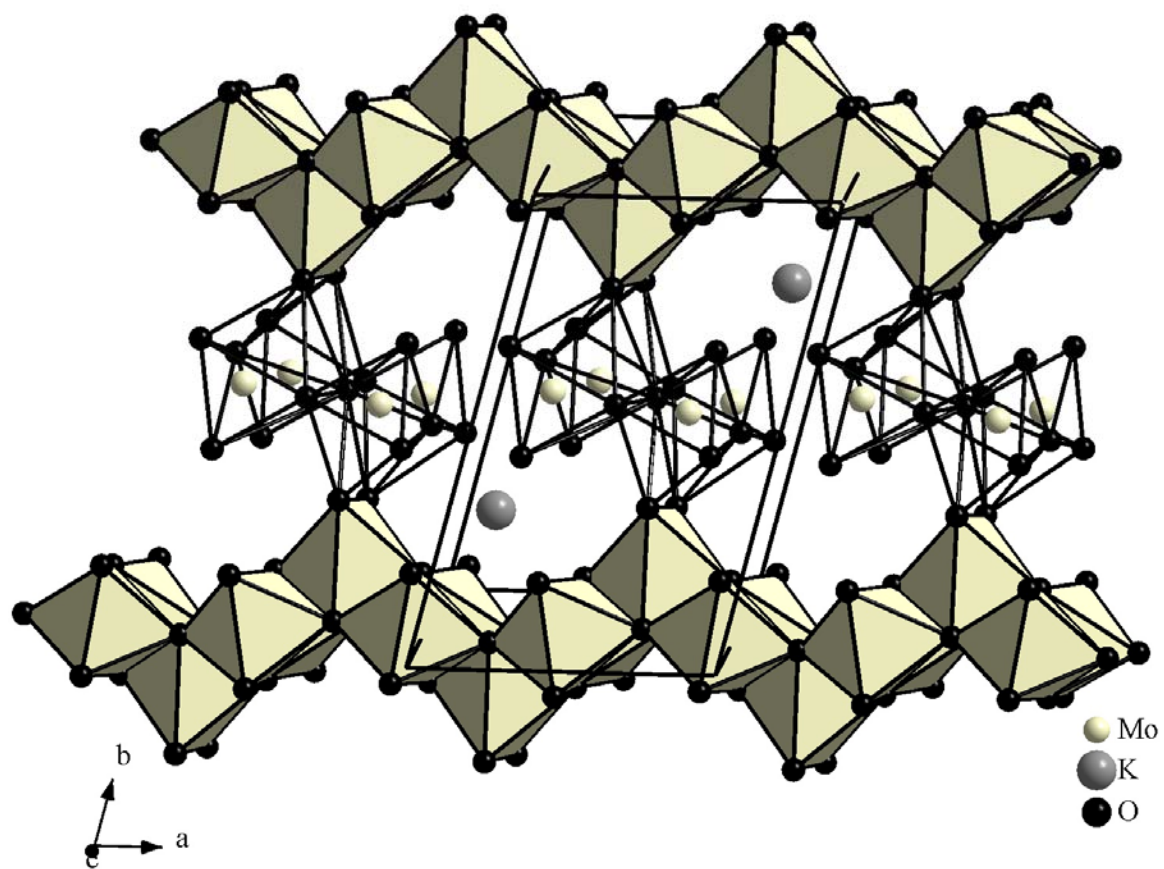


Figure 5-2: Perspective view of the crystal structure of $K_6Mo_{10}O_{33}$ along $[001]$.

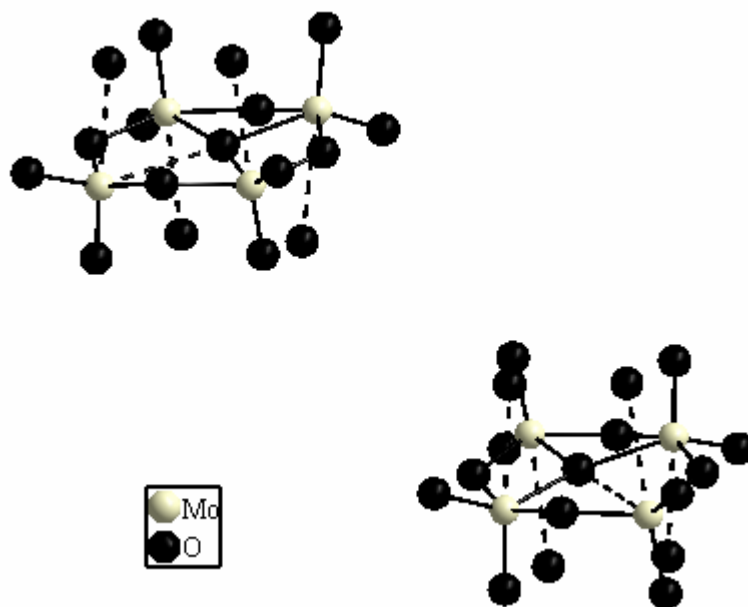


Figure 5-3: The two symmetrically independent Mo_4O_{17} groups of the structure solution in $P1$, dotted lines represent bonds longer than 2.64 Å.

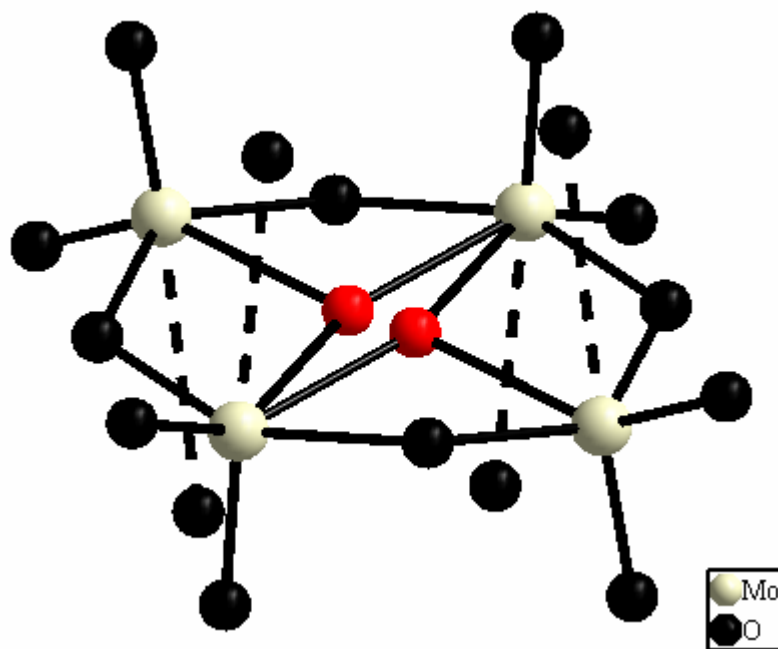


Figure 5-4: Mo_4O_{17} group of the centrosymmetric structure solution ($P\bar{1}$), positions of red oxygen atoms are half occupied, dotted lines represent bonds longer than 2.69 Å.

Studying the figure 5-2, one can expect to find an inversion centre in the crystal structure. As mentioned above, the main reason to exclude this symmetry element is a slight difference concerning the position of an oxygen atom. The relevant oxygen lies in the middle of the Mo_4 rhomb, but is shifted away from the exact centre. The more remote molybdenum atom appears in the distances of 2.907 Å and 2.965 Å for both symmetrically independent individuals, respectively. In the centrosymmetric structure solution, the central oxygen atom is created at two positions by the inversion centre (Figure 5-4) with an occupation factor of 0.5 each, resulting in significantly higher R values after complete refinement and so this disorder seems to be an artifact of the symmetry element.

Another distortion is observed for the Mo coordination. Although, the four molybdenum atoms of the Mo_4O_{17} groups are nearly in plane, they are displaced from the centre of the octahedra again. For each molybdenum atom, two short, two intermediate and two long Mo-O bonds were observed. But, here the larger distances are extremely long (bond lengths more than 2.645 Å are represented by dotted lines in figure 5-4). Due to the irregular and partially very large Mo-O distances in these Mo_4O_{17} units, the coordination polyhedra should be described as square pyramids and one tetrahedron instead of heavily distorted octahedra. In figure 5-5, the polyhedral representation of one Mo_4O_{17} unit is shown.

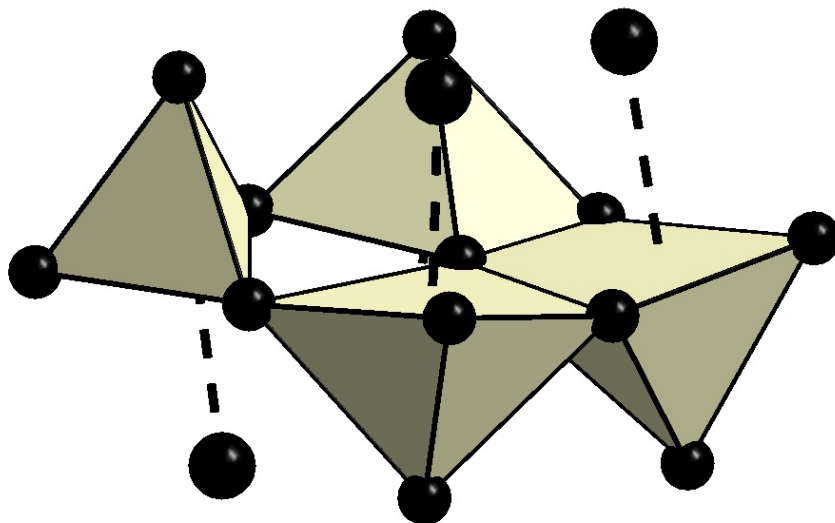


Figure 5-5: Mo_4O_{17} groups in polyhedral representation in $P1$.

The potassium atoms shown in figure 5-2 are lying in the sheet of plane, situated in the holes left by the MoO_6 octahedra. The other K^+ ions, in total eight of twelve over the whole unit cell, are spacing the sheets. The potassium ions are coordinated by irregular polyhedra of oxygen atoms with the K-O distances ranging continuously from 2.498 Å to higher values, so a sharp gap between the first and the higher coordination spheres cannot be observed. If only K-O distances below 3.3 Å are taken into account, these coordination polyhedra around K^+ are built from 7 to 9 oxygen atoms each.

The crystal structure of $K_6Mo_{10}O_{33}$ shows significant similarities to the related phases reported earlier by Gatehouse *et al.* containing sodium [3] and silver [177]. The infinite chains are identical to those found in both related compounds, including the 2+2+2 MoO_6 coordination. Also the connection of these chains into sheets of MoO_6 octahedra described here is found in the related silver phase, $Ag_6Mo_{10}O_{33}$, with an identical connection pattern. Nevertheless, the stacking of the sheets is differing (as seen in figure 5-6 and figure 5-7) which results in doubling of one crystallographic axis in the new compound.

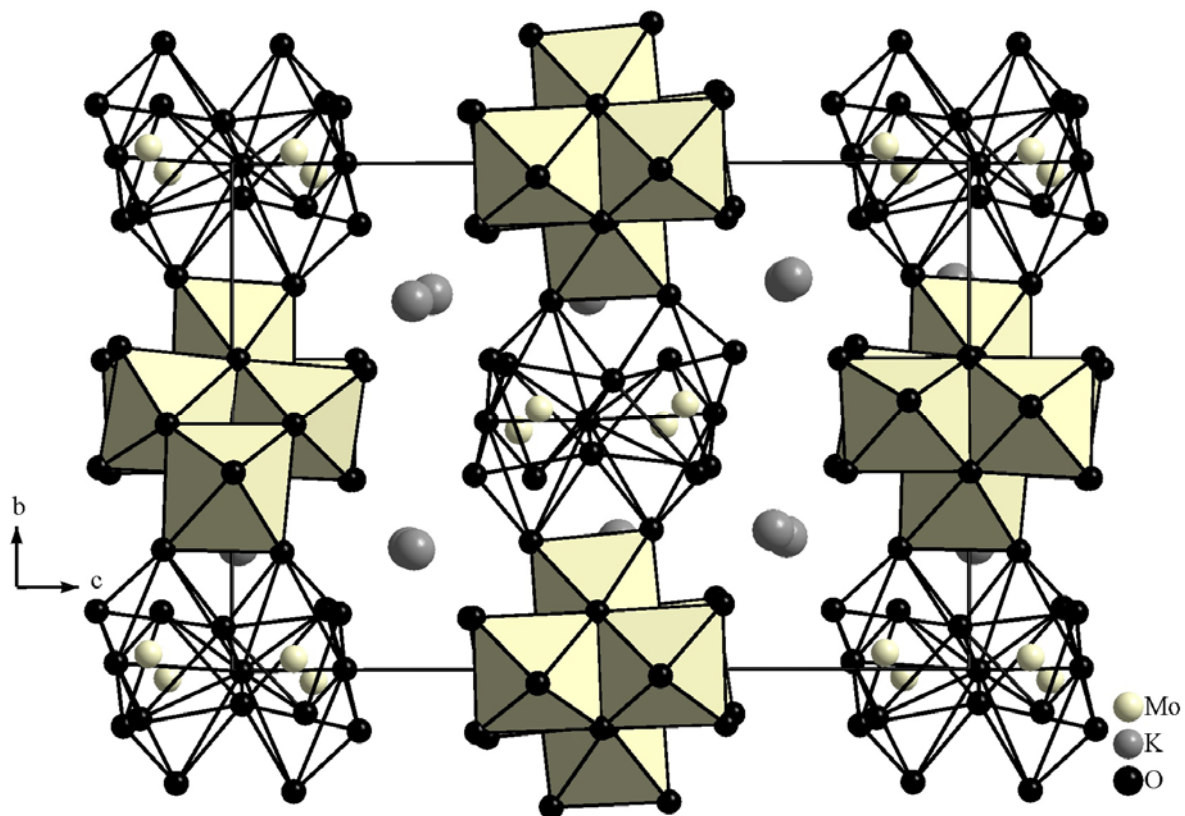


Figure 5-6: Crystal structure of $K_6Mo_{10}O_{33}$, viewing direction $[100]$.

The arrangement of the infinite chains in $Na_6Mo_{10}O_{33}$ (Figure 5-8) relative to the other chains is identical to that observed in $Ag_6Mo_{10}O_{33}$. So the silver compound shows features of both related alkali metal molybdates and can be regarded as a structural intermediate. The differences in the crystal structure are clearly effected by the variation of the cation, mainly due to the size of the cations. At first the lattice constant perpendicular to the sheets in the potassium and silver compounds, and parallel to the linking chain in $Na_6Mo_{10}O_{33}$ increases with the diameter of the respective cation (Na: $a = 8.05 \text{ \AA}$, Ag: $b = 8.31 \text{ \AA}$, K: $c = 17.13 \text{ \AA}$, which is $2 \times 8.57 \text{ \AA}$). While in $K_6Mo_{10}O_{33}$ and $Ag_6Mo_{10}O_{33}$, the sheet separations are too large to bridge them with an MoO_6 octahedron, this is possible in the sodium compound, so the unfavorable configuration of a quadrangle of MoO_6 octahedra can be avoided in favor of a configuration where no oxygen atom belongs to more than three different MoO_6 octahedra (Figure 5-9).

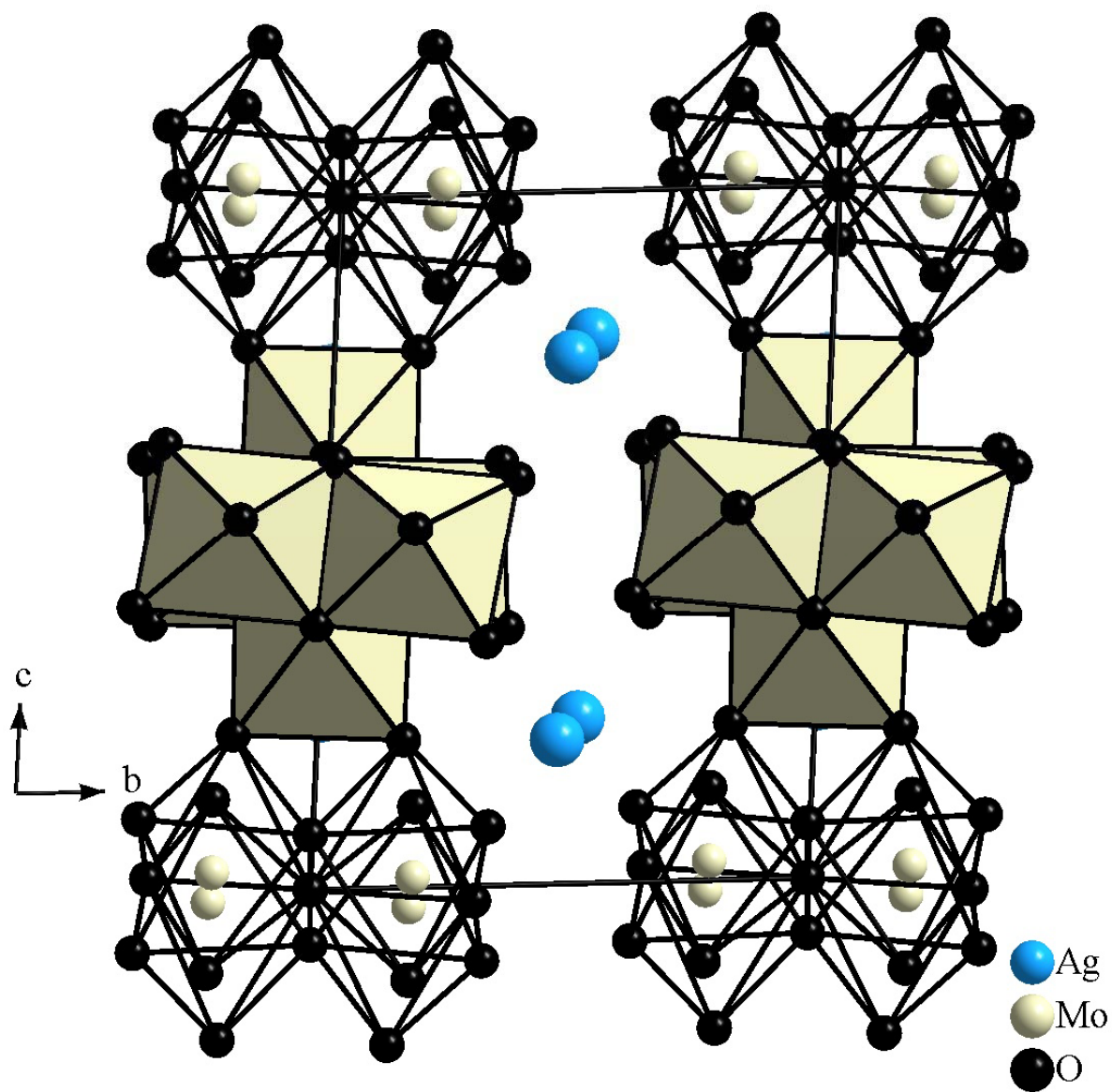


Figure 5-7: Crystal structure of $Ag_6Mo_{10}O_{33}$, viewing direction $[100]$.

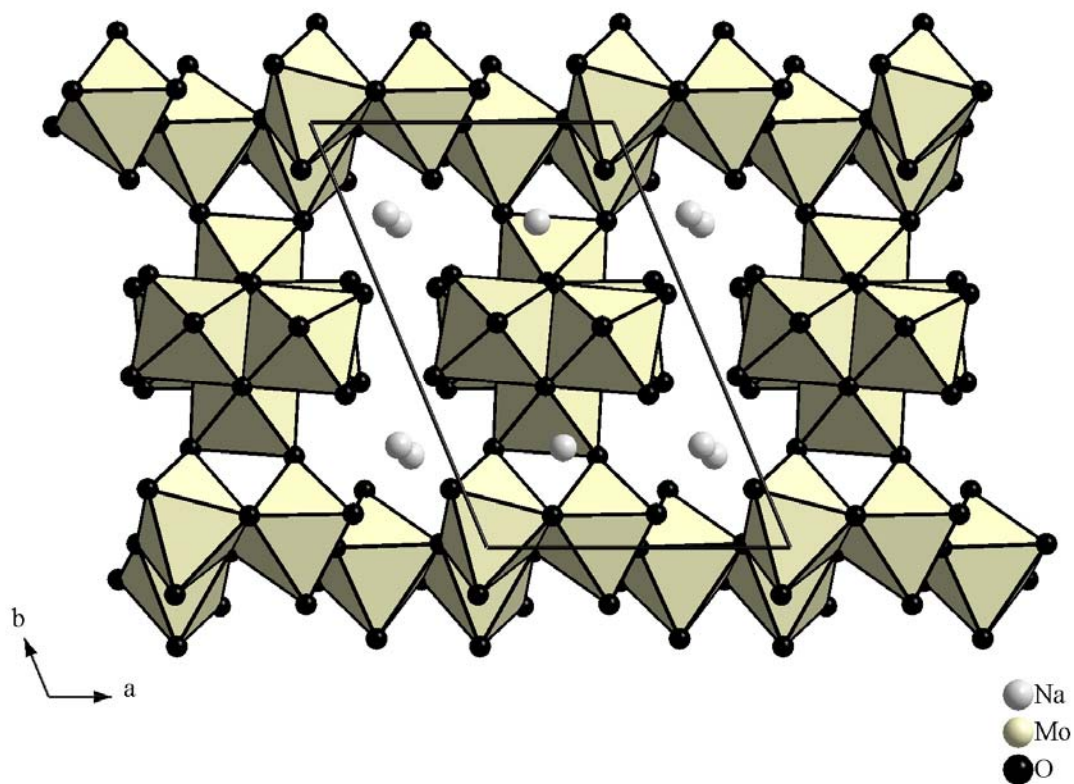


Figure 5-8: Crystal structure of $Na_6Mo_{10}O_{33}$. (The infinite chains identical in all structures shown are running parallel to viewing direction)

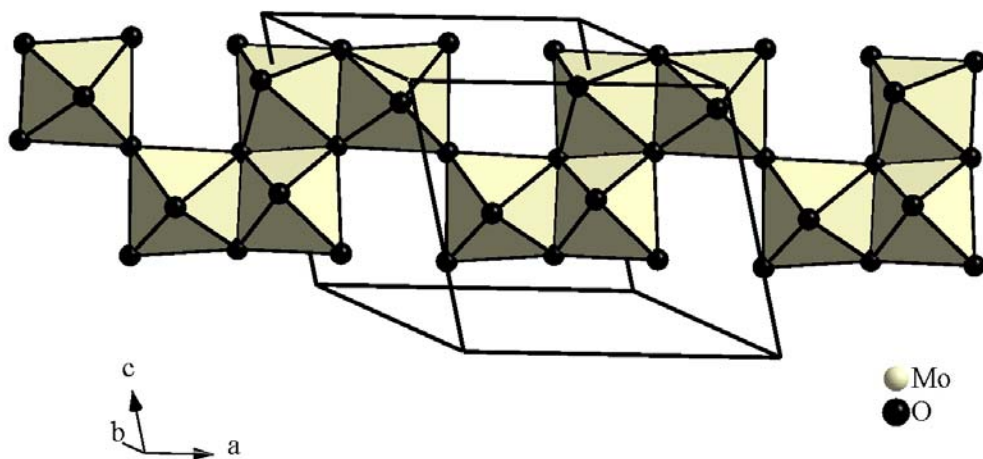


Figure 5-9: $\frac{1}{\infty}[Mo_4O_{17}]$ chains in $Na_6Mo_{10}O_{33}$.

The new potassium molybdate, $K_6Mo_{10}O_{33}$, shows close structural relationship with $Na_6Mo_{10}O_{33}$ and $Ag_6Mo_{10}O_{33}$ as mentioned above. Besides this, the synthetic conditions necessary to prepare the novel compound are close to those leading to $K_2Mo_3O_{10}$. Due to this, attempts to reproduce $K_6Mo_{10}O_{33}$ resulted in the neighboring phase, $K_2Mo_3O_{10}$, and a further characterization actually lack of a sufficient amount of pure samples.

5.2 Oxynitrides of the Nominal Composition $A_3MO_{4-n}N_n$

Cubic phases of formula $A_6M_2O_9$ with $A = K, Rb$ or Cs and $M = Nb, Mo$ or W , were obtained by the solid state reactions between A_2O and A_2MO_4 [21]. Their polymorphism was studied by using differential thermal analysis and high temperature X-ray diffraction. For $K_6Mo_2O_9$, three different phases have been found, an orthorhombic phase below 450 °C, a hexagonal one up to 750 °C and a face centered cubic elpasolite type one. The RT forms of Rb and K are isostructural, and their crystal structure is not known so far. Also the structures of related cubic phases such as K_3NbO_4 [180], $Na_6W_2O_9$ [21] etc. are not yet solved. The X-ray pattern of these compounds states that all these solids are of same kind with F - centered lattice. Former reports state that there are some kinds of disorder in the structure, and thus leading in problems in finding out the exact positions of the atoms. The problems in solving the crystal structures of these phases may also arise from insufficient data/methods for finding out the exact chemical formulae of the substances obtained. For the basic understanding of the material, solving the crystal structure became an important task and so, attempts have been made to synthesize and characterize these compounds.

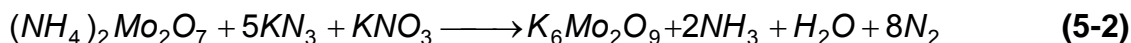
By using this azide–nitrate/nitrite route, we have produced plenty of oxometallates of molybdenum as well as tungsten. This is a very simple route for preparing many air or moisture sensitive molybdates. For synthesizing these cubic phases, azide-nitrate route was adopted. The results we found were quite different from the one which was reported. Here, the syntheses and characterizations of the above mentioned cubic phases are described.

5.2.1 K_3MoO_3N

5.2.1.1 Synthesis of “ $K_6Mo_2O_9$ ”

Preparations aiming in $K_6Mo_2O_9$ were performed via the azide route by the solid state reaction between potassium molybdate and potassium azide. The reactants are initially dried under vacuum for about 12 h. The dried starting materials, K_2MoO_4 and KN_3 were mixed in the ratio of 1:1. Then they were ground in a ball-mill, pressed as a pellet under 10^5 N, dried under vacuum (10^{-3} mbar) at 150 °C for 12 h, and placed under argon in a tightly closed steel container provided with a silver inlay. In a flow of dry argon, the following temperature treatment was applied: 25 °C → 260 °C (90 °C/h) → 380 °C (5 °C/h) → 600 °C (50 °C/h, 40 h) → 30 °C (20 °C/h).

Similar products are obtained when the reaction is modified considerably, e.g. from a $K_2MoO_4:KN_3$ of 1:4. The pure compound was obtained by the reaction of ammonium molybdate with corresponding alkali azide-nitrate mixture, as shown below. But, attempts to reproduce by this way were not successful.



Besides this, other reactions containing potassium oxide, potassium peroxide, elemental molybdenum and different molybdenum oxides were carried out, but the phase prospected was not detected from these experiments. These findings lead us to presume an oxynitride concealed behind “ $K_6Mo_2O_9$ ” as well as the related compounds with this nominal composition. The colorless hygroscopic product obtained from successful experiments was sealed and kept for further investigations in glass ampoules under dry argon. All the analyses have been performed in an atmosphere of dry argon.

5.2.1.2 Powder Diffraction Analysis

For X-ray powder diffraction analysis, the samples were sealed in Lindmann capillaries of 0.3 mm diameter. The measurement was effected on a STOE StadiP diffractometer with $Cu-K_{\alpha 1}$ radiation ($\lambda = 1.5406$ Å) at room temperature using a

position sensitive detector (angle range 6°) and a curved germanium monochromator in Debye-Scherrer geometry. The powder diffraction data were collected in the 2θ range of 5 and 120° . Silicon was used as an external standard. The XRD pattern (see Figure 5-10) obtained is found to be identical to that of the earlier reported compound named as “ $K_6Mo_2O_9$ ”, and that of cubic K_3NbO_4 phase. All reflections of the measured diffractogram were indexed ($a = 8.60 \text{ \AA}$) with the program WinXPOW [153].

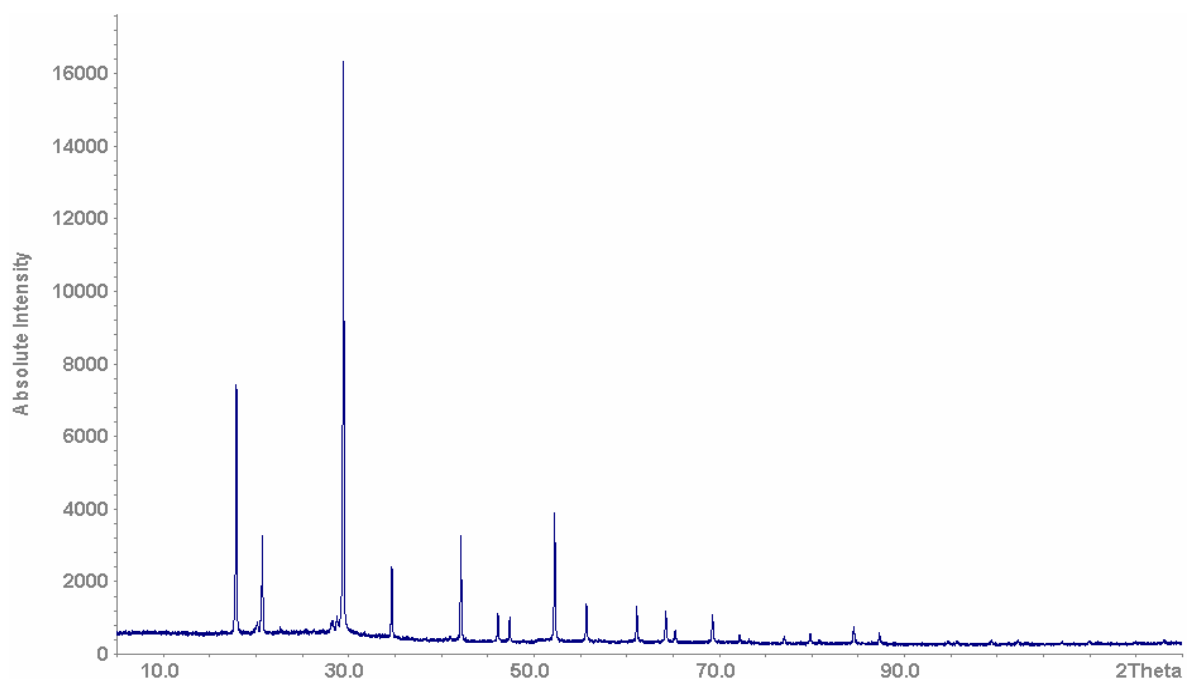


Figure 5-10: X-ray powder diffraction analysis of $K_6Mo_2O_9$ with $Cu-K_{\alpha 1}$ radiation ($\lambda = 1.5406$) at room temperature.

5.2.1.3 Single Crystal Measurement

In order to get the single crystals of the compound, the obtained product was annealed for 45 days at the temperature of about 550°C . Small colorless crystals were picked in the glove box using 0.1 mm glass capillary and were inserted into a 0.3 mm capillary which was sealed under dry argon. Single crystal diffraction data were recorded on a Bruker SMART-APEX CCD diffractometer at room temperature after mounting the crystals. The data from the single crystal shows the presence of disorder in the system which is explained in the structural part.

5.2.1.4 Thermal Analyses

The thermal behavior of the sample was investigated by DT/TG analyses (STA 409, Netzsch, Selb) coupled with a quadruple mass spectrometer. The sample was heated at the rate of 10 °C/min in a corundum crucible under the flow of dry argon. It was observed that the solid decomposes at around 700 °C. As the residue was in the molten state, a further analysis of the same was not performed.

5.2.1.5 Magnetic Measurement

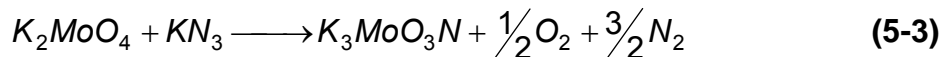
Approximately 40 milligrams of the sample was sealed in a quartz tube under the flow of dry helium. Magnetic measurement was performed by using a Superconducting Quantum Interference Device (SQUID), MPMS 5, 5-330 K (Quantity Design, San Diego, CA, USA). From the results of magnetic measurements, the sample was found to be diamagnetic which shows the molybdenum atom being in the oxidation state of +6.

5.2.1.6 DSC measurements

In order to detect phase transitions, high and low temperature DSC measurements were carried out. The result from the DSC measurement shows that there are no such phase transitions of the cubic phase obtained. This result is in contradiction to the one which has been reported earlier.

5.2.1.7 Chemical Analyses

As the solid is moisture sensitive, few milligrams of the solid was then sealed in small capsules/containers inside the glove box and were further chemically analyzed. From the result, it was found that the sample contains some amounts of nitrogen. The ratio of the cations, K: Mo, as well as that of the anions, O: N, is found to be 3:1 respectively. The chemical formula of the solid obtained according to the chemical formula was reduced to K_3MoO_3N . This formula is in accordance with the results obtained by the magnetic measurements. So, the synthesis equation can be written as



5.2.1.8 Raman Measurement

The powder sample was packed in a 0.3 mm quartz capillary under the flow of argon and a Raman measurement was recorded with a microscope laser Raman system (Jobin-Yvon, LabRam) operating at the laser lines of a He-Ne (632.8 nm) and a Diode-Laser (784.7 nm) at 20mW. Figure 5-11 shows the Raman spectrum of the cubic potassium molybdenum oxynitride, K_3MoO_3N .

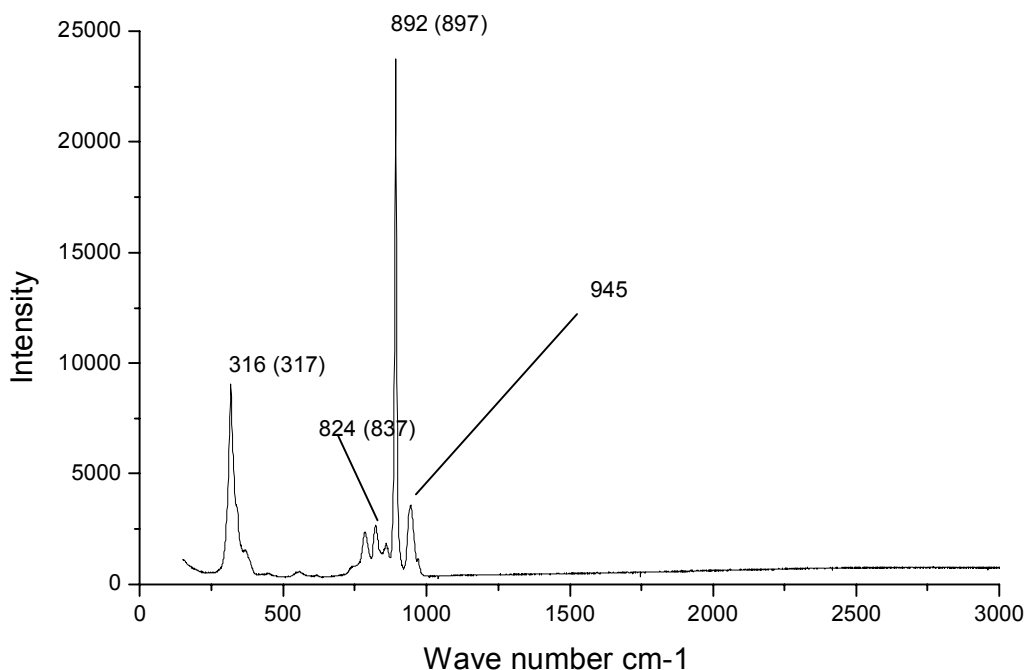


Figure 5-11: Raman spectrum of K_3MoO_3N (shifts of MoO_4 tetrahedra units [181] given in the brackets)

Raman spectra of molybdenum oxynitrides have not been reported earlier and so we had to compare the obtained fingerprints with the nearest known oxides. The measured Raman modes are very close to those of MoO_4 tetrahedra units (ν_1 : 897 cm^{-1} , ν_2 : 317 cm^{-1} and ν_3 : 837 cm^{-1} respectively [181]). The stronger modes observed at 316 , 824 and 892 cm^{-1} were obtained because of the presence of

MoO₃N tetrahedra, while the weaker modes and shoulders observed at around 330, 790 and 860 cm⁻¹ could be a result of undoped MoO₄ tetrahedra or other possible tetrahedra. This may be because of the possibility of co-crystallinity which exists between K₂MoO₄ and K₃MoO₃N solids (similar to the co-crystals of Na₃PO₄ and Na₂SO₄). The presence of K₂MoO₄ may be in a small quantity that it was not detected by X-ray diffraction but Raman measurements are more precise and sensitive for even smaller quantities, we observe the presence of MoO₄ tetrahedra along with MoO₃N tetrahedra in the sample.

5.2.1.9 Structure Description

The crystal structure of K₃MoO₃N was determined from single crystal data. X-rays are limited to find the presence of nitrogen in the sample, whereas it was detected by the elemental analysis. Because of the small difference in the scattering lengths of nitrogen and oxygen, we were unable to distinguish between fully ordered, fully disordered, or partially ordered anions. No systematic absences other than those due to the face centering condition are apparent and there are five possible space groups $F23$, $F\bar{4}3m$, $F432$, $Fm\bar{3}$ and $Fm\bar{3}m$. Many compounds, with a general formula A₃MO₄ (with A = Na, K, Rb, M = P, Nb), including the good ionic conductor Na₃PO₄, which can be seen as a parent compound for this family, were already investigated. All the results are similar and suggest that the MO₄ groups are subject to extensive (rotational) disorder. With the disorder of this type, a distinction of the possible space group is difficult to make and it is generally of limited significance. For all of the above space groups, the models of disordered oxygen positions are similar and thus here the group of the highest symmetry, $Fm\bar{3}m$ was assumed (as mentioned in the previous work [180]). Figure 5-12 shows the crystal structure of K₃MoO₃N with molybdenum polyhedra resulting from the anion disorder.

For K₃MoO₃N with $z = 4$, the solution in $Fm\bar{3}m$ lead to the single Mo site at the origin, $[0, 0, 0]$ ($4a$) and two sites of potassium ions, occupying $4b$ and $8c$. After that, the free electron density shows only one peak at $[0, 0, x]$ ($24e$), which being occupied by anions (O/N) forming a pseudo octahedral coordination for Mo. Since

the Raman spectrum strongly reveals the tetrahedral surrounding of Mo, this must be a following of a disorder of MoO_3N tetrahedra.

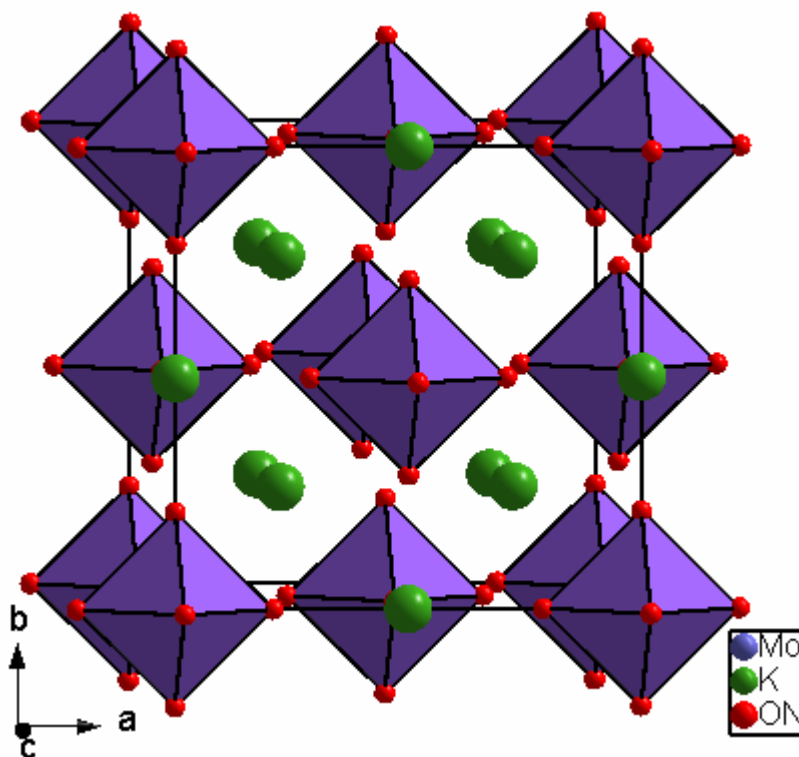


Figure 5-12: Crystal structure of K_3MoO_3N with distorted MoO_3N polyhedra.

According to the chemical analysis, the nitrogen/oxygen ratio in this compound is 1:3. The resulting formula K_3MoO_3N is in agreement with molybdenum in oxidation state of +6 as the most stable one for Mo. Thus this single 24e position for the anions was refined assuming an occupation factor 2/3, where $\frac{1}{2}$ corresponds to O and $\frac{1}{6}$ to N. The results of the structure refinement are given in table 5-4 and table 5-5. Table 5-6 gives the anisotropic displacement parameters of K_3MoO_3N . Figure 5-13 represents the molybdenum pseudo octahedron which is actually a disordered MoO_3N tetrahedron present in the sample while figure 5-14 represents the electron density mapping of the molybdenum polyhedron.

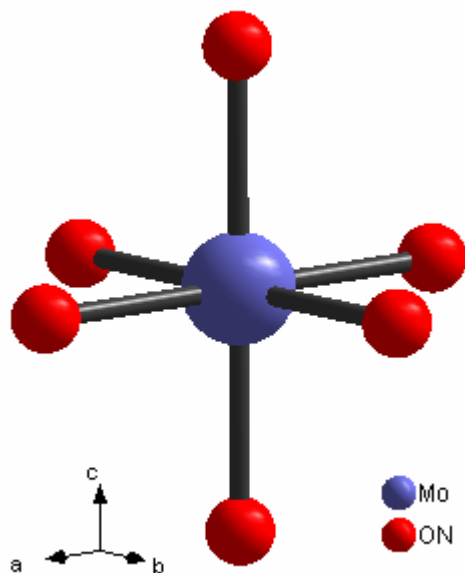


Figure 5-13: Molybdenum pseudo octahedron which is actually disordered MoO_3N tetrahedra.

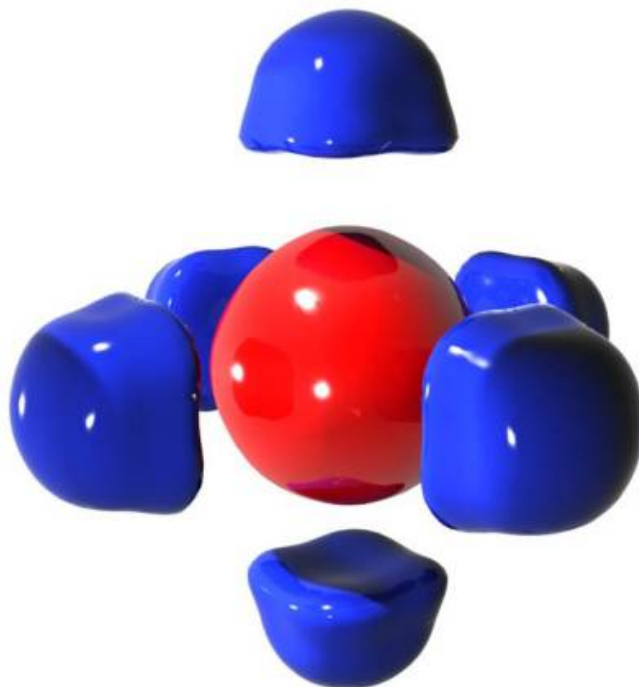


Figure 5-14: Probable electron density mapping of molybdenum polyhedra (Red sphere = Molybdenum, blue caps = Oxygen/Nitrogen).

The attempts to introduce a disorder to the structural refinement by the displacement of O and K atoms from “averaged” (introduce a splitting model) positions were unsuccessful, since atoms tend to the original position on the cell edge between Mo and K2.

Table 5-4: Crystallographic data and Structure Refinement of K_3MoO_3N .

Crystal system	Cubic
Space group	$Fm\bar{3}m$ (No. 225)
Lattice parameters / Å	$a = 8.612(1)$ Å
Z	4
Formula weight /g mol ⁻¹	226.9143
Cell Volume /Å ³	638.72
Density calc. /mg·m ⁻³	2.862
Crystal color	Colorless
Diffractometer	Brucker SMART-APEX CCD
X-rays/ Monochromator	Mo-K α_1 / Graphite
Method of the refinement	Full-matrix least-squares on F^2
Weight	$W = 1/(\sigma^2(F_0^2) + (0.1641 \times P)^2)$, where $P = (\max(F_0^2, 0) + 2 \times F_c^2)/3$
Maximum 2θ	69.75 °
Range of h, k, l	$-13 \leq h \leq 14, -13 \leq k \leq 13, -13 \leq l \leq 13$
Temperature (K)	295
No. of data points	2507
Absorption coefficient mm ⁻¹	3.94
R-Values	$R_1 = 0.058, wR_2 = 0.2066$

Table 5-5: Positional and isotropic displacement parameters for K_3MoO_3N .

Atom	Site	x	y	z	SOF
Mo1	4a	0	0	0	1.0000
K1	8c	¼	¼	¼	1.0000
K2	4b	½	½	½	1.0000
O1	24e	0	0	-0.21043	½
N1	24e	0	0	-0.21043	1/6

Because of the orientational disorder of the MoO_3N anion as in the figure 5-12, the Mo-O/N and K-O/N bond lengths cannot be reliable. In the structure of K_3MoO_3N , the disordered and almost spherical MoO_3N anion build up a cubic close packing where K1 and K2 occupy tetrahedral and octahedral sites, correspondingly to MoO_3N anions (Figure 5-12). The structure of K_3MoO_3N can be derived from the structure of Li_3Bi where Li positions are occupied by K and Bi atoms correspond to the averaged mass center of MoO_3N anions.

Table 5-6: Anisotropic displacement parameters of K_3MoO_3N in (\AA^2).

Atoms	U_{11}	U_{22}	U_{33}	U_{12}	U_{13}	U_{23}
Mo1	0.06247	0.06247	0.06247	0	0	0
K1	0.10445	0.10445	0.10445	0	0	0
K2	0.16325	0.16325	0.16325	0	0	0
O1	0.24148	0.24148	0.11708	0	0	0
N1	0.24148	0.24148	0.11708	0	0	0

5.2.2 Other Cubic Oxynitrides

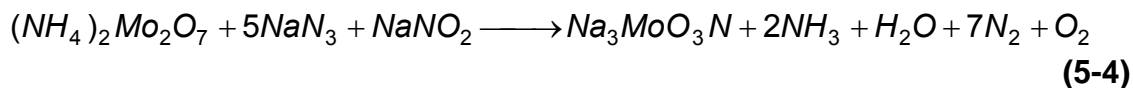
Similar to the K_3MoO_3N , some more compounds have been synthesized and characterized. The synthesis method of the other following oxynitrides is reported while the structural part remains the same as above.

1. Na_3MoO_3N
2. Rb_3MoO_3N
3. K_3WO_3N
4. K_3NbO_4

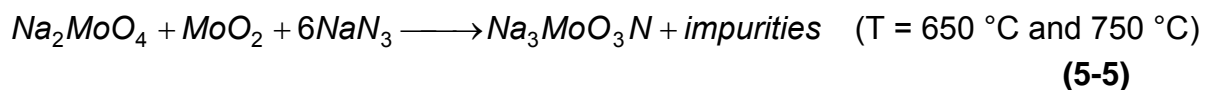
5.2.2.1 Sodium Molybdenum Oxynitride, Na_3MoO_3N

This sodium cubic oxynitride compound of molybdenum is prepared in the same way as K_3MoO_3N . All the dried reactants were mixed in the stoichiometric ratio and were ground in a ball-mill. Pellets have been prepared under 10^5 N and are dried under vacuum (10^{-3} mbar) at 150°C for 12 h. The dried reactants are placed in a tightly

closed steel container provided with a silver inlay. The crucible was then placed inside a furnace and the reaction was carried out under a flow of argon. A special temperature regime was applied: 25 °C → 260 °C (90 °C/h) → 380 °C (5 °C/h) → 600 °C (50 °C/h, 40 h) → 30 °C (20 °C/h).



The product has been firstly identified when the reaction between Na_2MoO_4 , MoO_2 and NaN_3 took place. Here, the cubic oxynitride is obtained along with known impurities such as Mo and Na_2MoO_4 . The reaction is given below.



The obtained oxynitride is highly sensitive to moisture and air and so, it is stored in small glass ampoules under dried argon. The reaction products were sealed in 0.3 mm capillary tubes and analyzed using X-ray diffraction. The XRD patterns obtained are found to be very similar to the cubic potassium oxynitride, K_3MoO_3N . A measured powder pattern of Na_3MoO_3N along with the known impurities (Na_2MoO_4 and Mo) is shown in figure 5-15. The cubic lattice constant $a = 7.8722(5) \text{ \AA}$ of Na_3MoO_3N was determined from single crystal data.

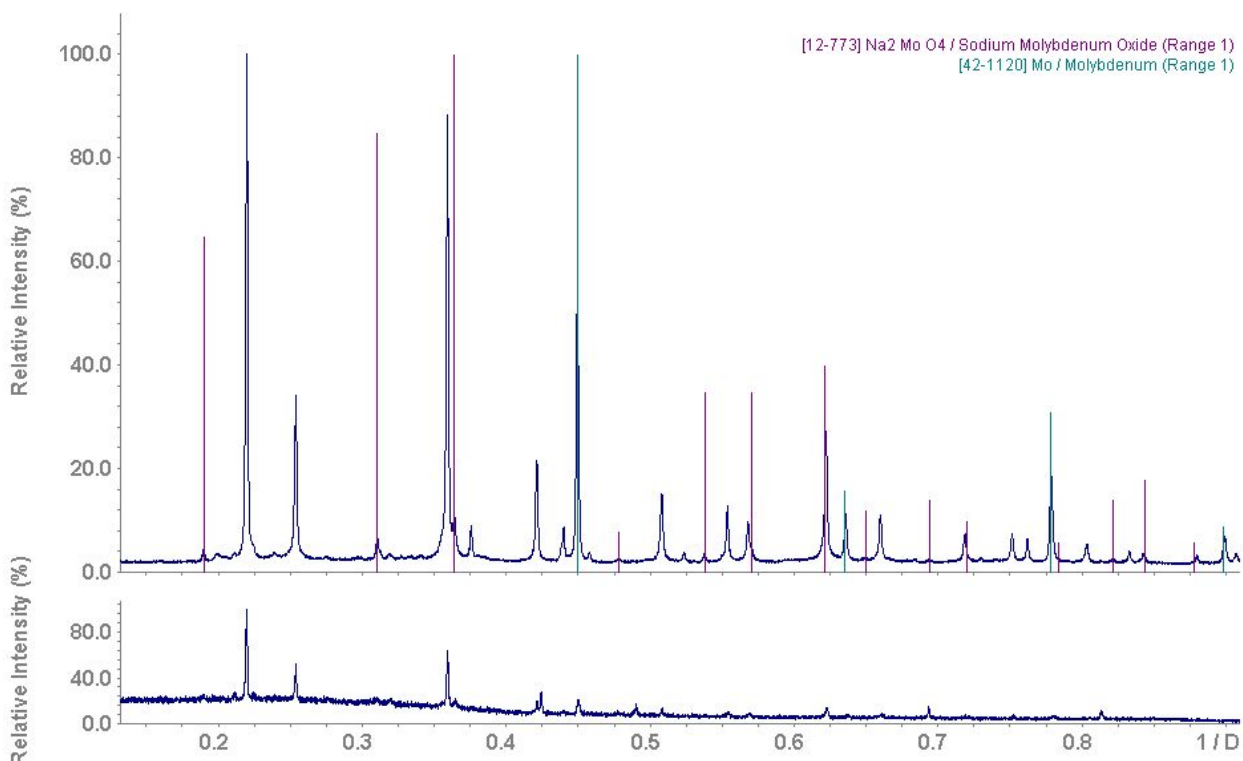
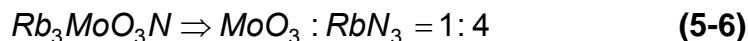


Figure 5-15: X-ray powder diffraction analysis of cubic Na_3MoO_3N with $Cu-K_{\alpha 1}$ radiation ($\lambda = 1.5406$) at room temperature.

5.2.2.2 Rubidium Molybdenum Oxynitride, Rb_3MoO_3N

The rubidium compound is also identical to the phase formerly mentioned as $Rb_6Mo_2O_9$. Analogous to the potassium compound, it actually turned out to be an oxynitride and will be named as Rb_3MoO_3N . It has been synthesized by reacting the relevant simple molybdenum oxide, MoO_3 with rubidium azide, RbN_3 in the appropriate ratio.



The reaction product was polycrystalline and is sensitive to air/moisture. The oxynitride was then sealed in the glass ampoules under the flow of dried argon and was kept for further analysis. Figure 5-16 shows the powder pattern of the cubic rubidium oxynitride.

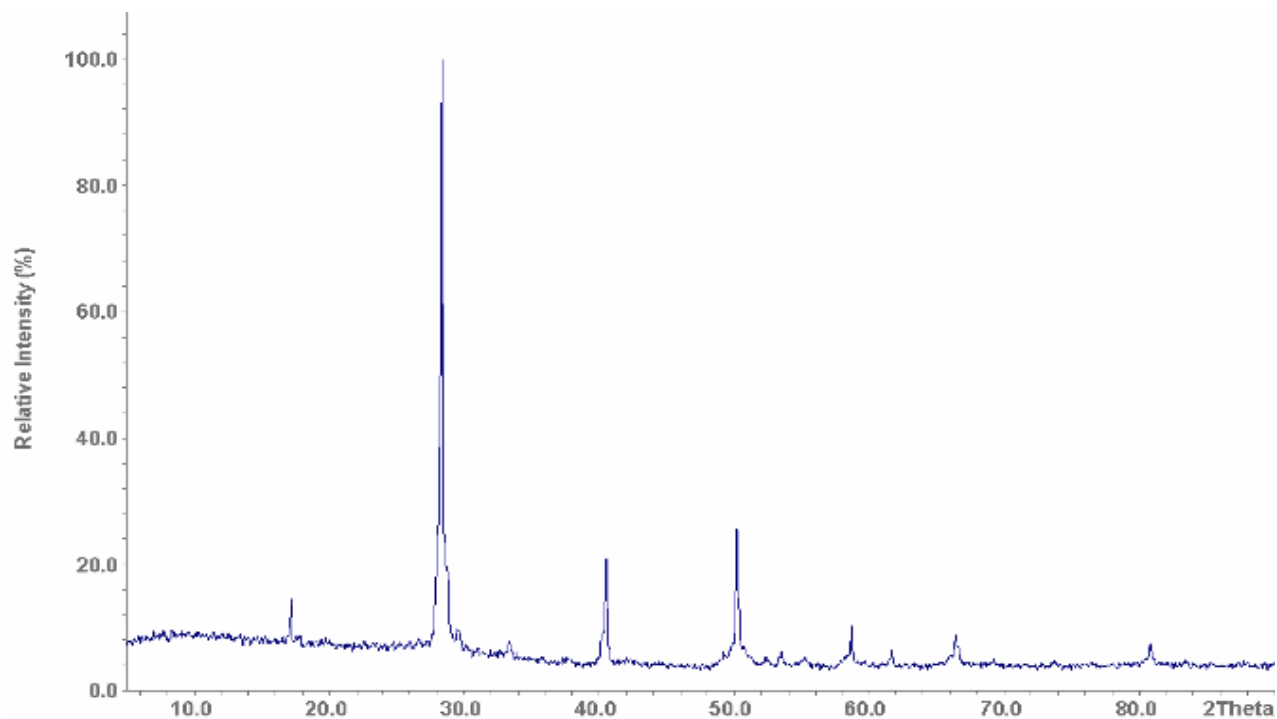
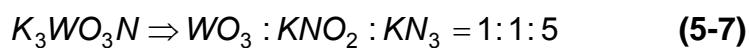


Figure 5-16: X-ray powder diffraction analysis of cubic Rb_3MoO_3N with $Mo-K_{\alpha 1}$ radiation ($\lambda = 0.7103$) at room temperature.

The indexing of the X-ray pattern of the above compound was carried out in STOE WinXPOW [153] program, it was indexed cubic with $a = 8.8958(2)$ Å.

5.2.2.3 Potassium Tungsten Oxynitride, K_3WO_3N

This compound is prepared by the reaction of tungsten oxide along with potassium azide and potassium nitrite in the silver crucible at the temperature of about 700 °C. An indexing of the X-ray pattern gives the cubic cell with $a = 8.624$ Å. The measured powder pattern is shown in the figure 5-17.



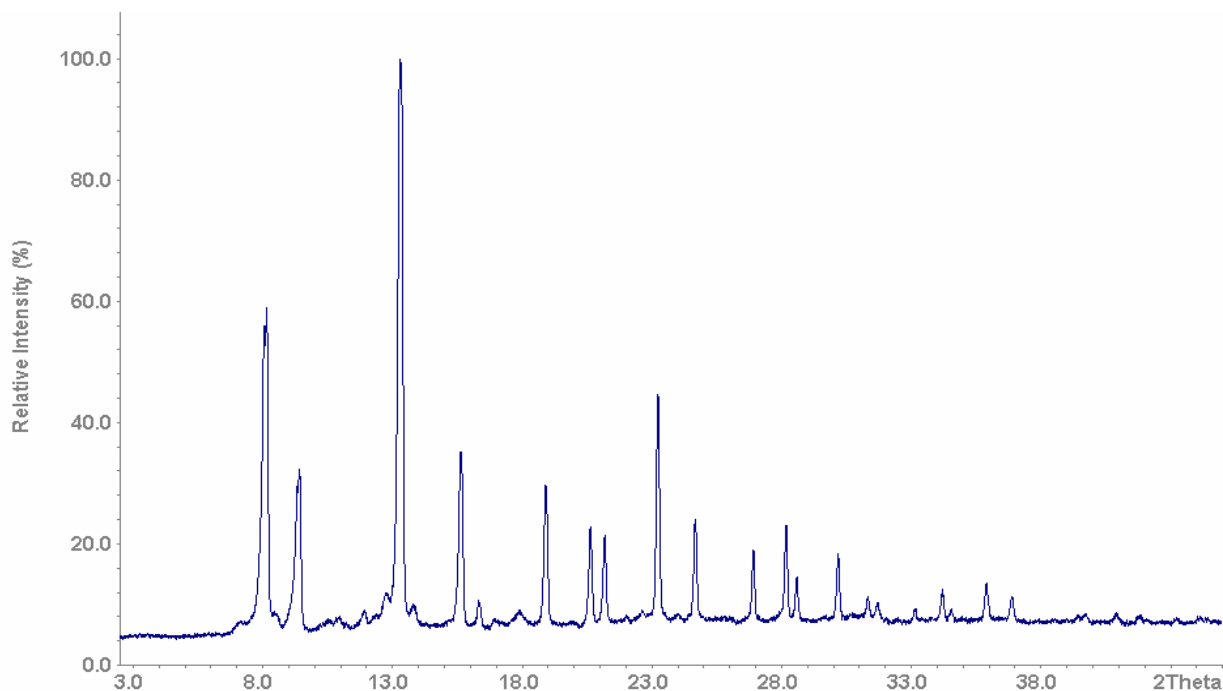


Figure 5-17: X-ray powder diffraction pattern of cubic K_3WO_3N with Mo- $K_{\alpha 1}$ radiation ($\lambda = 0.7103$) at room temperature.

5.2.2.4 Potassium Niobate Oxynitride, K_3NbO_4

This K_3NbO_4 was reported by Hoppe *et al.* [180], but the structure of this compound was not yet solved. This compound was obtained by the azide route by reacting potassium carbonate, potassium azide and niobium oxide in an appropriate stoichiometric ratio (3:4:1).

Colorless crystals were obtained. The crystal structure of K_3NbO_4 is very similar to that of cubic oxynitrides of molybdenum and tungsten of formula A_3MO_3N . Here, the structure consists of NbO_4 tetrahedra instead of disordered MO_3N tetrahedra as in the case of A_3MO_3N . The X-ray powder diffraction pattern is shown in figure 5-18. The obtained phase has been indexed cubic with the lattice constant, $a = 8.6228(3) \text{ \AA}$.

Table 5-7 represents the lattice constants of different cubic oxynitrides prepared via azide route.

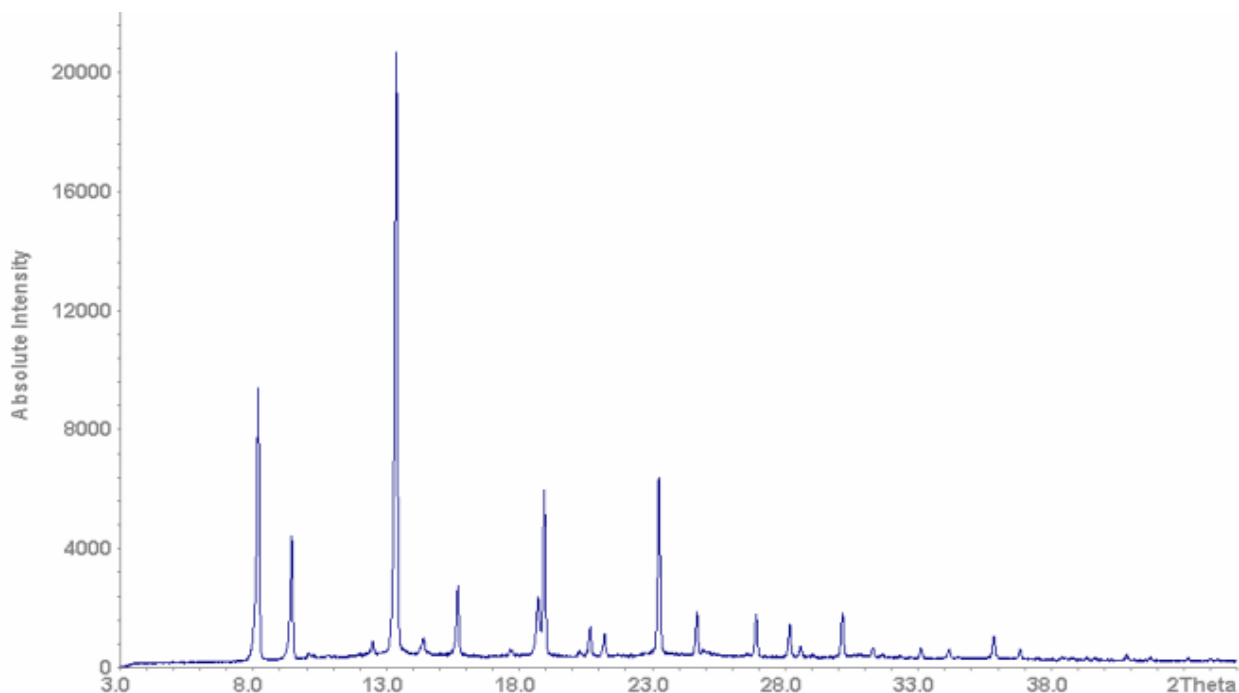


Figure 5-18: X-ray powder diffraction pattern of cubic K_3NbO_4 with Mo- $K_{\alpha 1}$ radiation ($\lambda = 0.7103$) at room temperature.

Table 5-7: Different cubic oxynitrides with their lattice constants.

Compound	Crystal system	Lattice constants (Å)	Data source
Na_3MoO_3N	Cubic, F- centered	7.8722(5)	Single crystal
K_3MoO_3N	Cubic, F- centered	8.5732(7)	Single crystal
Rb_3MoO_3N	Cubic, F- centered	8.8958(2)	Powder data
K_3WO_3N	Cubic, F- centered	8.624(2)	Powder data
K_3NbO_4	Cubic, F- centered	8.6228(3)	Single crystal

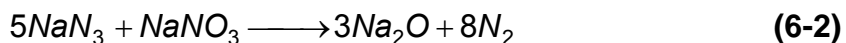
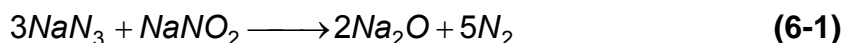
All these compounds are isotypic and contain tetrahedral $[MoO_{4-n}N_n]^{3-}$ anions, $M = Nb, Mo$ or W , which are rotationally disordered, so corresponding to the F- centering, an octahedral oxygen environment of M results. Thus, the azide-nitrate route paves the way in synthesizing many oxynitrides.

6. Chapter-6

Concluding Remarks

Concluding remarks concerning the azide/nitrate route as an access to alkali transition metal oxides/oxynitrides

The azide/nitrate route was found to be a promising route to access numerous ternary oxides with an alkali metal involved [123]. The use of alkali nitrates and azides (besides the respective metals or metal oxides) as starting compounds formally results in the *in-situ* formation of an alkali metal oxide as



According to this model of reaction progress, the alkali metal oxides are highly reactive and due to this, the reaction temperature and/or reaction time can be reduced relative to solid state reactions from (a mixture of) the respective oxides [12,21]. Nevertheless, the transition metal oxides used as starting materials often seem to react directly with the nitrate, possibly in the molten state [121], and an *in-situ* formation of an alkali oxide is not necessary to explain the reaction products. Due to the fact, that at high reaction temperatures the decomposition of the desired product can be initiated, also different and otherwise inaccessible compounds have been obtained by this route [121].

The main advantages of the azide/nitrate route can be formulated as follows:

- Insensitivity of the reactants to air and moisture.

The starting compounds involved into this method can be handled easily, e. g. they can be homogenised by using a ball-mill which is not possible with an alkali oxide as an educt.

- Moderate reaction conditions.

The reaction conditions are more moderate than usual solid state reactions. This is because of the *in-situ* formation of highly reactive alkali metal oxide and nitrogen which are very exothermic in nature.

- Different products compared to usual solid state reactions.

The reaction products can vary from those obtained by other methods of synthesis. Due to the moderate conditions, compounds with lower temperatures of decomposition are sometimes accessible by this preparation route.

- The formation of gaseous by-products, i.e. easily volatile products.

The products often do not have to be purified anymore.

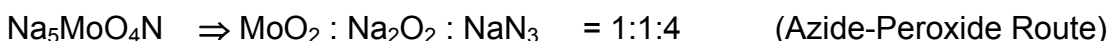
Applying the azide/nitrate route to transition metal elements of the groups IX and XI ternary oxides with the transition metals in reduced or even in mixed valence states are obtained, e. g. in the case of copper, depending on the reaction conditions, $\text{Na}_3\text{Cu}_2\text{O}_4$ with an average valence state of +2.5 for Cu [121] or the Cu(I) containing compound Na_3CuO_2 [121]. Compounds with copper purely in the oxidation state of +3 or even higher are not accessible by this route yet, cobalt is obtained as the usual (sometimes mixed) Co(II) or Co(III) [182] as well as in the “unusual” state of +1 in Rb_3CoO_2 [183], and silver actually remains in the Ag(I) state [184].

In the present work the azide/nitrate route was applied to group VI elements for the first time. In contrast to the former results with the later transition metal elements, here all products contain the metals in their highest possible valence states, i. e. for molybdenum and tungsten in +6. Although the transition metals were used in reduced valence states as starting materials like e. g. MoO_2 , WO_2 or elemental molybdenum, no reduced states were observed in the products. Obviously the nitrates or even the nitrogen formed during the reaction are able to oxidise the involved transition metals to their highest valence states.

Another characteristic feature of this method of preparation is the fact that, these reactions do not result in oxides exclusively, but also in oxynitrides, often as the main or even pure products. This is firstly a consequence of the energetically

preferred reaction of nitrogen with partially reduced molybdenum and tungsten compounds to Mo/W (VI) oxynitrides. As another reason, the affinity of molybdenum and tungsten for nitrogen as an associate in solids is consistent with the general tendency of the group IV, V, and VI elements for the easy formation of nitrides (from the elements). The mechanism of the reaction is not known, and it is not the case that the alkali oxide is formed in all azide nitrate reactions as mentioned in equations 6-1 and 6-2.

By the azide nitrate route, the oxynitrides were obtained along with impurities as well as by-products in some reactions. In some cases, they have been obtained as a pure phase. In order to get the pure single phase, several modifications have been performed to the well developed azide-nitrate route. These modifications were important for to get the pure phase of the compounds desired. Oxynitrides were obtained in the pure form when the reactant azide alone reacts with the TMO, and in some cases, pure compound is obtained by the addition of alkali peroxide along with alkali azide to TMO. So these modified routes can be called as “Azide Route” or “Azide-Peroxide Route”. Few examples were listed here.



As a conclusion, by applying the azide/nitrate route as well as the modification as the azide/nitrate/peroxide route to the heavy group VI elements, the products are restricted to those containing molybdenum and tungsten in the valence state +6, and that the formation of oxynitrides besides or instead of pure oxides has to be taken into account.

7. Summary

This work has focused on exploring the synthesis and characterization of new alkali oxides and oxynitrides of molybdenum and tungsten. In particular, the synthetic approach via the azide/nitrate route, which was developed recently, should be evaluated and extended to the oxides of the heavy group VI elements.

For characterization, the crystal structures have been determined by using X-ray diffraction data by means of single crystal or powder methods, and TGA/DTA, DSC and specific heat measurements, IR/Raman spectroscopy, and measurements of the magnetic and conducting behavior were performed.

In general, the following results can be depicted from this work:

- The azide/nitrate route has been turned out to be a very seminal and promising technique for the preparation of oxomolybdates and oxotungstates.
- This synthetic method provides an access to oxynitrides of molybdenum and tungsten, besides nitrogen free oxides. Nitrogen does not only serve as a volatile reaction product, but it can also be installed as a part of the solid state product at the applied reaction conditions.
- Several modifications of azide-nitrate route have been performed to obtain the desired product in the pure form.
- The usual oxidation state adopted by the transition metals involved here is +6. The oxidation potential of the reaction mixture is strong enough to oxidize molybdenum and tungsten to the highest possible state even when starting with the dioxide or the elemental metal.

The following compounds have been discovered and characterized in the course of this work.

1. $\text{Na}_3\text{MoO}_3\text{N}$

The new molybdenum oxynitride, $\text{Na}_3\text{MoO}_3\text{N}$, was prepared via the azide route from stoichiometric mixtures of MoO_3 and NaN_3 at 650 °C. Its crystal structure was solved and refined from X-ray powder data (orthorhombic, $Pmn2_1$, $a = 7.2463(1)$ Å, $b = 6.2498(1)$ Å, $c = 5.6386(1)$ Å, $Z = 2$, R_p : 0.0904; R_{wp} : 0.0983). The structure consists of isolated $[\text{MoO}_3\text{N}]^{3-}$ tetrahedra which are separated by Na^+ cations, also in a tetrahedral co-ordination. It is isostructural to $\text{Na}_3\text{WO}_3\text{N}$ which is a lower symmetry derivative of the Cu_3AsS_4 structure type. Due to the small difference in the scattering lengths of nitrogen and oxygen, it was impossible to decide between the borderline cases of completely ordered or disordered anions or a partial ordering. However, from the positive SHG responses, we can deduce the acentric space group being the correct one and based on the lattice energy calculations, we have been able to identify the position most probably being occupied by nitrogen.

2. $\text{Na}_5\text{MoO}_4\text{N}$

The new oxynitride, $\text{Na}_5\text{MoO}_4\text{N}$, was prepared from stoichiometric mixtures of the starting materials MoO_2 , Na_2O_2 and NaN_3 which were heated in a special regime up to 500 °C, and cooled down slowly. Its crystal structure was solved and refined from single crystal data (orthorhombic, $Cmcm$, $a = 9.911(2)$ Å, $b = 5.743(1)$ Å, $c = 10.677(2)$ Å, $Z = 4$, $R_1 = 0.0153$, $wR_2 = 0.0427$). The structure consists of isolated $[\text{MoO}_4\text{N}]^{5-}$ rectangular pyramids which are separated by Na^+ cations. This compound is structurally related to $\text{Na}_5\text{WO}_4\text{N}$ which crystallizes acentrically in space group $Cmc2_1$.

3. $K_3Na(WO_4)_2$

The new quaternary tungstate, $K_3Na(WO_4)_2$, was synthesized by heating the stoichiometric mixture of the corresponding alkali tungstates, anhydrous sodium tungstate and anhydrous potassium tungstate. The colorless oxide obtained was found to be stable till 1000 °C. $K_3Na(WO_4)_2$ is isostructural to the naturally occurring mineral glaserite, $K_3Na(SO_4)_2$. Similar to some glaserite type compounds, $K_3Na(WO_4)_2$ shows a phase transition which was observed from the HT-X-ray measurements. The room temperature phase was found to be monoclinic (space group: $C2/c$) with the lattice constants: $a = 10.4928(1)$ Å, $b = 6.0693(1)$ Å, $c = 15.2921(1)$ Å, $Z = 8$ and $\beta = 90.087(2)^\circ$ and, at the temperature above 250 °C, a hexagonal cell of space group $P\bar{3}m1$ with $a = 6.1305(1)$ Å and $c = 7.6944(1)$ Å was observed. The main building units of the crystal structure are WO_4 tetrahedra, which are linked by sodium and potassium cations. The main structural difference between the monoclinic and the trigonal structure is the tilting of the WO_4 tetrahedra and also the coordination of the potassium ions. The coordination number of potassium was found to be 10 and 12 for the HT-phase and, 9 and 10 for the RT-phase.

4. $K_6Mo_{10}O_{33}$

The new potassium molybdenum oxide, $K_6Mo_{10}O_{33}$, was synthesized by the solid state reaction from the appropriate quantities of the pre-dried metal oxide and potassium molybdate fired at around 650 °C for 2 days. The crystal structure of $K_6Mo_{10}O_{33}$ has been solved by using single crystal X-ray diffraction data, the structural refinement was performed by the full-matrix least squares calculation method. The compound adopts the space group $P1$ with the lattice constants $a = 7.7100(5)$ Å, $b = 11.9659(8)$ Å, $c = 17.1321(1)$ Å, $Z = 2$ with $\alpha = 86.42^\circ$, $\beta = 77.18^\circ$ and $\gamma = 74.14^\circ$. The compound is diamagnetic and decomposes at around 950 °C. The structure consists of infinite chains of edge-sharing MoO_6 octahedra which are linked in the second dimension by Mo_4O_{17} groups via common vertices. The structure of this compound is related to $Na_6Mo_{10}O_{33}$ and $Ag_6Mo_{10}O_{33}$.

5. Cubic Alkali Oxynitrides of Molybdenum, Tungsten and Niobium, $A_3MO_{4-n}N_n$

A group of cubic molybdates and tungstates of the formula $A_6M_2O_9$ with $A = \text{Na, K, Rb or Cs}$, $M = \text{Mo or W}$, is known for about 25 years, but the crystal structures have not been solved. After our attempts of syntheses and elemental analyses, it turned out that these compounds contain nitrogen and have to be regarded as oxynitrides. A number of these phases of molybdenum and tungsten and, for comparison, of niobium of the general formula $A_3MO_{4-n}N_n$ ($A = \text{Na, K, Rb}$; for $n = 1$: $M = \text{Mo, W}$; for $n = 0$: $M = \text{Nb}$) were synthesized by using the azide-nitrate/nitrite route, in detail there are

- $\text{Na}_3\text{MoO}_3\text{N}$
- $\text{K}_3\text{MoO}_3\text{N}$
- $\text{Rb}_3\text{MoO}_3\text{N}$
- $\text{K}_3\text{WO}_3\text{N}$
- K_3NbO_4 .

All the compounds are isostructural and crystallize in an F -centered cubic lattice. Single crystals for $\text{K}_3\text{MoO}_3\text{N}$ and $\text{Na}_3\text{MoO}_3\text{N}$, were successfully grown. According to crystal structure determinations in space group $Fm\bar{3}m$ ($\text{K}_3\text{MoO}_3\text{N}$: $a = 8.612(1) \text{ \AA}$, $Z = 4$, $R_1 = 0.058$, $wR_2 = 0.2066$), the cations are ordered, but the tetrahedral MoO_3N anions are rotationally disordered in a way that an octahedral surrounding of the transition metal is pretended. Also different positions of oxygen and nitrogen have not been observed. This phenomenon of rotational disorder remembers to the behavior of other compounds with the general formula $A_3\text{MO}_4$, e. g. the good ionic conductor Na_3PO_4 and other phosphates. All the phases obtained here are insulators. The cubic $\text{Na}_3\text{MoO}_3\text{N}$ has obviously the same composition as the orthorhombic phase presented in chapter 1. However, no way to transform one phase into the other has been found. The incurring of the cubic $\text{Na}_3\text{MoO}_3\text{N}$ is

restricted to the presence of another nitrogen-containing compound such as NaNO_3 or $(\text{NH}_4)_2\text{Mo}_2\text{O}_7$ in the reaction mixture besides the presence of azide.

Zusammenfassung

In dieser Arbeit wurde besonderes Gewicht auf Synthese und Charakterisierung neuer Alkalioxide und -oxynitride von Molybdän und Wolfram gelegt. Insbesondere der kürzlich entwickelte Ansatz zur Synthese über die Azid-Nitrat-Route sollte untersucht und gegebenenfalls auf die Oxide der schweren Elemente der Gruppe VI angewendet werden.

Zur Charakterisierung der erhaltenen, neuen Verbindungen wurden die Kristallstrukturen anhand von Röntgendaten mittels Einkristall- oder Pulvermethoden bestimmt, weiterhin wurden DTA/TG- und DSC-Messungen, Messungen der spezifischen Wärme, IR- und Ramanspektroskopie sowie Messungen der magnetischen Eigenschaften und der Leitfähigkeit durchgeführt.

Als allgemeine Ergebnisse dieser Arbeit können folgende Punkte festgehalten werden:

- Die Azid-Nitrat-Route hat sich als sehr fruchtbare und vielversprechende Methode zur Präparation von Oxomolybdaten und -wolframaten erwiesen.
- Die Synthesemethode bietet, außer zu reinen Oxiden, zusätzlich einen Zugang zu Oxynitriden von Molybdän und Wolfram. Stickstoff übernimmt hier nicht ausschließlich die Rolle eines flüchtigen Reaktionsproduktes, sondern kann unter den herrschenden Reaktionsbedingungen außerdem in den als Feststoff vorliegenden Teil der Produkte eingebaut sein.
- Um die gewünschten Produkte in Reinform zu erhalten, wurden Modifizierungen der Azid-Nitrat-Route vorgenommen.
- Die beteiligten Übergangsmetalle liegen in den Reaktionsprodukten durchweg in der Oxidationsstufe +6 vor. Das Oxidationspotential der Reaktionsmischung reicht aus, um Molybdän und Wolfram, auch bei Verwendung der Dioxide oder der Metalle als Ausgangsverbindung, in den höchstmöglichen Zustand zu oxidieren.

Die nachfolgenden Verbindungen wurden im Rahmen dieser Arbeit erstmals dargestellt und charakterisiert.

1. $\text{Na}_3\text{MoO}_3\text{N}$

Natriummolybdänoxynitrid, $\text{Na}_3\text{MoO}_3\text{N}$, wurde über die Azid-Nitrat-Route aus einer Mischung aus MoO_3 und NaN_3 bei $650\text{ }^\circ\text{C}$ dargestellt. Die Kristallstruktur wurde aus Röntgenpulverdaten gelöst und verfeinert (orthorhombisch, $Pmn2_1$, $a = 7.2463(1)$, $b = 6.2498(1)$, $c = 5.6386(1)\text{ \AA}$, $Z = 2$, $R_p = 0.0904$, $R_{wp} = 0.0983$). Die Kristallstruktur besteht aus isolierten $[\text{MoO}_3\text{N}]^{3-}$ -Tetraedern, welche von in ebenfalls tetraedrischer Umgebung befindlichen Na^+ -Kationen separiert werden. $\text{Na}_3\text{MoO}_3\text{N}$ ist isostrukturell zu $\text{Na}_3\text{WO}_3\text{N}$, einem niedersymmetrischen Verwandten des Cu_3AsS_4 -Strukturtyps. Aufgrund der geringen Unterschiede des Streuvermögens von Sauerstoff und Stickstoff läßt sich nicht entscheiden, ob einer der Grenzfälle vollständig ausgeordneter oder vollständig ungeordneter Anionen vorliegt, oder aber eine teilweise Ordnung. Durch Messungen des SHG-Effektes läßt sich jedoch eindeutig auf eine azentrische Raumgruppe schließen, und anhand von Berechnungen der Gitterenergie kann die am wahrscheinlichsten von Stickstoff besetzte Position bestimmt werden.

2. $\text{Na}_5\text{MoO}_4\text{N}$

Ein weiteres neues Molybdänoxynitrid, $\text{Na}_5\text{MoO}_4\text{N}$, wurde aus stöchiometrischen Mischungen von MoO_2 , Na_2O_2 und NaN_3 synthetisiert, die nach einem speziellen Temperaturprogramm auf $500\text{ }^\circ\text{C}$ erhitzt und anschließend langsam abgekühlt wurden. Die Kristallstruktur wurde anhand von Einkristalldaten gelöst und verfeinert (orthorhombisch, $Cmcm$, $a = 9.911(2)\text{ \AA}$, $b = 5.743(1)\text{ \AA}$, $c = 10.677(2)\text{ \AA}$, $Z = 4$, $R_1 = 0.0153$, $wR_2 = 0.0427$). Die Kristallstruktur setzt sich aus quadratischen $[\text{MoO}_4\text{N}]^{5-}$ -Pyramiden und Na^+ -Kationen zusammen. Die Anionen sind in diesem Fall ausgeordnet, das Stickstoffatom bildet die Spitze der $[\text{MoO}_4\text{N}]^{5-}$ -Pyramide. Die Verbindung ist nahe verwandt mit $\text{Na}_5\text{WO}_4\text{N}$, das azentrisch in der Raumgruppe $Cmc2_1$ kristallisiert.

3. $\text{K}_3\text{Na}(\text{WO}_4)_2$

Ein neues quaternäres Wolframat, $\text{K}_3\text{Na}(\text{WO}_4)_2$, wurde durch Erhitzen stöchiometrischer Mischungen der entsprechenden entwässerten ternären Alkaliwolframate, Na_2WO_4 und K_2WO_4 , dargestellt. Das erhaltene farblose Oxid ist bis 1000°C stabil. $\text{K}_3\text{Na}(\text{WO}_4)_2$ ist isostrukturell zum natürlich vorkommenden Mineral Glaserit, K_3NaSO_4 . Wie einige weitere, im Glaserittyp kristallisierende Verbindungen durchläuft $\text{K}_3\text{Na}(\text{WO}_4)_2$ einen Phasenübergang, der bei HT-Röntgenbeugungsmessungen beobachtet werden konnte. Die Raumtemperaturmodifikation kristallisiert monoklin mit $a = 10.4928(1) \text{ \AA}$, $b = 6.0693(1) \text{ \AA}$, $c = 15.2921(1) \text{ \AA}$, $Z = 8$ und $\beta = 90.087(2)^\circ$, bei 250°C wird ein hexagonales Gitter mit $a = 6.1305(1)$ und $c = 7.6944(1) \text{ \AA}$ beobachtet. Die wichtigsten Baugruppen der Kristallstruktur sind WO_4 -Tetraeder, die durch Kalium- und Natriumkationen verbunden werden. Der Hauptunterschied zwischen der monoklinen und der hexagonalen Phase besteht in der Neigung der WO_4 -Tetraeder sowie in der Umgebung der Kaliumionen. Die Koordinationszahl von Kalium ist 10 und 12 in der HT- bzw. 9 und 10 in der RT-Phase.

4. $\text{K}_6\text{Mo}_{10}\text{O}_{33}$

$\text{K}_6\text{Mo}_{10}\text{O}_{33}$ wurde aus geeigneten Mengen des vorgetrockneten Molybdänoxids und Kaliummolybdats durch zweitägiges Erhitzen bei 650°C präpariert. Die Kristallstruktur von $\text{K}_6\text{Mo}_{10}\text{O}_{33}$ wurde anhand von Einkristalldaten unter Verwendung des Verfahrens der kleinsten Fehlerquadrate bestimmt ($P1$, $a = 7.7100(5)$, $b = 11.9659(8)$, $c = 17.1321(1) \text{ \AA}$, $Z = 2$, $\alpha = 86.42^\circ$, $\beta = 77.18^\circ$, $\gamma = 74.14^\circ$). Die Verbindung ist diamagnetisch und zersetzt sich bei ungefähr 950°C . Die Kristallstruktur wird aus unendlichen Ketten von kantenverknüpften MoO_6 -Oktaedern gebildet, die von Mo_4O_{17} -Einheiten über gemeinsame Ecken zu Schichten verbunden werden. Die Struktur weist Ähnlichkeiten zu denen von $\text{Na}_6\text{Mo}_{10}\text{O}_{33}$ und $\text{Ag}_6\text{Mo}_{10}\text{O}_{33}$ auf.

5. Kubische Alkalioxynitride von Molybdän, Wolfram und Niob, $A_3MO_{4-n}N_n$

Eine Reihe kubischer Molybdate und Wolframate der Zusammensetzung $A_6M_2O_9$ mit $A = Na, K, Rb$ or Cs , $M = Mo, W$, ist seit etwa 25 Jahren bekannt, allerdings gelang es bisher nicht, deren Kristallstrukturen zu bestimmen. Nach unseren Syntheseversuchen und nach Elementaranalysen stellte sich heraus, daß diese Verbindungen Stickstoff enthalten und daher als Oxynitride angesehen werden müssen. Einige dieser molybdän-, wolfram- und, zum Vergleich, niobhaltigen Phasen der allgemeinen Zusammensetzung $A_3MO_{4-n}N_n$ ($A = Na, K, Rb$; für $n = 1$: $M = Mo, W$; für $n = 0$: $M = Nb$) wurden über die Azid-Nitrat/Nitrit-Route dargestellt, im einzelnen sind dies

- Na_3MoO_3N
- K_3MoO_3N
- Rb_3MoO_3N
- K_3WO_3N
- K_3NbO_4 .

Sämtliche Verbindungen sind isostrukturell und kristallisieren kubisch flächenzentriert. Von K_3MoO_3N and Na_3MoO_3N gelang die Zucht von Einkristallen, anhand derer die Kristallstruktur bestimmt werden konnte (K_3MoO_3N : $Fm\bar{3}m$, $a = 8.612(1) \text{ \AA}$, $Z = 4$, $R_1 = 0.058$, $wR_2 = 0.2066$) Während die Kationen ausgeordnet sind, können die Anionen nicht unterschiedlichen Positionen zugeordnet werden und sind fehlgeordnet. Zudem sind die $[MoO_3N]^{3-}$ -Anionen auf solche Weise rotationsfehlgeordnet, daß eine oktaedrische Umgebung des Übergangsmetallatoms vorgetäuscht wird. Das Auftreten von Rotationsfehlordnung tetraedrischer Baugruppen erinnert stark an das ähnlicher Verbindungen der allgemeinen Formel A_3MO_4 , darunter der gute Ionenleiter Na_3PO_4 sowie weitere Phosphate. Alle hier erhaltenen Phasen sind Isolatoren. Das hier erwähnte kubische Na_3MoO_3N hat die gleiche Zusammensetzung wie die orthorhombische Phase, die in Kapitel 1 dieser

Arbeit vorgestellt wurde. Allerdings wurde keine Möglichkeit gefunden, die beiden Modifikationen ineinander zu überführen. Der Erhalt des kubischen $\text{Na}_3\text{MoO}_3\text{N}$ ist an die Anwesenheit einer weiteren stickstoffhaltigen Komponente in der Reaktionsmischung neben dem Azid, d. h. NaN_3 oder $(\text{NH}_4)_2\text{Mo}_2\text{O}_7$, gebunden.

References

- 1 A. West, "Solid State Chemistry and its Applications", p 734. Wiley, New York, **1984**.
- 2 I. Lindqvist, Acta Chem. Scand. **1950**, 4, 1066.
- 3 B. M. Gatehouse, C. E. Jenkins, B. K. Miskin, J. Solid State Chem. **1983**, 46, 269.
- 4 P. Caillet, Bull. Soc. Chim. Fr. **1967**, 4750.
- 5 F. Hoermann, Z. Anorg. Allg. Chem. **1928**, 177, 145.
- 6 M. Seleborg, Acta Chem. Scand. **1967**, 21, 499.
- 7 H. Haas, M. Jansen, Z. Anorg. Allg. Chem. **2001**, 627, 755.
- 8 K. G. Bramnik, H. Ehrenberg, Z. Anorg. Allg. Chem. **2004**, 630, 1336.
- 9 S. E. Rasmussen, J. -E. Jorgensen, B. Lundtoft, J. Appl. Crystallogr. **1996**, 29, 42.
- 10 R. Hoffman, R. Hoppe, K. Bauer, K. J. Range, J. Less-Common Met. **1990**, 161, 279.
- 11 Pistorius, J. Chem. Phys. **1966**, 44, 4532.
- 12 H. Haas, M. Jansen, Z. Anorg. Allg. Chem. **2001**, 627, 755.
- 13 J. -M. Reau, C. Fouassier, P. Hagenmüller, Bull. Soc. Chim. Fr. **1967**, 3873.
- 14 K. V. Ramanujachary, M. Greenblatt, W. H. McCarroll, J. Cryst. Growth **1984**, 70, 476.
- 15 J. -M. Reau, C. Fouassier, P. Hagenmüller, J. Solid State Chem. **1970**, 1, 326.
- 16 N. C. Stephenson, Acta Cryst. **1966**, 20, 59.
- 17 J. Tarascon, G. Hull, Solid State Ionics **1986**, 22, 85.
- 18 J. -M. Reau, C. Fouassier, P. Hagenmüller, Bull. Soc. Chim. Fr. **1970**, 3827.
- 19 C. Ringenbach, H. Kessler, A. Hatterer, C. R. Seances Acad. Sci., Ser. C **1969**, 269, 1394.
- 20 G. L. Schimek, S. C. Chen, R. E. McCarley, Inorg. Chem. **1995**, 34, 6130.

- 21 M. Souland, H. Kessler, A. Hatterer, *Rev. Chim. Miner.* **1981**, *18*, 299.
- 22 H. Kessler, A. Hatterer, *C. R. Seances Acad. Sci., Ser. C* **1970**, *270*, 815.
- 23 A. Hatterer, H. Kessler, *C. R. Seances Acad. Sci., Ser. C* **1968**, *266*, 286.
- 24 T. Betz, R. Hoppe, *J. Less-Common Met.* **1985**, *105*, 87.
- 25 N. C. Stephenson, A. D. Wadsley, *Acta Cryst.* **1965**, *18*, 241.
- 26 J. Graham, A. D. Wadsley, *Acta Cryst.* **1966**, *20*, 93.
- 27 W. J. Schutte, J. L. de Boer, *Acta Cryst.* **1993**, *B49*, 579.
- 28 F. A. Schroeder, W. Schuckmann, *Z. Naturforsch.* **1977**, *B32*, 365.
- 29 H. Vincent, M. Chedira, J. Marcus, J. Mercier, C. Schlenker, *J. Solid State Chem.* **1983**, *47*, 113.
- 30 S. C. Chen, B. Wang, M. Greenblatt, *Inorg. Chem.* **1993**, *32*, 4306.
- 31 C. C. Torardi, J. C. Calabrese, *Inorg. Chem.* **1984**, *23*, 3281.
- 32 S. T. Triantafyllou, P. C. Christidis, *Acta Cryst.* **1999**, *C55*, 838.
- 33 K. J. Range, H. Haase, *Acta Cryst.* **1990**, *C46*, 317.
- 34 K. Okada, F. Marumo, S. I. Iwai, *Acta Cryst.* **1978**, *B34*, 3193.
- 35 K. Okada, H. Morikawa, F. Marumo, S. I. Iwai, *Acta Cryst.* **1978**, *B32*, 1522.
- 36 K. Okada, H. Morikawa, F. Marumo, S. I. Iwai, *Acta Cryst.* **1974**, *B30*, 1872.
- 37 R. Hoffman, R. Hoppe, *Z. Anorg. Allg. Chem.* **1989**, *573*, 143.
- 38 K. J. Range, H. Haase, *Acta Cryst.* **1990**, *C46*, 317.
- 39 K. Okada, H. Morikawa, F. Marumo, S. Iwai, *Acta Cryst.* **1975**, *B31*, 1200.
- 40 H. Kessler, A. Hatterer, *C. R. Seances Acad. Sci., Ser. C* **1972**, *274*, 623.
- 41 S. Triantafyllou, P. Christidis, Ch. Lioutas, *J. Solid State Chem.* **1997**, *133*, 479.
- 42 R. Slade, B. West, G. Hall, *Solid State Ionics* **1989**, *32*, 154.
- 43 F. Takusagawa, R. A. Jacobson, *J. Solid State Chem.* **1976**, *18*, 163.
- 44 M. Ghedira, J. Chenavas, M. Marezio, J. Marcus, *J. Solid State Chem.* **1985**, *57*, 300.
- 45 B. M. Gatehouse, P. Leverett, *J. Chem. Soc. A* **1969**, 849.
- 46 A. S. Koster, F. X. N. M. Kools, G. D. Rieck, *Acta Cryst.* **1969**, *B25*, 1704.
- 47 W. Gonschorek, T. Hahn, *Z. Kristallogr.* **1973**, *138*, 167.

- 48 S. A. Magarill, R. F. Klevtsova, *Kristallografiya* **1971**, *16*, 742.
- 49 M. Seleborg, *Acta Chem. Scand.* **1966**, *20*, 2195.
- 50 B. M. Gatehouse, P. Leverett, *J. Chem. Soc. A* **1968**, 1398.
- 51 R. Enjalbert, F. Guinneton, J. Galy, *Acta Cryst.* **1999**, *C55*, 273.
- 52 A. Foerster, H. U. Kreuzler, J. Fuchs, *Z. Naturforsch.* **1985**, *B40*, 1139.
- 53 B. M. Gatehouse, B. K. Miskin, *J. Solid State Chem.* **1974**, *9*, 247.
- 54 B. M. Gatehouse, B. K. Miskin, *J. Solid State Chem.* **1975**, *15*, 274.
- 55 B. M. Gatehouse, P. Leverett, *J. Chem. Soc. A* **1971**, 2107.
- 56 J. Marrot, J. M. Savariault, *Acta Cryst.* **1995**, *C51*, 2201.
- 57 M. Touboul, P. Toledano, *J. Appl. Crystallogr.* **1975**, *8*, 398.
- 58 M. Touboul, P. Toledano, *Acta Cryst.* **1978**, *B34*, 3547.
- 59 B. M. Gatehouse, B. K. Miskin, *Acta Cryst.* **1975**, *B31*, 1293.
- 60 M. Touboul, P. Toledano, P. Herpin, *Acta Cryst.* **1976**, *B32*, 1859.
- 61 F. Wöhler, *Ann. Chim. Phys.* **1825**, *29*, 43. (b) F. Wöhler, *Philos. Mag.* **1825**, *66*, 263 (English translation).
- 62 M. J. Sienko, In *Non-Stoichiometric Compounds*; R. F. Gould, Ed.; *Advances in Chemistry Series*; ACS: Washington DC, **1963**, p 224.
- 63 E. Banks, A. Wold, *Preparative Inorganic Reactions*; W. L. Jolly, Ed.; Interscience: New York, **1968**; Vol. 4, p 237.
- 64 P. G. Dickens, M. S. Whittingham, *Rev. Chem. Soc.* **1968**, *22*, 30.
- 65 P. Hagenmuller, *Progress in Solid State Chemistry*; H. Reiss, Ed.; Pergamon: New York, **1971**; Vol. 5, p 71.
- 66 H. R. Shanks, *J. Crystal Growth* **1972**, *13-14*, 433.
- 67 S. T. Triantafyllou, P. C. Christidis, Ch. B. Lioutas, *J. Solid State Chem.* **1997**, *133*, 479.
- 68 I. Tsuyumoto, T. Kudo, *Sensors Actuators B Chemical*, **1996**, *30*, 95.
- 69 P. R. Slater, J. T. S. Irvine, *Solid State Ionics*, **1999**, *124*, 61.
- 70 A. Wold, W. Kunmann, R. J. Arnott, A. Ferretti, *Inorg. Chem.* **1964**, *3*, 545.
- 71 R. Buder, J. Devenyi, J. Dumas, J. Marcus, J. Mercier, C. Schlenker, H. Vincent, *J. Physique Letters* **1982**, *43*, L59.

- 72 J. P. Pouget, K. Kagoshima, C. Schlenker, J. Marcus, *J. Physique Letters*. **1983**, *44*, L113.
- 73 R. Brusetti, B. K. Chakraverty, J. Devenyi, J. Dumas, J. Marcus, C. Schlenker, *Recent Developments in Condensed Matter Physics, Vol. 2*, Eds. J. T. Devreese, L. F. Lemmens, V. E. van Doren, J. van Royen (Plenum New York, **1982**), p. 181.
- 74 M. Greenblatt, W. H. McCarroll, R. Neifeld, M. Croft, J. V. Waszczak, *Solid State Commun.* **1984**, *51*, 671.
- 75 A.W. Sleight, T. A. Bither, P. E. Bierstedt, *Solid State Commun.* **1969**, *7*, 299.
- 76 J. Dumas, C. Schlenker, *Int. J. Mod. Phys.* **1983**, *B7*, 4045.
- 77 M. Greenblatt, *Chem. Rev.* **1988**, *88*, 31; (b) H. R. Shanks, *Solid State Commun.* **1974**, *15*, 753; (c) S. Reich, Y. Tsabba, *Eur. Phys. J.* **1999**, *B9*, 1; (d) A. Shengelaya, S. Reich, Y. Tsabba, K. A. Müller, *Eur. Phys. J.* **1999**, *B12*, 13; (e) R. Brusetti, P. Haen, J. Marcus, *Phys. Rev. B* **2002**, *65*, 144528.
- 78 B. W. Brown, E. Banks, *J. Am. Chem. Soc.* **1954**, *76*, 963.
- 79 A. Magneli, B. Blomberg, *Acta Chem. Scand.* **1951**, *5*, 375.
- 80 T. A. Bither, J. L. Gillson, H. S. Young, *Inorg. Chem.* **1966**, *5*, 1559.
- 81 K. Eda, T. Miyazaki, F. Hatayama, N. Sotani, *J. Solid State Chem.* **1998**, *137*, 12.
- 82 M. Onoda, K. Toriumi, Y. Matsuda, M. Sato, *J. Solid State Chem.* **1987**, *66*, 163.
- 83 M. Onoda, Y. Matsuda, M. Sato, *J. Solid State Chem.* **1987**, *69*, 67.
- 84 M. Ganne, M. Dion, A. Boumaza, M. Tournoux, *Solid State Commun.* **1986**, *59*, 137.
- 85 J. V. Dobson, J. Comer, *J. Electroanal. Chem.* **1987**, *220*, 225.
- 86 J. Fábry, V. Petříček, P. Vaněk, I. Císařová, *Acta Cryst.* **1997**, *B53*, 596.
- 87 M. Mokhosoev, K. Khal'baeva, E. Khaikina, A. Ogurtsov, *Russ. J. Inorg. Chem. (Engl. Transl.)*. **1990**, *35*, 1212.
- 88 L. Li, G. Wang, *Acta Phys. Sinica.* **1989**, *38*, 849.
- 89 R. Hoffmann, R. Hoppe, *Z. Anorg. Allg. Chem.* **1989**, *573*, 143.

- 90 C. N. R. Rao, *Chemical Approaches to the Synthesis of Inorganic Materials*, Wiley, New York, **1994**.
- 91 P. Hagenmuller, *Comprehensive Inorganic Chemistry*, Vol 4, Pergamon, New York, **1973**.
- 92 R. J. Cava, A. Santora, D. W. Murphy, S. Zahurak, R. S. Roth, *J. Solid State Chem.* **1982**, *42*, 251.
- 93 A. Wold, W. Kunmann, R. J. Arnott, A. Ferretti, *Inorg. Chem.* **1964**, *3*, 545.
- 94 A. K. Ganguli, J. Gopalakrishnan, C. N. R. Rao, *J. Solid State Chem.* **1988**, *74*, 228.
- 95 S. Ayyappan, C. N. R. Rao, *Mater. Res. Bull.* **1995**, *30*, 947.
- 96 Y. T. Zhu, A. Manthiram, *J. Solid State Chem.* **1994**, *110*, 187.
- 97 K. J. Rao, B. Vaidhyanathan, M. Ganguli, P. A. Ramakrishnan, *Chem. Mater.* **1999**, *11*, 882.
- 98 K. J. Rao, P. D. Ramesh, *Bull. Mater. Sci.* **1995**, *18*, 447.
- 99 D. M. P. Mingos, D. R. Baghurst, *Chem. Soc. Rev.* **1991**, *20*, 1.
- 100 J. Guo, C. Dong, L. Yang, G. Fu, *J. Solid State Chem.* **2005**, *178*, 58.
- 101 P. E. Rauch, F. J. DiSalvo, N. E. Brese, D. E. Partin, M. O'Keeffe, *J. Solid State Chem.* **1994**, *110*, 162.
- 102 N. E. Brese, M. O'Keeffe, *Structural Bonding* **1992**, *79*, 309.
- 103 W. Schnick, *Angew. Chem., Int. Ed. Engl.* **1993**, *32*, 806.
- 104 R. Marchand, Y. Laurent, J. Guyader, P. l'Haridon, P. Verdier, *J. Eur. Ceramic. Soc.* **1991**, *8*, 197.
- 105 M. Jansen, H. P. Letschert, *Nature* **2000**, *404*, 980.
- 106 V. Peltier, R. Conanec, R. Marchand, Y. Laurent, S. Delsarte, E. Guéguen, P. Grange, *Mat. Sci. Eng.* **1997**, *B47*, 177.
- 107 N. Fripiat, P. Grange, *J. Chem. Soc., Chem. Commun.* **1996**, 1409.
- 108 N. Fripiat, R. Conanec, A. Auroux, Y. Laurent, P. Grange, *J. Catal.* **1997**, *167*, 543.
- 109 S. Esmailzadeh, J. Grins, T. Hörlin, *Mat. Sci. Forum* **2000**, 325-326, 11.
- 110 P. l'Haridon, R. Pastuszak, Y. Laurent, *J. Solid State Chem.* **1982**, *43*, 29.

- 111 Y. Laurent, R. Pastuszak, P. l'Haridon, R. Marchand, *Acta Cryst.* **1982**, *B38*, 914.
- 112 A. Muller, B. Krebs, W. Holtje, *Spectrochim. Acta* **1967**, *23A*, 2753.
- 113 M. Jansen, R. Hoppe, *Z. Anorg. Allg. Chem.* **1974**, *409*, 152.
- 114 F. Bernhardt, R. Hoppe, *Z. Anorg. Allg. Chem.* **1993**, *619*, 969.
- 115 C. Feldmann, M. Jansen, *Z. Anorg. Allg. Chem.* **1995**, *621*, 201.
- 116 M. Jansen, R. Hoppe, *Z. Anorg. Allg. Chem.* **1975**, *417*, 31.
- 117 E. Zintl, H. H. von Baumbach, *Z. Anorg. Allg. Chem.* **1931**, *198*, 88.
- 118 M. Sofin, E.-M. Peters, M. Jansen, *Solid State Sci.* **2004**, *6*, 339
- 119 M. Sofin, E.-M. Peters, M. Jansen, *J. Solid State Chem.* **2004**, *177*, 2550.
- 120 M. Sofin, E.-M. Peters, M. Jansen, *Z. Anorg. Allg. Chem.* **2002**, *628*, 2697.
- 121 M. Sofin, Dissertation, Max-Planck Institut für Festkörperforschung (MPI-FKF), Stuttgart, **2003**.
- 122 W. Schlenk, A. Thal, *Ber. Dtsch. Chem. Ges.* **1913**, *46*, 2840.
- 123 D. Trinschek, M. Jansen, *Angew. Chem.* **1999**, *111*, 234; *Angew. Chem., Int. Ed.* **1999**, *38*, 133.
- 124 Firma Stoe & Cie, Software-Packet Stoe Stadi P, Darmstadt, 1999.
- 125 JCDPS-ICDD, USA, PCPDFWIN 1.22; www.icdd.com.
- 126 H. M. Rietveld, *J. Appl. Cryst.* **1969**, *2*, 65.
- 127 J. E. Post, *Reviews in Mineralogy: Modern Powder Diffraction Vol. 20*, Washington D. C., USA **1989**, S278.
- 128 J. Rodriguez-Carvajal, Program: FullProf 2000, CEA-CNRS **2000**.
- 129 J. Rodriguez-Carvajal, *Physica B* **1993**, *192*, 55.
- 130 Crystal Impact GbR, Endeavour 0.9.0 Structure Solution from Powder Diffraction, Bonn **1999**
- 131 H. Putz, J. C. Schön, M. Jansen, *J. Appl. Crystallogr.* **1999**, *32*, 864
- 132 V. Pareto, *Cours d'Economie Politique 1896-97*.
- 133 Bruker AXS, Programmpaket SMART, Madison, USA, **1998**.
- 134 G. M. Sheldrick, SHELXS-97, Programm zur Lösung von Kristallstrukturen, Göttingen **1997**.

- 135 G. M. Sheldrick, SHELXL-97, Programme zur Verfeinerung von Kristallstrukturen, Göttingen **1997**.
- 136 U. Henseler, M. Jansen, Sigma-Messung: Ein Programm zur Messung der elektrischen Eigenschaften eines Festkörpers, Bonn **1996**
- 137 U. Köhler, M. Jansen, Dissertation U. Köhler, Hannover **1987**
- 138 Landolt-Börnstein, Zahlenwerte und Funktionen aus Naturwissenschaften und Technik; Neue Serie, Gruppe II: Atom- und Molekularphysik, Bd. 2, Magnetische Eigenschaften der Koordinations- und Metallorganischen Verbindungen der Übergangselemente, Springer, Berlin, **1966**.
- 139 Microcalc Software Inc., Microcalc Origin, Version 6.0 DE, Northampton, **2000**.
- 140 G. Liu, X. Zhao, H. A. Eick, J. Alloys Comp. **1992**, 187, 145.
- 141 F. Pors, R. Marchand, Y. Laurent, Ann. Chim. Fr. **1991**, 16, 547.
- 142 R. Marchand, F. Pors, Y. Laurent, Ann. Chim. Fr. **1991**, 16, 553.
- 143 P. Bacher, P. Antoine, R. Marchand, P. L' Haridon, Y. Laurent, G. Roult, J. Solid State Chem. **1988**, 77, 67.
- 144 R. Marchand, F. Pors, Y. Laurent, O. Regreny, J. Lostec, L. M. Haussonne, J. Phys. Colloq. **1986**, 47(2), C1-901.
- 145 P. Antoine, R. Marchand, Y. Laurent, C. Michel, B. Raveau. Mat. Res. Bull. **1988**, 23, 953.
- 146 H. Jacobs, E. von Pinkowski, J. Less-Common Met. **1989**, 146, 147.
- 147 S. H. Elder, F. J. DiSalvo, J. B. Parise, J. A. Hriljac, James W. Richardson, J. Solid State Chem. **1994**, 108, 73.
- 148 D. Ostermann, H. Jacobs, Z. Anorg. Allg. Chem, **1993**, 619, 1277.
- 149 M. J. Capitan, C. Lowis dir Picard, Y. Laurent, J. A. Odriozola, Mat. Sci. Forum. **2000**, 325-326, 25.
- 150 V. Peltirer Bara, R. Marchand, A. O. Mallen, B. K. Hodnett, Mat. Sci. Forum. **2000**, 325-326, 45.
- 151 C. Chordes Yu, S. Ted Oyama, J. Solid State Chem. **1995**, 116, 205.
- 152 D. Trinschek, M. Jansen, Angew. Chem., Int. Ed. Engl. **1999**, 38, 133.

- 153 WinXPOW Ver 1.2, STOE & Cie GmbH, Darmstadt **2001**.
- 154 G. Adiwidjaja, J. Löhn, *Acta Crystallogr.* **1970**, B26, 1878.
- 155 I. Lindqvist, *Acta Chem. Scand.* **1959**, 4, 1066.
- 156 R. Hoppe, *Adv. Fluorine. Chem.* **1970**, 6, 387.
- 157 R. Hoppe, *Angew. Chem., Int. Ed. Engl.* **1966**, 5, 95.
- 158 S. K. Kurtz, J. Jerphagnon, M. M. Choy, *Landolt-Börnstein, Rev. ed., Vol III/11*, Springer-Verlag, Berlin, **1979**, 671.
- 159 N. Arumugam, A. Hönnerscheid, M. Jansen, *Z. Anorg. Allg. Chem.* **2003**, 629, 939.
- 160 H. Jacobs, D. Ostermann, *Z. Anorg. Allg. Chem.* **1994**, 620, 535.
- 161 W.H. Zachariasen, H. A. Plettinger, *Acta Cryst.* **1961**, 14, 229.
- 162 A. S. Koster, F. X. N. M. Kools, G. D. Rieck, *Acta Cryst.* **1969**, B25, 1704.
- 163 B. N. Mehrotra, W. Eysel, T. Hahn, *Acta Cryst.* **1977**, B33, 305.
- 164 K. M. Mogare, W. Klein, M. Jansen, *Z. Anorg. Allg. Chem.* **2005**, 2-3, 468.
- 165 M. E. Hilmy, *Am. Mineral.* **1953**, 38, 118.
- 166 K. Okada, J. Ossaka, *Acta Cryst.* **1980**, B36, 919.
- 167 A. Eichner, M. Kaczmarek, M. Wiesner, B. Mroz, *Ferroelectrics* **2004**, 303, 31.
- 168 A. Goldberg, W. Eysel, T. Hahn, *Neues Jahrb. Mineral. Monatsc.* **1973**, 6, 241.
- 169 T. Krajewski, B. Mróz, P. Piskunowicz, T. Breczewski, *Ferroelectrics* **1990**, 106, 225.
- 170 G. Madariaga, T. Breczewski, *Acta Cryst.* **1990**, C46, 2019.
- 171 B. Gossner, *Neues Jahrb. Mineral., Geol. Palaeontol., Abh. Abt. A.* **1928**, 57, 89.
- 172 H. F. Fischmeister, *Monatsh. Chem.* **1962**, 93, 420.
- 173 J. Fábry, T. Breczewski, V. Petříček, *Acta Cryst.* **1993**, B49, 826.
- 174 W. Abriel, F. Rau, K. –J. Range, *Mat. Res. Bull.* **1980**, 15, 1099.
- 175 K. G. Bramnik, H. Ehrenberg, *Z. Anorg. Allg. Chem.* **2004**, 630, 1336.
- 176 G. L. Schimek, S. C. Chen, R. E. McCarley, *Inorg. Chem.* **1995**, 34, 6130.

-
- 177 B. M. Gatehouse, P. Leverett, *J. Solid State Chem.* **1970**, *1*, 484.
- 178 L. Kihlborg, *Arkiv Kemi*, **1963**, *21*, 357.
- 179 B. M. Gatehouse, P. Leverett, *Chem. Commun.* **1968**, *15*, 901.
- 180 G. Meyer, R. Hoppe, *Rev. Chim. Miner.* **1975**, *12*, 454.
- 181 K. Nakamoto, "Infrared and Raman Spectra of Inorganic and Coordination Compounds", 4th edition, p 138, Wiley, New York, **1986**.
- 182 M. Sofin, H. -U. Güdel, R. Bircher, E. -M. Peters, M. Jansen, *Angew. Chem.* **2003**, *115*, 3651; *Angew. Chem., Int. Ed.* **2003**, *42*, 3527.
- 183 M. Sofin, M. Jansen, *Z. Anorg. Allg. Chem.* **2001**, *627*, 2115.
- 184 M. Sofin, K. Friese, J. Nuss, E. -M. Peters, M. Jansen, *Z. Anorg. Allg. Chem.* **2002**, *628*, 2500.

Appendix

Table A: Bond lengths between atoms in $K_6Mo_{10}O_{33}$.

Atoms	Atoms	Distance(Å)
Mo1	O5	1.7299
	O3	1.7455
	O1	1.9204
	O6	1.9583
	O4	2.2518
	O2	2.2945
Mo2	O11	1.6751
	O9	1.8022
	O10	1.9660
	O8	1.9690
	O7	2.2452
Mo3	O12	2.3407
	O14	1.6006
	O16	1.6996
	O15	1.8494
	O13	1.8534
Mo4	O34	2.1574
	O5	2.8855
	O18	1.6856
	O20	1.7244
	O19	1.9805
Mo5	O17	1.9893
	O33	2.1216
	O44	2.6784
	O28	1.7264
	O21	1.7414
Mo6	O36	1.9452
	O7	1.9913
	O10	2.1504
	O35	2.3080
	O22	1.6759
	O32	1.6796

Atoms	Atoms	Distance(Å)
Mo7	O7	1.9654
	O36	2.0277
	O38	2.2015
	O8	2.2569
	O23	1.7075
Mo8	O24	1.7086
	O39	1.9581
	O2	1.9923
	O6	2.2209
	O41	2.2763
Mo9	O31	1.6147
	O25	1.7263
	O19	1.8374
	O63	1.9044
	O9	2.7118
Mo10	O33	2.9065
	O30	1.6470
	O29	1.7973
	O2	1.9451
	O39	2.0106
Mo11	O37	2.0911
	O1	2.2345
	O27	1.7485
	O26	1.7927
	O15	1.9525
	O54	1.9921
	O34	2.0796
	O42	2.7631
	O55	1.6810
	O45	1.7381
	O40	1.9597
	O4	2.0238

Atoms	Atoms	Distance(Å)
Mo12	O1	2.2052
	O37	2.2857
	O52	1.6712
	O50	1.7024
	O4	1.9338
	O40	1.9933
Mo13	O6	2.2103
	O41	2.2141
	O53	1.6728
	O49	1.6756
	O12	1.9492
	O47	2.0436
Mo14	O35	2.1366
	O10	2.2869
	O51	1.7092
	O48	1.7229
	O47	1.9378
	O12	1.9693
Mo15	O8	2.1510
	O38	2.2481
	O46	1.6552
	O44	1.7593
	O35	1.9088
	O38	1.9176
Mo16	O36	2.1965
	O47	2.2617
	O42	1.6997
	O43	1.7070
	O41	1.9086
	O37	1.9591
Mo17	O39	2.2110
	O40	2.3166
	O58	1.6214
	O57	1.6738
	O56	1.9044
	O13	1.9523
	O34	2.1666
	O3	2.6448

Atoms	Atoms	Distance(Å)
Mo18	O64	1.5025
	O66	1.6424
	O62	1.8722
	O63	1.9528
	O33	2.0797
	O11	2.7239
Mo19	O60	1.7537
	O61	1.7926
	O54	1.8501
	O56	1.8868
	O43	2.8657
	O34	2.9651
Mo20	O59	1.7060
	O17	1.8065
	O65	1.8361
	O62	1.9221
	O33	2.2500
	O46	2.8975
K1	O29	2.4985
	O9	2.5997
	O60	2.8223
	O23	2.8446
	O58	2.8460
	O21	2.8767
K2	O22	3.0009
	O25	3.0509
	O19	3.2134
	O50	2.6979
	O48	2.7024
	O42	2.7285
K3	O59	2.7450
	O53	2.9677
	O26	3.0764
	O55	3.1026
	O15	3.1480
	O60	2.6149
	O1	2.6318
	O6	2.6750

Atoms	Atoms	Distance(Å)
K4	O13	2.7066
	O27	2.7090
	O29	2.9846
	O58	3.1725
	O23	3.2665
	O51	2.5984
	O45	2.6099
	O52	2.6859
	O65	2.7089
	O14	2.7658
	O66	2.8109
K5	O49	2.8182
	O10	2.5915
	O8	2.5964
	O63	2.6176
	O18	2.6601
	O65	2.6759
K6	O44	2.7653
	O43	2.8092
	O24	2.8508
	O28	2.8569
	O30	2.8959
	O32	3.0643
	O61	3.0877
	O20	3.1052
	O19	3.1167
	O61	2.5212
K7	O30	2.7172
	O20	2.7181
	O24	2.7377
	O32	2.7540
	O28	2.8822
	O31	2.9363
	O38	2.6650
	O31	2.7038
K8	O17	2.7164
	O35	2.7440
	O64	2.9526

Atoms	Atoms	Distance(Å)
K9	O20	3.1481
	O28	3.1636
	O5	2.7776
	O11	2.8825
	O49	2.9119
	O52	3.0199
	O51	3.0333
	O66	3.0410
	O45	3.0524
	O14	3.1124
K10	O62	3.1251
	O54	2.6568
	O37	2.6799
	O41	2.6993
	O16	2.7143
	O57	2.7429
	O55	3.1197
	O26	3.1409
K11	O4	3.2875
	O22	2.6277
	O25	2.6956
	O21	2.7144
	O3	2.7768
	O23	2.8629
	O56	2.9742
	O58	3.0202
	O29	3.1965
	K12	O26
O53		2.7228
O46		2.7234
O55		2.7259
O16		2.9159
O50		2.9364
O48		3.0080
O59		3.1672

AUTOBIOGRAPHICAL STATEMENT

NACHIAPPAN ARUMUGAM

Education Background

- Ph. D., Inorganic Chemistry** **2001-2005**
Max-Planck-Institute for Solid State Research (*MPI*), Germany.
Dissertation: New Alkali Oxides and Alkali Oxy-Nitrides of Molybdenum and Tungsten
Advisor: Prof. Dr. Martin Jansen
- M. Sc., Physical Chemistry** **1998-2000**
Indian Institute of Technology (*IIT*), Bombay, India
Thesis: Removal (Recovery) of Oil from Water using Camphoric Carbon
Advisor: Prof. Dr. Maheshwar Sharon
- B. Sc., Chemistry** **1995-1998**
University of Madras, Chennai, India.

Work Experience

- Research Assistant, **NCL**, Pune, India. **2000-2001**
- Synthesized AMPS based water soluble polymers and hydrogels for enhanced oil recovery.

Personal Information

Date of Birth: 31st January 1978
Nationality: Indian
Gender: Male

Languages Known

- Fluent in English, Tamil and Hindi.
- Basic knowledge of German.

List of Publications

- "Synthesis and Structure of Sodium Tetraoxo Nitrido Molybdate, Na_5MoO_4N " **Nachiappan Arumugam**, Eva -M Peters, and Martin Jansen, *Z. Naturforsch.* **2004**, 59b, 274.
- "A New Oxynitride Compound of Molybdenum, Na_3MoO_3N – Synthesis via the Azide Route and Structure" **Nachiappan Arumugam**, Andreas Hönnerscheid, and Martin Jansen, *Z. Anorg. Allg. Chem.* **2003**, 629, 939